Nonlinear Vibrations of Metallic and Composite Structures

by

Tony J. Anderson

Dissertation submitted to the Faculty of the

Virginia Polytechnic Institute and State University

in Partial fulfillment of the requirements for the degree of

Doctor of Philosophy

in

Engineering Mechanics

APPROVED:

Ali H. Nayfeh, Chairman

Dean T. Mook

Mahendra P. Singh

Rakesh K. Kapania

Scott L. Hendricks

April 1993

Blacksburg, Virginia

Nonlinear Vibrations of Metallic and Composite Structures

by

Tony J. Anderson

Ali H. Nayfeh, Chairman

Engineering Mechanics

(ABSTRACT)

In this work, several studies into the dynamic response of structures are made. In all the studies there is an interaction between the theoretical and experimental work that lead to important results. In the first study, previous theoretical results for the single-mode response of a parametrically excited cantilever beam are validated. Of special interest is that the often ignored nonlinear curvature is stronger than the nonlinear inertia for the first mode. Also, the addition of quadratic damping to the model improves the agreement between the theoretical and experimental results. In the second study, multi-mode responses of a slender cantilever beam are observed and characterized. Here, frequency spectra, psuedo-phase planes, Poincaré sections, and dimension values are used to distinguish among periodic, quasi-periodic, and chaotic motions. Also, physical interpretations of the modal interactions are made. In the third study, a theoretical investigation into a previously unreported modal interaction between high-frequency and low-frequency modes that is observed in some experiments is conducted. This modal interaction involves the complete response of the first mode and modulations associated with the third and fourth modes of the beam. A model that captures this type of modal interaction is developed. In the fourth study, the natural frequencies and mode shapes of several composite plates are

experimentally determined and compared with a linear finite-element analysis. The objective of the work is to provide accurate experimental natural frequencies of several composite plates that can be used to validate future theoretical developments.

Acknowledgments

I would like to thank my advisor, Professor Ali H. Nayfeh, for the opportunity to work with him and for his guidance and support through my research. I would like to thank Dr. Scott L. Hendricks for his friendship and help both at and away from school. I would like to thank Professors Dean T. Mook and Mahendra P. Singh for their teaching and advise. In addition, I would like to thank Rakesh K. Kapania for his helpful comments about my work. I would like to thank Edmund G. Henneke and the ESM Department for financial support. I would like to thank all the people at Virginia Polytechnic Institute and State University who have taught me and provided an excellent educational opportunity.

I would like to thank Balakumar Balachandran and Perng-Jin F. Pai for their freely given input to my work and for their friendship, and special thanks for Balakumar Balachandran's patience on reviewing my publications. I would like to express my appreciation to Kyoyul Oh and the other students working in the Vibrations Laboratory and Sally Shrader for their help and friendships that made my work more enjoyable.

I am most thankful to my wife and children. They provide both support for my work and a life away from school that is required for the maintenance of my sanity.

This work was support by the Army Research Office under Grant No. DAAL03-89-K-0180, the Center for Innovative Technology under Contract No. MAT-91-013, and the Air Force Office of Scientific Research under Grant No. F49620-92-J-0197.

Table of Contents

List of Figures

List of Tables

1. Introduction

Performance requirements for structures are becoming more difficult to meet. Often the requirements on structures are conflicting. For example, due to the expense of carrying components into orbit, the structure for the Space Station Freedom must be light weight. In addition, low-gravity experiments require stable platforms. The Hubble Space Telescope required light-weight components and extremely tight pointing accuracy. After the Hubble Space Telescope was in orbit and operating, scientists found that low-frequency structural vibrations initiated by the release of thermal stresses were large enough that the pointing accuracy did not meet the requirements of the observation missions and valuable time was lost due to the vibrations. Light weight and high strength are requirements for structures, such as the blades of hubless helicopter rotors. This certainly is not an all inclusive list of high-performance structures, but it is enough to show that the requirements on these structures are contradictory. For example, the easiest way for engineers to make a stable platform for the space station is to make it big and stiff and not worry about the structure's dynamics, but this violates the other requirement of light-weight components. This trend of ever more difficult requirements on structures is sure to continue.

Engineers must consider the dynamics in the modeling of a structure in order to meet high-performance requirements. Linear models are often used to approximate the response of structures. Linear models have many desirable characteristics. For many linear systems, exact solutions are known and a single solution exists for a given set of parameters. Also, superposition holds, modes do not exchange energy, and the frequency content of the steady-state response is the same as that of the excitation. Light-weight structures tend to be flexible. As the flexibility of structures increases, linear

approximations often no longer adequately predict the behavior and engineers must resort to nonlinear models. This leads to a fundamental problem; the aforementioned characteristics of linear systems do not hold for nonlinear systems.

When engineers deal with systems that require nonlinear models, they generally resort to approximate techniques. The books by Nayfeh and Mook (1979), Bolotin (1964), Evan-Ivanowski (1976), and Tondl (1965) show some of the tremendous amount of work and success in this area. The responses of nonlinear systems exhibit complicated phenomena, such as multiple solutions, frequency entrainment, superharmonic resonances, subharmonic resonances, combination resonances, modal interactions, saturation, quenching, Hopf bifurcations, limit cycles, symmetry-breaking and period-multiplying bifurcations, and chaos. Even with this long list of different phenomena, there is apparently no way of knowing if all types of nonlinear phenomena that can occur have been found. Due to the approximate nature of the analytical techniques and the many possible types of responses, it is difficult for an engineer to know with a high level of confidence that the analytical results will capture the motion that will occur in practice. This leads to the need for experiments to validate predicted results. In the process, experiments can reveal previously unknown nonlinear responses.

1.1 Literature Review

Often, knowledge about nonlinear systems develops by the observation of a phenomenon that is not understood, which leads to an analysis that explains the observation, which in turn predicts additional phenomena not previously observed, which is verified by experimental observations. A description of a classic example of this process follows. Froude (1863) reported that a ship whose frequency in heave is twice its frequency in roll has undesirable seakeeping characteristics. Nayfeh, Mook, and Marshall (1973) considered the response of a ship whose frequency in pitch is

approximately twice its frequency in roll to primary-resonant excitations. They found nonlinear periodic and modulated responses when the first (roll) mode was excited by a primary-resonant excitation. This type of response could be interpreted as undesirable seakeeping characteristics. In their study, they also discovered the saturation phenomenon. Haddow, Barr, and Mook (1984) conducted a theoretical and experimental investigation of the response of a two-degree-of-freedom beam structure to a harmonic excitation. They were the first to experimentally verify the saturation phenomenon.

Examples of theory and experiments complimenting each other are common throughout the literature on nonlinear systems. A review of pertinent works on the nonlinear vibration of structures follows.

1.1.1 Beam Studies

The exact analysis of structures is a nonlinear three-dimensional elasticity problem. This is an extremely difficult problem for engineers. Typically, the analyst makes some approximations to simplify the problem. For beam-like structures, beam theories are very useful tools that reduce the three-dimensional elasticity problem to a one-dimensional problem. The simplest beam theory is the well known Euler-Bernoulli beam theory and can be found in any strength of materials text. It is applicable to the in-plane deflections of long-slender isotropic beams. For this case, the shear deflection and nonlinearities are ignored. For beams with high aspect ratios h/L, where h and L are the length and thickness of the beam, respectively, or short wavelengths, the shear deflection is not negligible. In these cases a first-order shear theory, known as Timoshenko's beam theory (Thomson, 1981; Timoshenko, 1921, 1922), is often used. In this theory, the shear stress is assumed to be the same at every point over a given cross section. A shear correction coefficient, which depends on the shape of the cross section, is introduced to account for the fact that the shear stress and shear strain are not uniformly distributed

over the cross section. Heyliger and Reddy (1988) presented a higher-order shear deformation theory, in which some quadratic terms are included and no shear correction coefficient is needed.

Often nonlinearities due to finite deflections are important in the study of the response of beam structures. Eringen (1951) included nonlinear inertia terms in his investigation of the planar response of simply-supported beams. He investigated the single-mode response of a simply-supported beam with immovable hinged ends. Evensen and Evan-Iwanowski (1966) included the effect of longitudinal inertia on the parametric response of an elastic column. They assumed an inextensional beam and a single-mode response. Their study combined analytical and experimental investigations and found good agreement between the two. Sato et al. (1978) included both geometric and inertia nonlinearities in their study of the parametric response of a horizontal beam carrying a concentrated mass under gravity. They assumed a planar single-mode response. Their results show that, in addition to parametric resonances, external resonances occur due to initial static deflections.

The previously mentioned studies of the nonlinear response of beams investigated planar responses. In the development of beam theories in three-dimensional space, studies that combine theoretical and experimental results have proven to be important. Haight and King (1971) analytically and experimentally investigated the stability of the planar response of a parametrically excited cantilever beam. In the analysis, the three-dimensional motion of a beam with approximately equal moments of inertia was considered. For this case, the twisting of the beam can be neglected. Haight and King found regions of forcing and frequency values that resulted in the planar motion losing stability, resulting in an out-of-plane motion. Hodges and Dowell (1974) used Hamilton's principle and Newton's second law to develop a comprehensive set of equations with quadratic nonlinearities that describe the dynamics of beams in three-dimensional space.

Dowell, Traybar, and Hodges (1977) devised a simple experiment to investigate the static deflections and natural frequency shifts to evaluate the theory of Hodges and Dowell (1974). The results show that there are systematic differences between the theory and experiment when tip deflections become large. Later Hodges et al. (1988) pointed out that the nonlinear equations of motion governing flexural deformations cannot be consistent unless all nonlinear terms through third order are included. Crespo da Silva and Glynn (1978a) formulated a set of consistent governing differential equations of motion describing the nonplanar, nonlinear dynamics of an inextensional beam. In order to include the twisting of the beam, they used three Euler angles to relate the deformed and undeformed states. They also included nonlinearities due to both inertia and curvature. Crespo da Silva and Glynn (1978b) showed that when the lower frequency modes are considered the often ignored nonlinearities due to curvature are important. Pai and Nayfeh (1992) presented a very general beam theory valid for metallic and composite beams. The twisting curvature of the beam was used to define a twist angle, resulting in equations of motion that are independent of the rotation sequence of the Euler angles. They included both inertial and geometric nonlinearities as well as a third-order shear-deformation model.

Several studies experimentally investigated the response of slender cantilever beams similar to the one we study in this dissertation. Dugundji and Mukhopadhyay (1973) experimentally and theoretically investigated the response of a thin cantilever beam excited by a base motion transverse to the axis of the beam and along the direction of the beam's larger cross-section dimension. They observed three resonances: a primary resonance of the first torsional mode, a combination resonance involving the first and second bending modes, and a combination resonance involving the first bending and first torsional modes. For the combination resonance involving the first bending and first torsional modes, the frequency relationship between the excitation frequency and the

lowest-frequency component in the response was 18:1. Dugundji and Mukhopadhyay's study demonstrates that high-frequency excitations can excite low-frequency modes through external combination resonances. This type of resonance can be explained with current analytical models. Haddow and Hasan (1988) experimentally investigated the response of a parametrically excited flexible cantilever beam to an excitation whose frequency was near twice the fourth natural frequency ($2f_4$) and found various periodic and chaotic responses. They also reported that an "extremely low subharmonic response" occurred under certain conditions. Burton and Kolowith (1988) analytically and experimentally studied the response of a parametrically excited flexible cantilever beam to an excitation having a frequency near $2f_4$. They obtained experimental results similar to those reported by Haddow and Hasan (1988). In the studies of Haddow and Hasan (1988) and Burton and Kolowith (1988), prior to a chaotic response, a single-mode periodic response was observed. Cusumano and Moon (1989) and Cusumano (1990) presented results for an externally excited cantilever beam. They observed a "cascading of energy" to low-frequency components in the response after the planar motion lost stability, resulting in a nonplanar chaotic motion. The transition to a nonplanar chaotic motion was the focus of the works of Haddow and Hasan (1988), Burton and Kolowith (1988), and Cusumano and Moon (1989).

Several experimental studies have focused on chaotic vibrations of elastic beams. Moon and Holmes (1979), Moon (1980), and Moon and Holmes (1985) investigated the planar motion of buckled beams. In these test setups, the beam had two static equilibrium positions. This lead to a two-well potential problem. The beam would vibrate about a static equilibrium but then chaotically jump from one equilibrium to another. Moon and Shaw (1983) experimentally and theoretically investigated chaotic vibrations in a planar beam with impact boundary conditions.

Cusumano (1990) extensively studied a slender cantilever beam subjected to an external base excitation. His work focused mainly on chaotic out-of-plane motions. He characterized these motions with time histories, frequency spectra, and dimension calculations. In the excitation frequency-amplitude plane, he observed seven regions where chaotic motions occurred. In all of the cases, the loss of planar stability was preceded by the first in-plane bending mode being excited. He did not investigate how the first mode was excited. For the modeling of the system, he set the curvature associated with the largest area moment of inertia equal to zero. This defined a nonlinear mode that consisted of out-of-plane bending and twisting. His experiment using a near circular rod to verify this assumption is erroneous because, for this case, the assumption of zero curvature is not valid. One area moment of inertia must be much larger than the other to make this assumption. Cusumano also found that when the damping of the system was reduced, the qualitative nature of the motion of the beam did not change. He tested this by conducting experiments in a bag filled with helium. This suggests that the damping model will change the analytical results quantitatively but not qualitatively.

1.1.2 Damping

Damping is a crucial element in the dynamics of structures. Without damping, transient motions would not die out. Damping can also affect the stability boundaries. Despite its importance, a well defined method for determining the type of dominant damping mechanisms that are involved in a structure does not seem to exist. This is due, in part, to the large number of possible mechanisms involved. Linear viscous damping is often chosen because of modeling convenience. We present a brief review of studies on damping to give some insight into the topic and present a background for the selection of the damping models.

Bert (1973) reviewed material damping models. He compared the energy loss per cycle of the models and discussed their shortcomings. Also discussed are various measurement techniques. Crandall (1970) discussed damping mechanisms and presented results that show that damping depends on the amplitude and frequency of cyclic motions. He described some models and noted their limitations. He also presented examples where damping affects the stability of the dynamical system. Nelson and Greif (1970) reviewed which of these models was incorporated into general purpose shock and vibration computer programs.

Because the mechanisms involved in damping are not very well known, experiments are typically conducted to determine the damping coefficients. Generally the form of the damping is assumed and the coefficients are determined. Baker, Woolam, and Young (1967) investigated damping of thin cantilever beams. They introduced internal damping and external air damping into the governing equations. They obtained solutions by energy methods and computer simulations. Predicted decrements of free-vibration decay were compared with experiments on cantilevers run in atmospheres with standard and reduced pressures. Banks and Inman (1991) investigated damping mechanisms in composite beams. They found that a spatial hysteresis model combined with a linear viscous air damping model results in the best quantitative agreement with experimental time histories. Adams and Bacon (1973) investigated the flexural damping capacity and dynamic Young's modulus of metals and reinforced plastics. They tested their specimens in vacuum in order to obtain material damping properties. Rades (1983) presented two methods to determine coefficients for linear viscous and drag-type quadratic damping. These methods were based on variations to polar plots due to the quadratic damping. Rice and Fitzpatrick (1991) presented a method to determine nonlinear elements in a system by reformulating the nonlinear problem as a multiple input/output linear system. They applied the method to a single-degree-of-freedom

system with a drag-type quadratic damping. All these studies point out the large effect air damping can have on a system. The models assumed for air damping are linear viscous or linear viscous and quadratic damping. These are the models used in this work.

1.1.3 Nonlinear Dynamic Phenomena in Other Structures

In this section, we give a brief review of studies that investigated nonlinear phenomena in structures other than cantilever beams. The review emphasizes but is not restricted to studies with experimental and theoretical work.

Evan-Iwanowski (1976) presented quite general theoretical results for various nonlinear systems. These results were used to guide theoretical and experimental results presented later in the text. He presented theoretical and experimental results for the cases of principal parametric resonance ($f_e = 2f_i$) of a simply-supported plate, principal parametric and summation combination resonances ($f_e=f_i+f_j$) of a circular cylinder, summation combination resonances($f_e=f_i+f_j+f_k$) of a three-degree-of-freedom lumped mass system with cubic nonlinearities, principal parametric resonance of a column, and electric motor and cantilever beam interaction, where f_e is the excitation frequency and the f_m are the natural frequencies of the system.

Haddow, Barr, and Mook (1984) theoretically and experimentally investigated the response of an "L" shaped structure to a harmonic excitation. The structure had two lumped masses which had the effect of reducing the continuous system to a two-degree-of-freedom system having the frequencies f_1 and f_2. The dominant nonlinearities in the system were quadratic. They observed the influences of a two-to-one internal resonance (i.e., $f_2 \approx 2f_1$). They were also the first to experimentally verify the saturation phenomenon when $f_e \approx f_2$. Nayfeh and Zavodney (1988) experimentally observed amplitude- and phase-modulated motions in a similar structure when $f_e \approx f_1$. Nayfeh, Balachandran, Colbert, and Nayfeh (1989) studied a similar "L" shaped structure. Balachandran (1990)

and Balachandran and Nayfeh (1990) treated the beam sections of the structure as continuum, and used a time-averaged Lagragian to obtain the governing equations of motion. They found that, in the presence of autoparametric resonances, extremely small excitation levels may to produce chaotic motions, whereas large excitation levels are required to produce chaotic motions in single-degree-of-freedom systems.

Nayfeh (1983) investigated the response of a bowed structure (systems with quadratic and cubic nonlinearities) to a combination resonance. He showed that the combination resonance of the difference type can never be excited. He also found that, for certain ranges of the forcing level and phase, the combination resonance can be quenched or enhanced. Nayfeh (1984) studied the response of bowed structures to a two-frequency excitation with no internal resonances. He found up to seven equilibrium solutions. However, only one of these solutions is stable. He also found that when the amplitude of the excitation is higher than that necessary for both modes to be nonzero, there were no periodic steady-state responses.

Nayfeh, Nayfeh, and Mook (1990) investigated a T-shaped beam-mass structure subjected to a harmonic excitation of the third mode. The first three natural frequencies of the structure are such that the third natural frequency is approximately the sum of the first and second natural frequencies. The experiments and associated analysis show the existence of modal saturation, quasiperiodic, and phase-locked responses.

Miles (1965), Anand (1966), Narasimha (1968), and Nayfeh and Mook (1979) analyzed motions of strings subjected to harmonic in-plane excitations and found that nonplanar responses are possible for some excitation frequencies. Johnson and Bajaj (1989) investigated the same problem and showed that periodically and chaotically modulated responses are possible. Nayfeh, Nayfeh, and Mook (1992) experimentally investigated the motion of a stretched string subjected to external and parametric excitations. The combination of parametric and external excitations leads to whirling

motions where modes at the excitation frequency as well as modes at one-half the excitation frequency can be excited. They showed that under certain conditions the whirling motions lose stability, giving rise to complicated modulated motions.

1.1.4 Composite Plate Studies

To meet the ever more stringent requirements placed on structures, engineers often use advanced composite materials because of their high specific moduli and high specific weights. Much of the research on composite structures has been on plates.

Leissa (1981) surveyed the literature on the vibration and buckling of composite plates. Bert (1985) reviewed the dynamic response of laminated composites. Reddy (1983, 1985) reviewed the literature concerning the application of the finite-element method for the vibration of plates. Kapania and Raciti (1989a,b) presented a summary of recent advances in the analysis of laminated beams and plates. They reviewed the free-vibration analysis of symmetrically laminated plates for various geometric shapes and edge conditions.

In the study of the vibrations of laminated composite plates, the shear deflection is important because of the large ratio between the tensile and shear moduli. Kapania and Raciti (1989a) reviewed developments in the analysis of laminated beams and plates with an emphasis on shear effects and buckling. They presented a discussion of various shear-deformation theories for plates and beams and a review of the recently developed finite-element method for the analysis of thin and thick laminated beams and plates. Librescu and Reddy (1989) compared several shear-deformation theories and showed their connection with first-order shear-deformation theory. Reddy (1984) and Bhimaraddi and Stevens (1984) presented a higher-order shear-deformation theory that contains the same dependent unknowns as the first-order shear-deformation theory, but accounts for a parabolic distribution of the transverse shear strains through the thickness of the plate. It

also predicts zero shear on the surface of the plate and does not require a shear correction factor.

Bert and Mayberry (1969) experimentally and theoretically investigated the natural frequencies and mode shapes of laminated anisotropic plates with clamped edges. They presented the material properties used in the analysis but did not indicate how these were obtained. They used the maximum response amplitude as a criterion to determine the natural frequencies. In the theoretical investigation they neglected shear deflections and used a Rayleigh-Ritz approximation. The error between the experimental and theoretical results was approximately 10%. Clary (1972) investigated the natural frequencies and mode shapes of unidirectional composite material panels. He investigated the change in frequencies and mode shapes as the angle between the fibers and boundaries is changed. He presented the material properties used in the analysis but did not indicate how these were obtained. He used the maximum response amplitude to determine the natural frequencies. Also, relatively large masses were attached to the plate to monitor the response and to excite the plate. The percentage error between experiment and theory is between 2% and 3% for the beam-type modes and between 2% and 10% for the plate modes. Crawley (1979) experimentally and theoretically investigated the natural frequencies and mode shapes of composite cantilever plates and shells. He used the 90° phase difference between the periodic excitation and the response as a criterion to determine the natural frequencies. This is a somewhat better method than the maximum response amplitude method previously mentioned. He obtained material properties from static tests of the specimens. The difference between experimental and theoretical natural frequencies is approximately 12%. He suggested the difference could be due to the dynamic moduli being different from the static moduli. Ashton and Anderson (1969) experimentally and theoretically investigated the natural frequencies and mode shapes of laminated boron-epoxy plates with clamped edges. They sprinkled

aluminum granules on the plates. They took the excitation frequency at which the granules had definite model patterns to be the natural frequency. The error between the theoretical and experimental values for the natural frequencies ranges between 1-30 %.

There have been very few experimental investigations of the nonlinear response of composite plates. Mayberry and Bert (1968) experimentally and theoretically investigated the nonlinear vibrations of composite plates. They investigated a glass-epoxy plate clamped on all edges. They observed that the plates frequencies increased as the excitation level was increased. The predicted linear natural frequencies did not match the measured linear natural frequencies. They normalized the results so that they match in the linear case, then they found that the trend of increase in frequency with excitation levels between theory and experiment matched for one case. The other cases did no match.

Yamaki and Chiba (1983a, 1983b) experimentally and theoretically investigated the nonlinear response of a thin isotropic rectangular plate clamped on all edges. They observed many types of responses, such as internal and combination resonances. The theory and experiments matched for some cases but not for most. The main limitation of the analysis was their assumption that three symmetric modes participated in the response. For most of the cases observed in the experiments, other modes participated in the response.

The nonlinear analysis of laminated composite plates has been a subject of significant current interest. Whitney (1968) and Whitney and Leissa (1969) were the first to formulate the equations of motion for the large-deflection behavior of laminated anisotropic plates by accounting for the von Karman geometrical nonlinearity. Chia (1980) presents in his text a comprehensive literature review, which covers the work in the field until 1979. Most nonlinear plate theories (Schmidt 1977; Reissner 1948, 1953; Reddy 1984; and Bhimaraddi 1987) account for von Karman type nonlinearities with

classical plate theory as well as first-order and higher-order shear theories. Pai and Nayfeh (1991) presented a theory that accounts for nonlinear curvatures, mid-plane strains, and third-order shear deformations. Singh, Rao, and Iyengar (1991) showed that it is important to include nonlinearities in the analysis of composite plates even for small loads because they observed nonlinear effects even in the small-deflection range

1.2 Summary and Overview of the Dissertation

In this work, several studies were conducted that combined experimental and theoretical investigations. I believe the most significant results are presented in Chapters 4 and 5. In these Chapters, we present results pertaining to a newly found modal interaction. This modal interaction could have implications for any structure that has excitations with frequencies that are high relative to the lowest natural frequencies of the structure. Following is an overview of the Dissertation.

In Chapter 2, we present the starting points for the investigation of the motion of the metallic cantilever beam. For the theoretical investigation of the beam, we start with the nonlinear equation and boundary conditions governing the planar motion of an isotropic cantilever beam in a nondimensionalized and scaled form. For the experimental investigation of the beam, we start with the test set-up and instrumentation. We also present the tools used to characterize both the theoretical and experimental responses.

In Chapter 3, we present a theoretical and experimental investigation of single-mode motions of the beam in the presence of a principal parametric resonance; that is, the excitation frequency f_e is near twice a natural frequency f_i of the beam and the base motion is along the undeformed axis of the beam. The nonlinearities in the system are due to both nonlinear inertia (a softening-type nonlinearity) and the often ignored nonlinear curvature (a hardening-type nonlinearity). Hence, the nonlinearity is of the hardening or softening type depending on whether the curvature or inertia nonlinearity

dominates the response. We experimentally verified that the nonlinearity for the first mode is of the hardening type due to the dominance of the nonlinear curvature. Also, we observed that the second mode is of the softening type, which is due to the dominance of the nonlinear inertia.

In Chapter 4, we present the results of experimental investigations into the transfer of energy from high-frequency excitations to low-frequency components in the response of the flexible cantilever beam. Four cases were considered, three with periodic base motions along the axis of the beam, and one with a band-limited random base motion transverse to the axis of the beam. A transfer of energy from high-frequency modes of the system to low-frequency modes of the system was observed in all four cases.

In Chapter 5, we present a theoretical investigation of the resonances reported in Chapter 4. We used the method of averaging to obtain equations that describe the evolution of the slowly varying terms in the system. A nonclassical transformation is used in the variation of parameters prior to the averaging process. This transformation was required to capture the slow-time scale evolution of the low-frequency first mode compared to the high-frequency third and fourth modes. The theoretical and experimental results are in good agreement.

In Chapter 6, we present the results of an experimental and theoretical investigation into the vibrations of advanced composite plates. We obtain the natural frequencies and mode shapes of composite plates with several layup sequences and boundary conditions. These results are compared to results obtained from linear finite-element models. For the cases where the boundary conditions are well known, the present experimental and finite-element results are in better agreement than what has been previously reported.

2. Test Setup and Tools

In this chapter, we introduce items that are common to Chapters 3-5. These items include the nonlinear equations of motion for a flexible metallic cantilever beam, the test setup used to investigate the nonlinear vibrations of the beam, and the tools used to characterize the motions of the beam. Work on composite plates is presented in Chapter 6, it is essentially self contained and includes a description of the test setup and system.

2.1 Nonlinear Equations of Motion

As mentioned in Chapter 1, the nonlinear responses of flexible cantilever beams has been extensively investigated. For this study, we use the equations developed by Crespo da Silva and Glynn (1978a). Crespo da Silva and Glynn (1978a) made the following assumptions for a long slender isotropic beam experiencing small strains and moderate deflections and rotations: (a) warping, shear deformations, and Poisson effects are negligible and (b) bending and twisting moments at any arbitrary position along the beam are proportional to the nonlinear expressions of the local bending and twisting curvatures, respectively. In addition, we restrict our attention to planar motions and assume that the damping is composed of linear viscous and quadratic terms. This leads to the following partial-differential equation:

$$m\frac{\partial^2\hat{v}}{\partial\hat{t}^2}+\hat{\mu}\frac{\partial\hat{v}}{\partial\hat{t}}+EI\frac{\partial^4\hat{v}}{\partial\hat{s}^4}=-EI\frac{\partial}{\partial\hat{s}}\left(\frac{\partial\hat{v}}{\partial\hat{s}}\frac{\partial}{\partial\hat{s}}\left(\frac{\partial\hat{v}}{\partial\hat{s}}\frac{\partial^2\hat{v}}{\partial\hat{s}^2}\right)\right)-\frac{\partial}{\partial\hat{s}}\left(\frac{1}{2}\frac{\partial\hat{v}}{\partial\hat{s}}\int_L^{\hat{s}}m\frac{\partial^2}{\partial\hat{t}^2}\left(\int_0^{\hat{s}}\left(\frac{\partial\hat{v}}{\partial\hat{s}}\right)^2 d\hat{s}\right)d\hat{s}\right)$$
$$-m\left(\frac{\partial^2\hat{v}}{\partial\hat{s}^2}(\hat{s}-L)+\frac{\partial\hat{v}}{\partial\hat{s}}\right)\left(\hat{a}_b\cos\left(\hat{\Omega}\hat{t}\right)+\hat{g}\right)-\hat{c}\frac{\partial\hat{v}}{\partial\hat{t}}\left|\frac{\partial\hat{v}}{\partial\hat{t}}\right| \qquad (2.1)$$

where the variables are defined in Table 2.1. The associated boundary conditions are

$$\hat{v} = \hat{v}' = 0 \text{ at } \hat{s} = 0$$

$$\hat{v}'' = \hat{v}''' = 0 \text{ at } s = L. \tag{2.2}$$

Table 2.1 Definitions of Variables.

Variable	Variable Definition	Variable Dependence
m	mass per unit length	s
E	Young's modulus	s
I	area moment of inertia	s
$\hat{v}$	displacement	t, s
$\hat{s}$	position along the length of the beam of the undeformed element	independent variable
$\hat{t}$	time	independent variable
L	length of undeformed beam	constant
$\hat{\Omega}$	base motion frequency	control parameter
$\hat{a}_b$	acceleration of the base of the beam along the axis of the undeformed beam	control parameter
$\hat{g}$	acceleration due to gravity	constant
$\hat{c}$	coefficient of quadratic damping	s
$\hat{\mu}$	coefficient of viscous damping	s

A schematic of the beam defining the variables is shown in Fig. 2.1. On the right-hand side of Eq. (2.1), the first term is due to nonlinear curvature and the second term is due to

nonlinear inertia. The third term represents the parametric excitation due to the base motion and the effect of gravity. The last term is due to quadratic damping.

If the cross-section dimensions of the beam are uniform (i.e., m, E, and I are constant), the equation of motion can be considerably simplified. We introduce nondimensional variables by using the characteristic length L and time $L^2\sqrt{m/EI}$ and obtain

$$s=\frac{\hat{s}}{L},\quad v=\frac{\hat{v}}{L},\quad t=\hat{t}\sqrt{\frac{EI}{mL^4}},\quad \tilde{\mu}=\hat{\mu}\frac{L^2}{\sqrt{mEI}},\quad \tilde{c}=\hat{c}\frac{L}{m},$$
$$\tilde{\Omega}=\hat{\Omega}\sqrt{\frac{mL^4}{EI}},\quad \tilde{a}_b=\hat{a}_b\frac{mL^3}{EI},\quad \tilde{g}=\hat{g}\frac{mL^3}{EI}.$$

This leads to the following equation of motion:

$$\begin{aligned}\ddot{v}+\tilde{\mu}\dot{v}+v^{iv} =& -\left(v'\left(v'v''\right)'\right)' -\left(\tfrac{1}{2}v'\int_1^s \tfrac{\partial^2}{\partial t^2}\left(\int_0^s v'^2 ds\right)ds\right)' \\ & -\left(v''(s-1)+v'\right)\left(\tilde{a}_b\cos\left(\tilde{\Omega}t\right)+\tilde{g}\right)-\tilde{c}\dot{v}|\dot{v}|.\end{aligned} \tag{2.3}$$

where $v'=\partial v/\partial s$ and $\dot{v}=\partial v/\partial t$. The boundary conditions become

$$\begin{aligned} v=v'=0 \text{ at } s=0 \\ v''=v'''=0 \text{ at } s=1\end{aligned} \tag{2.4}$$

With a continuous system, there are an infinite number of vibration modes and associated natural frequencies. The natural frequencies ω_m are determined by the roots of the equation

$$1+\cos(z_m)\cosh(z_m)=0,$$

where $\omega_m=z_m{}^2$. To help in ordering the derivatives of the dependent variable, we perform an additional scaling to make the natural frequency ω_n of interest equal one. To this end, we let $s^*=z_n s$ and $t^*=z_n{}^2 t$. This leads to the following equation of motion:

$$\ddot{v}+\frac{\tilde{\mu}}{z_n^2}\dot{v}+v^{iv}=-z_n{}^2\left(v'(v'v'')'\right)'-\frac{1}{2}z_n{}^2\left(v'\int_{z_n}^{s}\frac{\partial^2}{\partial t^2}\left(\int_0^s v'^2 ds\right)ds\right)'$$
$$-\left(v''(s-z_n)+v'\right)\left(\frac{\tilde{a}_b}{z_n^4}\cos\left(\frac{\tilde{\Omega}}{z_n^2}t\right)+\frac{\tilde{g}}{z_n^4}\right)-\tilde{c}\dot{v}|\dot{v}|. \tag{2.5}$$

In Eq. (2.5), the derivatives $\dot{()}$ and $()'$ are with respect to t^* and s^* and the superscript * is dropped. The boundary conditions (2.4) become

$$\begin{aligned} v = v' = 0 \quad &\text{at } s=0, \\ v'' = v''' = 0 \quad &\text{at } s=z_n. \end{aligned} \tag{2.6}$$

2.2 Test Setup and Measurements

The experimental setup for the beam experiments with periodic excitation is shown schematically in Fig. 2.2. The beam was clamped to a 250 lbf modal shaker in a cantilever configuration with the long axis of its undeformed shape in a vertical position. The shaker head motion was in the vertical direction along the long axis of the beam. There was a slight bend in the beam with about 0.25 inch tip deflection in the static configuration. The motion along the axis of the beam produced a parametric excitation of the beam. In addition, the bend caused the base motion to produce a small external excitation.

The experimental setup for the beam experiments with random excitation is shown schematically in Fig. 2.3. The beam was clamped to a 100 lbf shaker in a cantilever configuration with the long axis of its undeformed shape in a vertical position. The shaker head motion was in the horizontal direction transverse to the long axis of the beam.

The test specimen was a carbon steel beam with dimensions 33.56" x 0.75" x 0.032 ". In Table 2.2, we summarize the physical properties of the beam. The resulting length to thickness ratio was 1049 and the width to thickness ratio was 23.44. Strain gages were used to obtain a measure of the beam response. In Table 2.3, we present the first five measured and calculated natural frequencies along with the measured log decrements. Because the third mode was a main component of several of the responses, the frequency ratios relative to the third modes natural frequency are also given in Table 2.3.

Because the base motion was along the long axis of the beam and hence produced a parametric excitation, common frequency-domain methods of experimental modal analysis cannot be used to measure natural frequencies and damping values (Ewins, 1984). To measure the frequencies, we excited the beam at approximately twice the natural frequency of interest, thereby excited the associated mode in a principal parametric resonance. We then stopped the excitation and monitored the locations of peaks in the response spectrum that was continually updated. As the amplitudes of the peaks shrank into the noise floor, we noted the frequencies. We used an additional method to measure the natural frequency of the first mode (Zavodney 1987). We plotted on the oscilloscope the output of the signal generator versus a strain-gage signal after the excitation was turned off to produce a Lissajous pattern. The frequency from the signal generator was adjusted until the figure eight was stationary. We interpreted the frequency setting of the signal generator to be twice the first natural frequency. The results of this method agree with those obtained by using the frequency-spectrum method. A similar procedure was used to measure the damping. The beam was excited at twice the natural frequency of the mode of interest. The excitation was turned off and a time history was

recorded as the motion died out. A log decrement was measured over the last fifty cycles that the signal was large enough to be reliable.

Table 2.2 Physical Parameters of the Beam.

Parameter	Value	Definition
L	33.56 in	beam length
b	3/4 in	beam width
h	1/32 in	beam thickness
I	1.9073×10^{-6} in^4	area moment of inertia
E	30.0×10^{6} psi	Young's modulus
m	$1.745\times10^{-5}\ \frac{\text{lb}\cdot\text{s}^2}{\text{in}^2}$	mass per unit length

Table 2.3 Beam Frequency Data.

Calculated Natural Frequencies (Hz)	Measured Natural Frequencies (Hz)	Log Decrement	Measured Frequency Ratio f_i/f_3
0.641*	0.647	0.050	0.00383
5.623	5.648	0.014	0.349
16.136	16.188	0.0061	1.00
32.061	31.906	0.012	1.971
52.993	52.872	0.007	3.266

*Corrected for the effect of gravity.

The modal shaker is capable of 250 lbf peak harmonic force, and has a rated dynamic stroke of 4.0 inches. The shaker is driven by a 2,500 watt power amplifier.

Because the shaker armature has no suspension stiffness of its own, we used a custom suspension system to keep the shaker motion centered in the middle of the stroke (Zavodney, 1987). We attached a sixty pound mass to the shaker armature to reduce the amount of feedback to the shaker from the experiment. We attached the shaker system to an isolation pad. The pad consists of a 4' x 8' x 0.75" plate of steel that is anchored to a concrete block that weighs approximately 33,000 lbs. The isolation pad is attached to ground and is isolated from the building.

The base motion of the beam was monitored with an accelerometer. A measure of the response of the beam was obtained from two strain gages: one located at $s / L = 0.06$ and the other located at $s / L = 0.25$. These gages will be referred to as "Base Strain Gage" and Mid-Span Gage", respectively, in the figures.

We processed the accelerometer and strain-gage signals with an oscilloscope and signal analyzer. At certain settings of the control parameters, long time histories were recorded for post-processing with a PC computer configured with an analog-to-digital board.

The excitation and response spectra were monitored through stationary sweeps of a single control parameter: either the excitation frequency or the excitation amplitude. A stationary sweep is one in which the control parameter is changed a small increment and a steady response is realized before the data is recorded and the next step in the control parameter is made. For our experiments, a stationary response is one whose Poincaré section ceased to evolve and peaks in the frequency spectra had nearly constant magnitudes.

To obtain the contribution of each mode to the response, we measured the magnitudes of the main peaks near each modes' natural frequency in the spectrum. A drawback to this method is that if a mode has a component at a frequency away from its

natural frequency it will not be attributed to that mode. Two cases are of particular interest. First, if the response of a mode is periodic, only the basic frequency will be attributed to the mode of interest. In addition, if one of the harmonics falls close to the natural frequency of a higher-frequency mode, it will be erroneously attributed the response of the higher-frequency mode. Second, if a mode has a static response it will not be attributed to the response of the mode. We use the described method to obtain the contribution of each mode to the response because of the difficulty of measuring spatial data on such light structures. The spatial data is required to separate the contribution of each mode if they have response components at a common frequency. We note that even with the mentioned drawbacks good results can be obtained if care is taken in interpreting the results.

During the stationary sweeps the spectrum was used to characterize the motion. Also, the two strain-gage signals were plotted against each other on the oscilloscope , thereby producing a pseudo-phase plane. To construct a Poincaré section, we used the excitation frequency as the sampling frequency for the oscilloscope. This resulted in a 512 point Poincaré section. These tools are discussed further in the next section.

Experiments on the models were conducted with sinusoidal signals generated by a two-channel, variable-phase wave synthesizer. It has a 0.0001 Hz resolution. The harmonic distortion of the signal generator is less than -90 db.

2.3 Tools for Characterizing Motions

The following is a list of analytical tools used to characterize the responses measured in experiments and predicted by the analysis:

Frequency spectra

Pseudo-phase planes

Poincaré sections

Dimensions.

This discussion of the tools contains my impressions and comments, which may be useful to somebody wanting to perform similar experiments. References are given for detailed discussions, definitions, and theorems.

2.3.1 Frequency Spectra

A frequency spectrum helps in distinguishing periodic, quasiperiodic, and chaotic motions from each other. It is determined as a fast Fourier transform (FFT) of a time series. A thorough treatment of FFT's is given by Brigham (1974). The spectrum of a periodic motion has discrete spectral lines at a basic frequency and its multiples. The spectrum of an n-period quasiperiodic motion is composed of n basic frequencies and different integer combinations of these n frequencies, while the spectrum of a chaotic motion has a broadband character. We can not draw strong conclusions about the nature of the signal from the frequency spectrum alone because of the finiteness of the resolution. When taking an FFT the signal is assumed to be periodic with period T, where T is the record length. Therefore even a signal whose frequency spectrum has broadband character may be periodic with a basic period of T. Even with this limitation we found the frequency spectrum to be the most useful way to characterize the motion "real time" during experiments.

The manner in which we conducted the experiments made the frequency spectra very useful. During the stationary sweeps, we observed the frequency spectra on the signal analyzer. The analyzer can be set to continuously sample data and calculate and display the frequency spectra. Typically the frequency spectrum of the initial response of an experiment would consist of a single peak at the excitation frequency. In many of the

experiments, as the frequency was varied, additional peaks would come into the response spectrum. This indicated that a bifurcation had occurred and a different type of motion was present. At this point, psuedo-phase planes were observed, Poincaré sections were investigated, and long time histories could be taken for post experimental calculation of dimension and high-resolution frequency spectra. In this manner, the evolution of the frequency spectra throughout an experiment was found to be a very useful tool.

Whenever a frequency analysis is performed on experimental data, a weighting function or "window" must be used to prevent leakage. A very readable discussion of windows is given by Gade and Henrik (1988). A more complete treatment is given by Harris (1978). Leakage is due to the finite-time interval of the sampled data. Only components in the signal whose frequency are an integer multiple of the basic frequency 1/T will project into a single line of resolution; all others will exhibit nonzero projections over the entire frequency span. Windows are weighting functions applied to data to reduce the spectral leakage associated with a finite record length.

In the process of reducing the effect of leakage, windowing distorts the signal. Hence, there are several things to keep in mind when interpreting experimentally obtained frequency spectra. One is the ripple caused by the window. The ripple can be understood with the following experiment. The frequency of a signal consisting of a single constant amplitude sine wave is incrementally swept. If the peak amplitude is measured at each frequency setting, then due to the finiteness of the resolution the measured peak amplitude will vary depending on what the frequency of the signal is compared to the center lines in the spectrum. This can show up as false variations in the response of a mode in an experiment. A commonly used filter that has the least amount of ripple (0.01 dB) is the "Flat Top" window. Another concern with the use of windows is their bandwidths. The bandwidth is the number of lines in the spectrum that the energy

of a signal is smeared across. This limits the analyzer's ability to resolve two closely spaced frequencies, particularly if one has a magnitude much smaller than the other. In Fig. 2.4 we show two frequency spectra of a signal that consists of $y(t) = \sin(f_1 2\pi t) + \frac{1}{2}\sin(f_2 2\pi t)$, where both f_1 and f_2 are integer multiples of the basic frequency 1/T and $f_2 - f_1 = \frac{2}{T}$. No window (or rectangular window) is used for Fig. 2.4a and we see that two separate peaks are present in the spectrum. A Kaiser-Bessel window is used for Fig. 2.4b and we see that the two peaks are smeared together and can not be distinguished. The Flat Top window has a 3 dB bandwidth of $\frac{3.72}{T}$. Therefore, with the use of a Flat Top window, if the spectrum resolution (1/T) is 0.1 Hz the closest that two frequencies can be resolved is about 0.3 Hz. If separating closely spaced frequencies is important, the Kaiser-Bessel window is a good choice with a 3 dB bandwidth of $\frac{1.71}{T}$. A third item that should be kept in mind is the sidelobes caused by the windows. These can show up as small peaks about the main peak in the response spectrum. Typically the sidelobes are not a problem unless the experimenter is trying to locate a bifurcation very accurately and is looking for when sidebands are first observed as an indicator. In this case the sidelobes could be misinterpreted as sidebands.

2.3.2 Psuedo-Phase Plane

We constructed a psuedo-phase plane by plotting one stain-gage signal versus the other on an oscilloscope (Zavodney, 1987). A psuedo-phase plane shows the same qualitative characteristics as a phase plane.

The space whose coordinates are the state variables is also known as the state space. In the study of structures, a convenient set of coordinates is the modal coordinates. The state space would consist of the modal coordinates and their time derivatives. The strain measured with a strain gage on a structure will consist of components of all the

modes present unless the stain gage is located at a strain node of a mode. With more than one strain gage located at different locations on the structure, each one will measure all the modes present with a varying contribution from each. If enough strain gages are attached to distinguish all the modes present, these measured values could be transformed into modal coordinates, thereby producing the displacement part of the phase space. Two of the modal coordinates plotted against each other would produce a two dimensional projection of the phase portrait. If two modes are present, two strain-gage signals plotted against each other can be thought of as transformed modal coordinates plotted against each other, thus giving the same qualitative information as two modal coordinates plotted against each other. Even if more than two modes are present, the plot of the two strain-gage signals versus each other gives qualitative information about the response. Therefore we call this plot a psuedo-phase plane.

If too many modes are present, the psuedo-phase plane becomes very complicated and difficult to interpret. Also, even with a low-order system, if the motion becomes complicated the psuedo-phase plane may be difficult to interpret.

2.3.3 Poincaré Sections

Often psuedo-phase planes become very complicated or "messy". Poincaré sections contain the same information as the psuedo-phase planes but from a reduced set of data. For instance, a periodic signal with a frequency equal to the clock frequency produces a closed loop in a psuedo-phase plane but produces a single point in a Poincaré section.

For our experiments, we constructed Poincaré sections from the psuedo-phase planes by sampling the signals at the excitation frequency. This has the effect of taking the known fast time scale associated with the excitation frequency out of the data and

displaying only the slowly varying components that characterize the motion. We interpret Poincaré sections as follows: a single point or a collection of a finite number of points in the Poincaré section corresponds to a periodic attractor, a collection of points that fall on a closed curve corresponds to a two-period qausiperiodic attractor, and a collection of points in the Poincaré section that do not lie on any simple geometrical form possibly corresponds to a strange attractor (Seydel, 1988). Here, we refer to the motion that the beam evolves to after a long time as an attractor.

2.3.4 Pointwise Dimension

The dimension is one of the geometrical properties that characterizes an attractor. It is a measure of the minimum number of essential variables necessary to model the dynamics of a system. A fixed point attractor has a dimension of zero, a periodic attractor has a dimension of one, and an n-period quasiperiodic attractor has a dimension of n. A chaotic attractor has a noninterger or fractal dimension.

For the calculation of the dimension d_p, we plot the logarithm of the number of points N(r) in an n-dimensional ball of radius r on the ordinate and the logarithm of the radius of the ball on the abscissa. Curves for different embedding dimension n are plotted. The value of the dimension d_p is estimated from the slope in the "scaling" region of the curves. An example of this type of plot is shown in Fig. 2.5. The slopes found in the scaling region are then plotted versus the embedding dimension to determine if the dimension converges to a constant value, as shown in Fig. 2.6.

In the method used in this work, we obtained a scalar time signal Y(t) from the system. We constructed an n-dimensional space from the scalar time signal Y(t) by forming the additional coordinates $Y(t+\tau)$, $Y(t+2\tau)$, ... , $Y(t+(n-1)\tau)$. Here, n is the embedding dimension mentioned earlier. The value for n where the slope of the scaling

region ceases to change is chosen as the minimum embedding dimension. In choosing τ, several considerations have to be taken into account. If τ is too small, the trajectories in the state space of Y(t) and Y(t+τ) are highly correlated. On the other hand, if τ is too large the delayed coordinates become uncorrelated. For this work, we use the first zero crossing of the autocorrelation function as a starting point in choosing τ. Various values of τ are used near this value until one is found for which the slopes converge to a constant value.

The dimension characterizes the motion and provides a lower bound on the number of essential variables needed to model the dynamics. Therefore, a small finite value for the dimension of the response of a continuous system, such as the cantilever beam, gives hope to capturing the essential dynamics of such a system with a low-order model. Also, if the dimension calculated numerically from a model of a system and the dimension calculated from experimental data match, it indicates that the model and the actual system have some common characteristics. Further discussion of dimension can be found in Farmer et al. (1983).

The dimension of an attractor does not provide as much information as one might hope. Here we discuss some shortcomings.

The dimension of an attractor is a measure of the minimum number of essential variables necessary to model the dynamics of a system. For a structure, these essential variables are not necessarily the modal coordinates. The dimension is not a measure of the number of modes that are participating in the response. For instance, in the study by Balachandran et al. (1990), in some cases the response consisted of two modes with a periodic response. In this case, the dimension is 1.0, although the number of participating modes is two. As this example points out, the essential variables that the dimension measures are not modal coordinates but some generally unknown functions.

A noninteger dimension from experimental data does not necessarily mean the motion is chaotic. Noise can influence the calculations. Cusumano (1990) calculated a dimension of 1.11 from experimental data and still concluded that the motion was periodic and that the noninterger value was due to noise. Dimension values farther from an integer may be considered fractal.

More than one scaling region can exist in the plot for the dimension as can be seen in Fig. 2.5. In Figs. 2.6a and 2.6b, we show variation of the dimension with the embedding dimension. We see that, for this case, the dimension value converges in both scaling regions. However, the dimension of 2.25 associated with the smaller radius is chosen. In this case, the lowest region that converges to approximately a constant value is used. If one of the scaling regions fails to converge, we assume that it represents length scales dominated by noise. If one of the essential variables is of this scale it is not measured and the calculated dimension is less than the true dimension of the motion. Associated with this limitation is the observation that the noise floor often increases as bifurcations are approached (Jeffries and Wiesenfeld, 1985; Wiesenfeld, 1985). This makes it difficult to determine accurate dimension values near bifurcations.

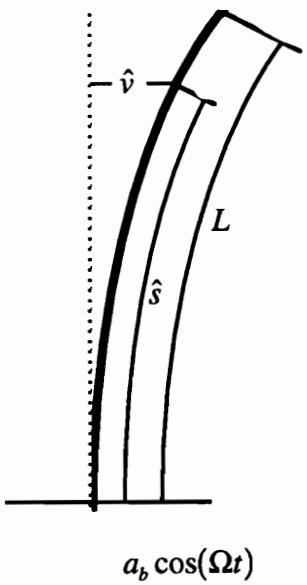

Fig. 2.1 A cantilever beam subjected to a base excitation.

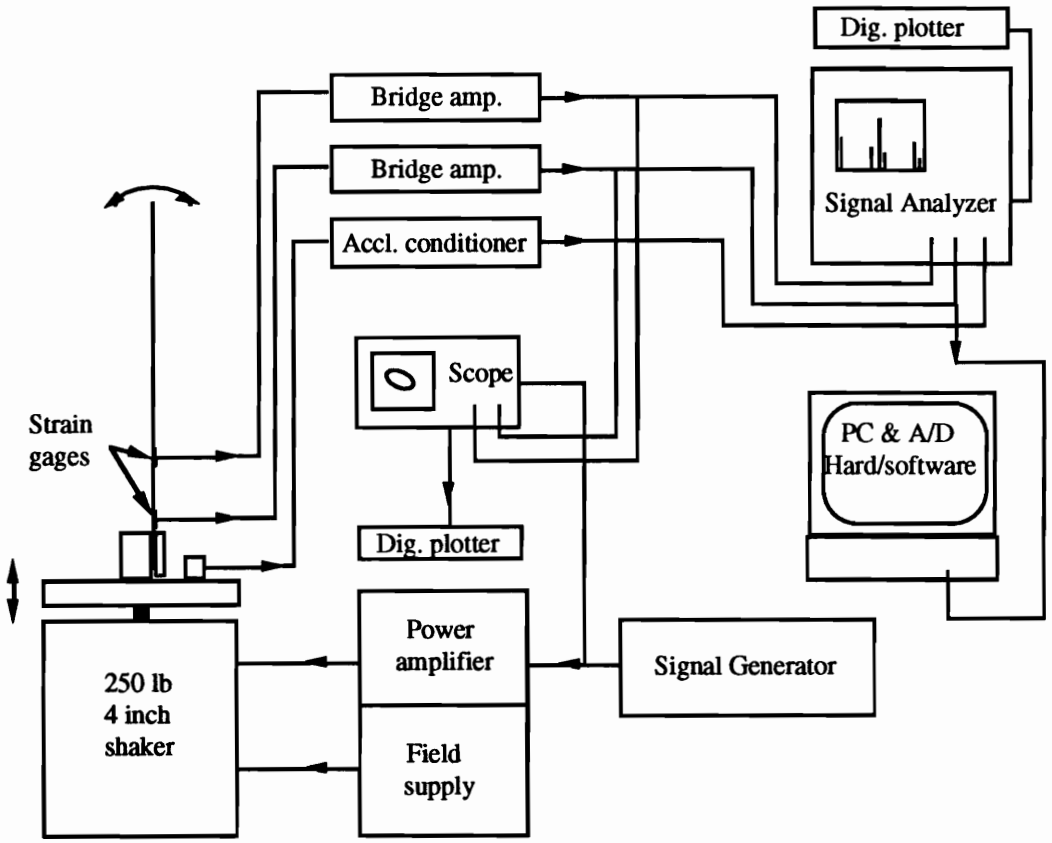

Fig. 2.2 A schematic of the experimental setup for periodic excitation.

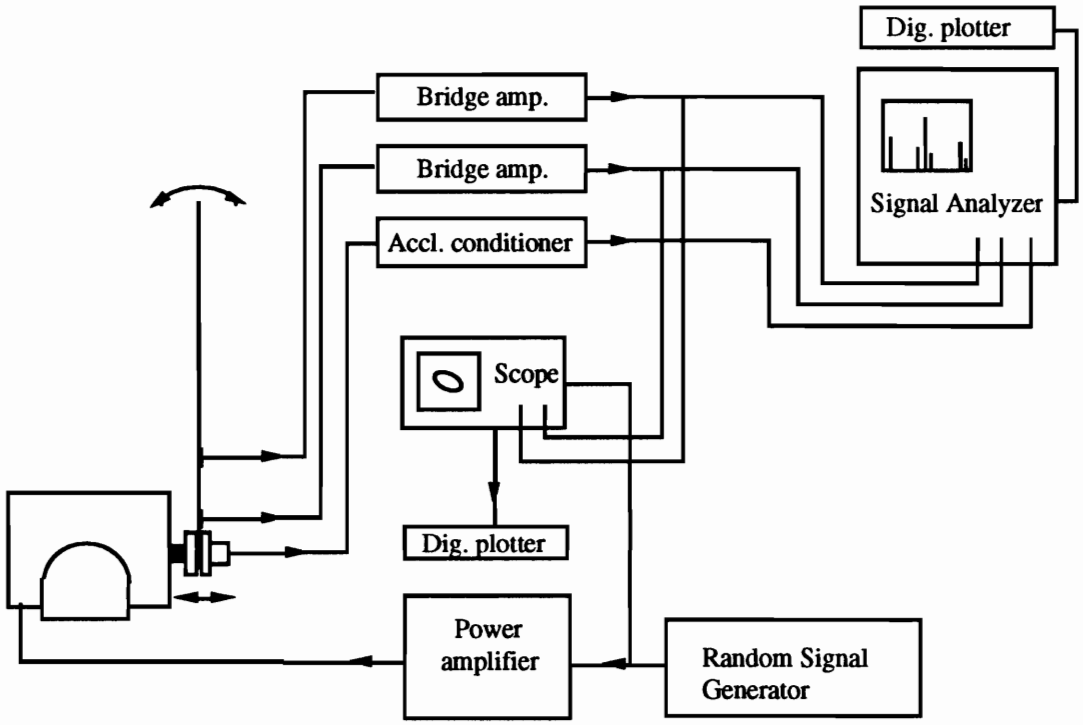

Fig. 2.3 A schematic of the experimental setup for random excitation.

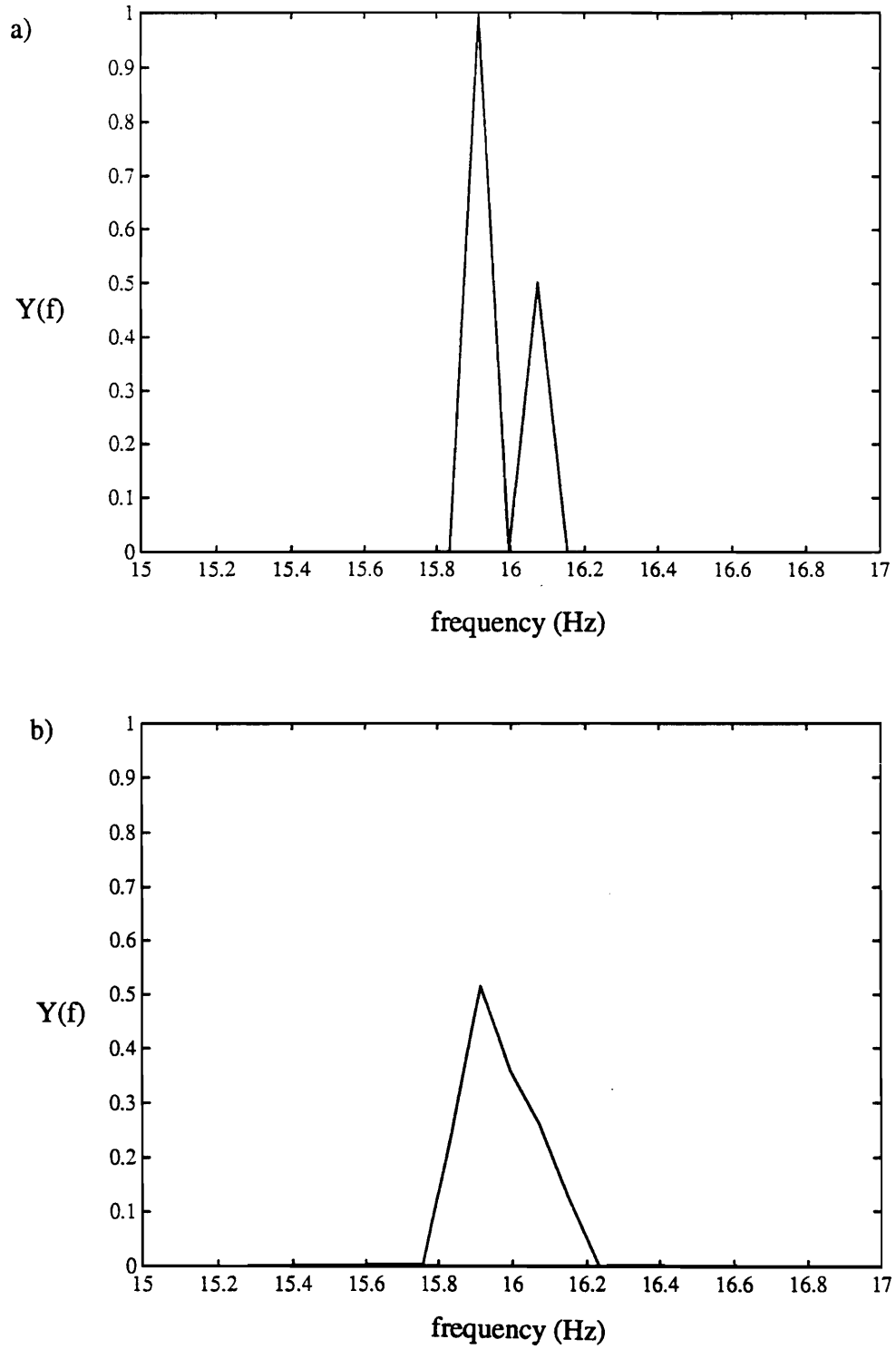

Fig. 2.4 Frequency spectra of a periodic signal composed of two sine waves with the record length being an integer multiple of the periods: a) no window, b) Kaiser-Bessel window.

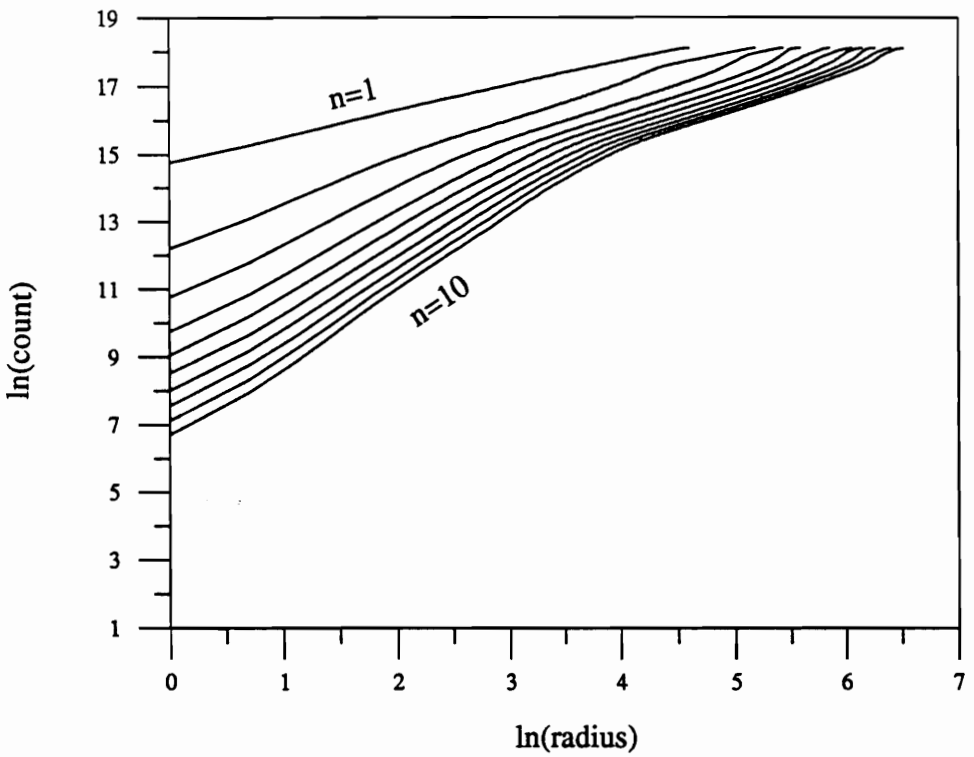

Fig. 2.5 Plot for dimension calculation.

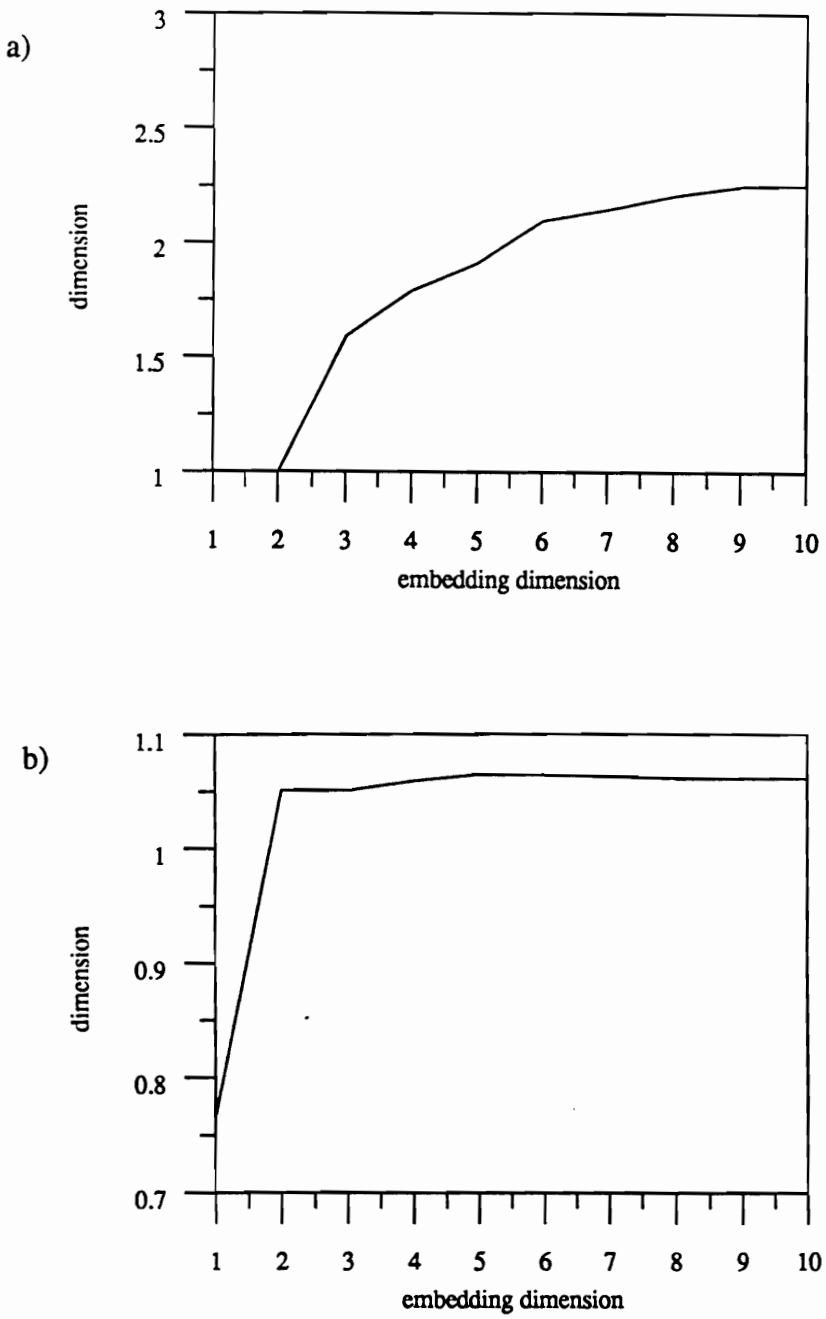

Fig 2.6 Plots of dimension versus embedding dimension for two scaling regions: a) 1<log(radius)<3, b) 4.5<log(radius)<6.

3. Experimental Verification of the Importance of Nonlinear Curvature in the Response of a Cantilever Beam

In this Chapter, we present the results of an experimental and theoretical investigation into the single-mode responses of a parametrically excited metallic cantilever beam. During excitation of the first mode, we found a hardening-type frequency-response curve. This experimentally verifies that, for the first mode, the often ignored nonlinear curvature terms are stronger than the nonlinear inertia terms. Adding quadratic damping in the analysis improves the agreement between the experimental and theoretical results for both the frequency-response and force-response curves of the first mode.

During excitation of the second mode, we found softening-type frequency-response curves, in agreement with the analysis. The addition of quadratic damping to the model improves the agreement between the experimental and theoretical results some what but not nearly as much as for the first mode. This indicates that it may be necessary to consider different nonlinear damping terms for different modes.

3.1 Multiple-Scales Analysis

In this chapter, we use the equations presented in Chapter 2 and restrict our investigation to a single-mode response. Equations (2.5) and (2.6) are repeated here for convenience:

$$\ddot{v}+\frac{\tilde{\mu}}{z_n^2}\dot{v}+v^{iv}=-z_n{}^2\left(v'\left(v'v''\right)'\right)'-\frac{1}{2}z_n{}^2\left(v'\int_{z_n}^{s}\frac{\partial^2}{\partial t^2}\left(\int_0^s v'^2 ds\right)ds\right)'$$
$$-\left(v''(s-z_n)+v'\right)\left(\frac{\tilde{a}_b}{z_n^4}\cos\left(\frac{\tilde{\Omega}}{z_n^2}t\right)+\frac{\tilde{g}}{z_n^4}\right)-\tilde{c}\dot{v}|\dot{v}|. \tag{3.1}$$

$$v = v' = 0 \quad \text{at } s=0,$$
$$v'' = v''' = 0 \quad \text{at } s=z_n. \tag{3.2}$$

To analyze the solutions of the nonlinear equation (3.1) subject to the boundary conditions (3.2), we employ the method of multiple scales (Nayfeh, 1981). Toward this end, we introduce a small parameter ε as a bookkeeping device. Then, we seek a uniform expansion of the form

$$v(s,T_0,T_2;\varepsilon) = \varepsilon v_1(s,T_0,T_2,\ldots) + \varepsilon^3 v_3(s,T_0,T_2,\ldots) + \ldots, \tag{3.3}$$

where $T_0 = t$ is a fast scale characterizing motions at the frequencies ω_n and Ω; and $T_2 = \varepsilon^2 t$ is a slow scale characterizing the time variations of the amplitude and phase. In addition, we replace $\tilde{\mu}/z_n^2$, $\tilde{a}_b/z_n^4$, $\tilde{g}/z_n^4$, $\tilde{c}$, and $\tilde{\Omega}/z_n^2$ with $\varepsilon^2\mu$, $\varepsilon^2 a_b$, $\varepsilon^2 g$, εc, and Ω, respectively. Substituting these expressions and Eq. (3.3) into Eqs. (3.1) and (3.2) and equating coefficients of like powers of ε, we obtain

Order ε:

$$D_0^2 v_1 + v_1^{iv} = 0 \tag{3.4}$$

$$v_1 = v_1' = 0 \quad \text{at } s = 0,$$
$$v_1'' = v_1''' = 0 \quad \text{at } s = z_n \tag{3.5}$$

Order ε^3:

$$D_0^2 v_3 + v_3^{iv} = -2D_0D_2 v_1 - \mu D_0 v_1 - z_n^2\left(v_1'(v_1'v_1'')'\right)' - \frac{1}{2}z_n^2\left(v_1'\int_{z_n}^{s} D_0^2\left(\int_0^s v_1'^2 ds\right)ds\right)'$$
$$-\left(z_n v_1''(s-z_n) + z_n v_1'\right)\left(a_b\cos(\Omega T_0) + g\right) - c D_0 v_1 |D_0 v_1| \tag{3.6}$$

$$v_3 = v_3' = 0 \quad \text{at s} = 0,$$
$$v_3'' = v_3''' = 0 \quad \text{at s} = z_n \tag{3.7}$$

where $D_n = \partial/\partial T_n$.

The general solution of Eqs. (3.4) and (3.5) can be expressed as

$$v_1(s, T_0, T_2) = \sum_{m=1}^{\infty} \Phi_m(s) A_m(T_2) e^{i\omega_m T_0} + cc \tag{3.8}$$

where cc stands for the complex conjugate of the preceding terms,

$$\omega_m = \frac{z_m^{\,2}}{z_n^{\,2}}$$

and

$$\Phi_m(s) = \cosh(\frac{z_m s}{z_n}) - \cos(\frac{z_m s}{z_n}) + \frac{\cos(z_n) + \cosh(z_n)}{\sin(z_n) + \sinh(z_n)} \left(\sin(\frac{z_m s}{z_n}) - \sinh(\frac{z_m s}{z_n}) \right).$$

We note that

$$\int_0^{z_n} \Phi_n^{\,2} ds = z_n . \tag{3.9}$$

The A_m are unknown functions of T_2 at this order of approximation and will be found by imposing the solvability condition at the next order of approximation.

The general solution, Eq. (3.8), of Eqs. (3.4) and (3.5) consists of an infinite number of modes corresponding to an infinite number of frequencies. However, any mode that is not directly or indirectly excited will decay to zero with time due to the presence of damping. In this paper, we restrict our attention to the case where only one mode is directly excited and assume that this mode is not excited by an internal resonance, that is, we consider a single-mode approximation. Thus, the nondecaying first-order solution can be expressed as

$$v_1(s, T_0, T_2) = \Phi_n(s) \left(A_n(T_2) e^{iT_0} + \overline{A}_n(T_2) e^{-iT_0} \right) \tag{3.10}$$

where the overbar denotes the complex conjugate and the index n corresponds to the mode being excited.

Substituting Eq. (3.10) into Eq. (3.6) yields

$$
\begin{aligned}
D_0^2 v_3 + v_3^{iv} = & -2i\Phi_n D_2 A_n e^{iT_0} - i\mu\Phi_n A_n e^{iT_0} - z_n\left(\Phi_n''(s-z_n)+\Phi_n'\right)gA_n e^{iT_0} \\
& -z_n^2\left(\Phi_n'\left(\Phi_n'\Phi_n''\right)'\right)'\left(A_n^3 e^{3iT_0} + 3A_n^2\overline{A}_n e^{iT_0}\right) \\
& -\frac{1}{2}z_n^2\left(\Phi_n'\int_{z_n}^{s}\int_0^s \Phi_n'^2 dsds\right)'\left(-4A_n^3 e^{3iT_0} - 4A_n^2\overline{A}_n e^{iT_0}\right) \\
& -z_n\left(\Phi_n''(s-z_n)+\Phi_n'\right)a_b\left(A_n e^{i(\Omega+1)T_0} + \overline{A}_n e^{i(\Omega-1)T_0}\right) + cc \\
& -c\left(\Phi_n\left(iA_n e^{iT_0} - i\overline{A}_n e^{-iT_0}\right)\right)\left|\Phi_n\left(iA_n e^{iT_0} - i\overline{A}_n e^{-iT_0}\right)\right|.
\end{aligned}
\tag{3.11}
$$

Here, we restrict our discussion to the case of principal parametric resonance of the nth mode (i.e., $\Omega \approx 2$). To express the nearness of this resonance, we introduce the detuning parameter σ defined by $\Omega = 2 + \varepsilon^2\sigma$. Because the homogeneous part of Eqs. (3.11) and (3.7) has a nontrivial solution, the inhomogeneous Eqs. (3.11) and (3.7) have a solution only if a solvability condition is satisfied (Nayfeh, 1981). To determine this solvability condition, we seek a particular solution free of secular terms in the form

$$v_3 = V_3(s, T_2)e^{iT_0} + cc. \tag{3.12}$$

Substituting Eq. (3.12) into Eqs. (3.11) and (3.7), multiplying the result by e^{-iT_0}, and integrating over the interval $T_0 = 2\pi$,we obtain

$$
\begin{aligned}
-V_3 + V_3^{iv} = & -2i\Phi_n D_2 A_n - \mu i\Phi_n A_n - z_n\left(\Phi_n''(s-z_n)+\Phi_n'\right)gA_n \\
& -z_n\left(\Phi_n''(s-z_n)+\Phi_n'\right)a_b\overline{A}_n e^{i\sigma T_2} - 3z_n^2\left(\Phi_n'\left(\Phi_n'\Phi_n''\right)'\right)'A_n^2\overline{A}_n \\
& +2z_n^2\left(\Phi_n'\int_{z_n}^{s}\int_0^s \Phi_n'^2 dsds\right)'A_n^2\overline{A}_n - \Gamma_n c\Phi_n|\Phi_n|
\end{aligned}
\tag{3.13}
$$

$$
\begin{aligned}
V_3(0,T_2) &= V_3'(0,T_2) = 0 \\
V_3''(0,T_2) &= V_3'''(0,T_2) = 0
\end{aligned}
\tag{3.14}
$$

where

$$\Gamma_n = \frac{1}{2\pi}\int_0^{2\pi} i\left(A_n e^{i\tau} - \bar{A}_n e^{-i\tau}\right)\left|A_n e^{i\tau} - \bar{A}_n e^{-i\tau}\right| e^{-i\tau} d\tau. \tag{3.15}$$

To determine the solvability condition, we multiply Eq. (3.13) by the adjoint Ψ, integrate over the interval 0 to z_n, and obtain

$$\int_0^{z_n} \Psi\left(-\omega_n{}^2 V_3 + V_3{}^{iv}\right) ds = \int_0^{z_n} \Psi \mathrm{H}\, ds, \tag{3.16}$$

where H is the right-hand side of Eq. (3.13). Here H is a function of A_n, V_3, and Φ_n. Next, we integrate the left-hand side of Eq. (3.16) by parts to transfer the derivatives from V_3 to Ψ and obtain

$$\left[\Psi V_3''' - \Psi' V_3'' + \Psi'' V_3' - \Psi''' V_3\right]_0^{z_n} + \int_0^{z_n} V_3\left(\Psi^{iv} - \Psi\right) ds = \int_0^{z_n} \Psi \mathrm{H}\, ds. \tag{3.17}$$

The equation governing the adjoint Ψ is obtained by setting the coefficient of V_3 in the integrand in Eq. (3.17) equal to zero. The result is

$$\Psi^{iv} - \Psi = 0. \tag{3.18}$$

Using Eq. (3.18) and the boundary conditions given in Eq. (3.14), we have

$$\left[\Psi'' V_3' - \Psi''' V_3\right]^{z_n} - \left[\Psi V_3''' - \Psi' V_3''\right]^0 = \int_0^{z_n} \Psi \mathrm{H}\, ds. \tag{3.19}$$

To determine the boundary conditions needed to define Ψ, we consider the homogeneous problem in which H = 0. Then Eq. (3.19) becomes

$$\left[\Psi'' V_3' - \Psi''' V_3\right]^{z_n} - \left[\Psi V_3''' - \Psi' V_3''\right]^0 = 0. \tag{3.20}$$

We choose the adjoint boundary conditions such that the coefficients of $V_3(z_n)$, $V_3'(z_n)$, $V_3''(0)$, $V_3'''(0)$ in Eq. (3.20) vanish independently. This results in the following boundary conditions:

$$\begin{aligned} &\Psi = \Psi' = 0 \text{ at } s = 0 \\ &\Psi'' = \Psi''' = 0 \text{ at } s = z_n \end{aligned} \tag{3.21}$$

We note that Eqs. (3.18) and (3.21) are the same as the spatial part of Eqs. (3.4) and (3.5). Hence, the system is said to be self-adjoint. So the solution to the adjoint system, Eqs. (3.18) and (3.21), is $\Psi = \Phi_n$.

Having defined the adjoint, we let $\Psi = \Phi_n$ in Eq. (3.19) and obtain the solvability condition

$$\int_0^{z_n} \Phi_n \, \mathrm{H} \, ds = 0. \tag{3.22}$$

Using the definition of H, we find that the solvability condition yields

$$-2i\mathrm{D}_2 A_n - i\mu_n A_n - (3\alpha_1 - 4\alpha_2) A_n^2 \overline{A}_n - \frac{1}{2}\alpha_3 a_b \overline{A}_n e^{i\sigma T_2} + \alpha_3 A_n g - \alpha_4 \Gamma_n = 0 \tag{3.23}$$

where

$$\begin{aligned}
&\mu_n = \frac{1}{z_n}\int_0^{z_n} \mu \Phi_n{}^2 ds, \quad \alpha_1 = \int_0^{z_n} z_n \Phi_n \left(\Phi_n' \left(\Phi_n' \Phi_n'' \right)' \right)' ds \\
&\alpha_2 = \frac{1}{2}\int_0^{z_n} z_n \Phi_n \left(\Phi_n' \int_{z_n}^{s} \int_0^{s} \Phi_n'^2 ds ds \right)' ds, \quad \alpha_3 = \int_0^{z_n} \Phi_n \left(\Phi_n''(s - z_n) + \Phi_n' \right) ds \\
&\alpha_4 = \int_0^{z_n} c \Phi_n{}^2 |\Phi_n| ds
\end{aligned} \tag{3.24}$$

Numerical values for α_1, α_2, α_3, and α_4 are given in Table 3.1. Substituting the polar form

$$A_n = \tfrac{1}{2} a_n e^{i\beta_n} \tag{3.25}$$

into Eq. (3.23), multiplying the result by $e^{-i\beta_n}$, and separating real and imaginary parts, we obtain

$$\dot{a}_n = -\frac{1}{2}\mu_n a_n - \frac{1}{4} a_b \alpha_3 a_n \sin(\gamma_n) - C_n a_n^2 \tag{3.26}$$

$$a_n \dot{\gamma}_n = \sigma a_n - \left(\frac{3}{4}\alpha_1 - \alpha_2 \right) a_n^3 - \frac{1}{2} a_b \alpha_3 a_n \cos(\gamma_n) + \alpha_3 g a_n \tag{3.27}$$

where

$$\gamma_n = \sigma T_2 - 2\beta_n \tag{3.28}$$

and

$$C_n a_n^2 = -ie^{-i\beta_n}\alpha_4\Gamma_n = \frac{i\alpha_4 a_n^2}{2\pi}\int_0^{2\pi}(\cos\varphi - i\sin\varphi)\sin\varphi|\sin\varphi|d\varphi = \frac{8}{3\pi}\alpha_4 a_n^2 \tag{3.29}$$

Table 3.1 Values of Coefficients in Modulation Equations.

	First Mode	Second Mode
α_1	3.271	27.637
α_2	2.299	72.364
α_3	1.571	8.647
α_4	0.0589	0.1178

Equations (3.26) and (3.27), which describe the amplitude and phase for the nth mode, have the same form as those for a parametrically excited Duffing's equation (Nayfeh and Mook, 1979) with quadratic damping.

The sign of the coefficient of a_n^3 determines whether the nonlinearity is of the hardening or softening type. It follows from Eq. (3.27) that $\frac{3}{4}\alpha_1$ accounts for the nonlinear curvature and α_2 accounts for the nonlinear inertia. If $\frac{3}{4}\alpha_1 > \alpha_2$, the nonlinear curvature dominates and the effective nonlinearity is hardening. If $\frac{3}{4}\alpha_1 < \alpha_2$, the nonlinear inertia dominates and the effective nonlinearity is softening. Using the values of α_1 and α_2 from Table 3.1, we find that $\frac{3}{4}\alpha_1 - \alpha_2$ is negative for the first mode and positive for the second mode. Consequently, the nonlinearity is of the hardening type for the first mode and of the softening type for the second mode.

To determine the stability of the fixed points and hence the periodic solutions of the nth mode, we find it convenient to introduce the Cartesian coordinates p and q defined as

$$p = a_n \cos\left(\frac{1}{2}\gamma_n\right), \quad q = a_n \sin\left(\frac{1}{2}\gamma_n\right). \tag{3.30}$$

This yields the following set of first-order autonomous ordinary-differential equations:

$$\dot{p} = -\frac{1}{2}\mu_n p - \left(\frac{\sigma}{2} + \alpha_3\left(\frac{g}{2} + \frac{a_b}{4}\right)\right)q + \left(\frac{3}{8}\alpha_1 - \frac{1}{2}\alpha_2\right)q\left(p^2 + q^2\right) - C_n p\sqrt{p^2 + q^2} \tag{3.31}$$

$$\dot{q} = -\frac{1}{2}\mu_n q + \left(\frac{\sigma}{2} + \alpha_3\left(\frac{g}{2} - \frac{a_b}{4}\right)\right)p - \left(\frac{3}{8}\alpha_1 - \frac{1}{2}\alpha_2\right)p\left(p^2 + q^2\right) - C_n q\sqrt{p^2 + q^2}\,. \tag{3.32}$$

Equations (3.26) and (3.27) are used to obtain frequency-response and force-response curves and Eqs. (3.31) and (3.32) are used to determine the stability of the fixed points.

3.2 Experiments

We experimentally investigated the response of the slender cantilever beam described in Chapter 2 to a parametric excitation. We considered principal parametric resonances of the first and second modes. The beam was clamped to the 250 lb modal shaker to allow base excitation of the beam. This shaker provides a four-inch stroke, which is required for low-frequency vibration testing. The base motion, which was along the axis of the beam, provided the parametric excitation to the beam.

The base motion was measured with a DCLVDT for the first-mode experiments and with an accelerometer for the second-mode experiments. A measure of the response was obtained from two strain gages: one located at x/L = 0.06 and the other located at x/L = 0.25, where x is the distance along the undeformed beam measured from the base. Because the responses were measured in terms of bending strains in the experiments and predicted in terms of modal amplitudes in the theory, a constant scaling factor was applied to the strains to convert them to amplitudes. This constant was determined by choosing a single experimental data point and dividing the value by the theoretical value

that corresponds to the same control parameter. This value was then used for all the experimental data points of that experiment.

The excitation and response signals were monitored with a signal analyzer and an oscilloscope. For real-time spectral analyses, we used 1280 lines and a Flat Top window. We used a 10 Hz base-band to monitor the response of the first mode and a 20 Hz base-band to monitor the response of the second mode. The spectra were used to obtain the contribution of each mode to the response and characterize the observed motion. The excitation and response spectra were monitored through stationary sweeps of a single control parameter: either the excitation frequency or the excitation amplitude.

3.3 Results

Here, we compare the results of the theoretical and experimental frequency and amplitude sweeps. In Fig. 3.1, we theoretical frequency-response curves for the first mode in the absence of quadratic damping (i.e., C_1=0.000) along with experimental observations. The symbol ⧗ in the figures corresponds to observations obtained during a reverse sweep and the symbol ✱ corresponds to observations obtained during a forward sweep in the control parameter. For all the plotted theoretical results, solid lines indicate stable fixed points and broken lines indicate unstable fixed points. The theoretical frequency-response curve is bent to the right, indicating that the nonlinear curvature terms dominate the nonlinear inertia terms for this mode. Also the two theoretical branches in Fig. 3.1 never close as the excitation frequency is increased. The experimental frequency-response curve is also slightly bent to the right. The experimentally obtained response is obviously bounded and does not show any overhang. There is some qualitative agreement between the experimental and theoretical results with both curves being bent to the right.

In Fig. 3.2, we show and theoretical force-response curves for the first mode in the absence of quadratic damping (i.e., C_1=0.000) along with experimental observations. In the experiments, we measured the base displacements and converted them to accelerations for plotting. The theory predicts an overhang associated with a reverse (subcritical) pitchfork bifurcation of the trivial fixed point of Eqs. (3.31) and (3.32). This bifurcation results in a jump from a trivial state to a nontrivial state as the excitation amplitude is increased past the bifurcation point. However, the experiments do not show a jump. The observed smooth transition from a trivial to a nontrivial response observed in the experiments suggests a supercritical pitchfork or a transcritical bifurcation. The experimental and theoretical results shown in Fig. 3.2 are in qualitative disagreement.

In Figs. 3.3 and 3.4, we show theoretical frequency- and force-response curves for various values of the quadratic-damping coefficient. In the frequency-response plots (Fig. 3.3), the curves close for $C_1 \neq 0.000$ and the amplitudes are limited. In Fig. 3.4, the force-response curves for $C_1 \neq 0.000$ do not have an overhang. Also, the inclusion of quadratic damping appears to have changed the bifurcation of the trivial fixed point from pitchfork to transcritical (Nayfeh and Balachandran, 1993). These results are much like those found experimentally. Comparing these figures with the experimental results in Figs. 3.1 and 3.2 suggests that C_1=0.050 yields the best match of the experimental and theoretical results. Thus, in Figs. 3.5 and 3.6, we show experimental and theoretical frequency- and force-response curves with C_1=0.050 for the analysis. The agreement between the experiment and theory is very good.

In Fig. 3.7, we show theoretical frequency-response curves for the second mode in the absence of quadratic damping (i.e., C_2=0.000) along with experimental observations. The theoretical curve is bent to the left, indicating that the nonlinear inertia terms are stronger than the nonlinear curvature terms for this mode. As in the previous case, the upper and lower theoretical branches never close. The experimental curve is bent to the

left with a definite overhang. The experimental response jumps from a large amplitude solution to a trivial solution at 11.07 Hz, whereas the theory predicts that the response continues to grow as the frequency is reduced. In Fig. 3.8, we show the theoretical force-response curves for the second mode in the absence of quadratic damping (i.e., C_2=0.000) along with experimental observations. They agree very well except that during the reverse sweep in excitation amplitude the observed response jumps down to a trivial response at $a_b = 221.7$ in/sec^2 whereas the predicted response jumps down to a trivial response at $a_b = 130.0$ in/sec^2 .

In Figs. 3.9 and 3.10, we show theoretical frequency- and force-response curves for various values of the quadratic-damping coefficient. As in the previous case, the frequency-response curves close for $C_2 \neq 0.000$. Above a certain value of C_2, the frequency-response curve is stable throughout. In Fig. 3.10, as C_2 is increased, the turning points occur at higher excitation amplitudes. The inclusion of quadratic damping in the model for the second mode does not change the bifurcation of the trivial response from pitchfork to transcritical as much as it did for the first mode.

In Figs. 3.11 and 3.12, we show and theoretical frequency- and force-response curves with C_2=0.100 for the analysis along with corresponding experimental observations respectively. As with the previous case, we tried to choose C_2 to produce the best match of the experimental and theoretical results. For this case, we chose C_2 such that the excitation amplitude at which the large-amplitude response jumps down to the trivial response match in the theoretical and experimental frequency-response curves. However, for this value of C_2 the location of the jump in the force-response curves does not match. The value C_2=0.100 is a compromise between matching the locations of the jumps from the large-amplitude solution to the trivial solution in the frequency- and force-response curves.

3.4 Discussion and Conclusions

We conducted an experimental and theoretical investigation into the single-mode responses of a parametrically excited cantilever beam. During excitation of the first mode, we found a hardening-type frequency-response curve. This experimentally verifies that, for the first mode, the often ignored nonlinear curvature terms are stronger than the nonlinear inertia terms. Adding quadratic damping in the analysis improves the agreement between the experimental and theoretical results for both the frequency- and force-response curves of the first mode.

During excitation of the second mode, we found softening-type frequency-response curves, in agreement with the analysis. The addition of quadratic damping to the model improves the agreement between the experimental and theoretical results some what but not nearly as much as for the first mode. This indicates that it may be necessary to consider different nonlinear damping terms for different modes.

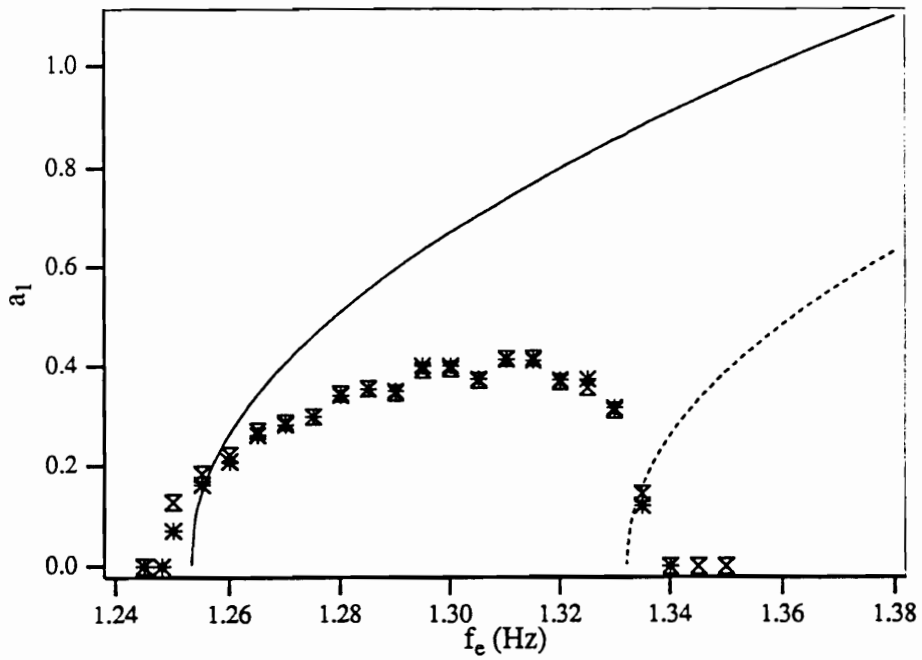

Fig. 3.1 Experimental and theoretical frequency-response curves for the first mode when C_1=0.000 and a_b = 46.53 in/sec^2.

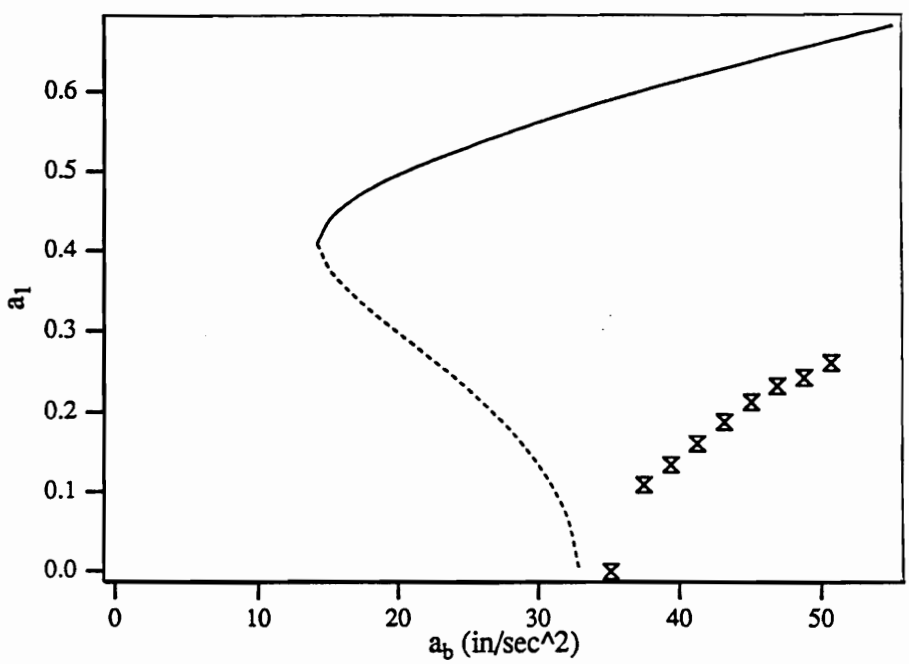

Fig. 3.2 Experimental and theoretical force-response curves for the first mode when C_1=0.000 and f_e=1.253 Hz.

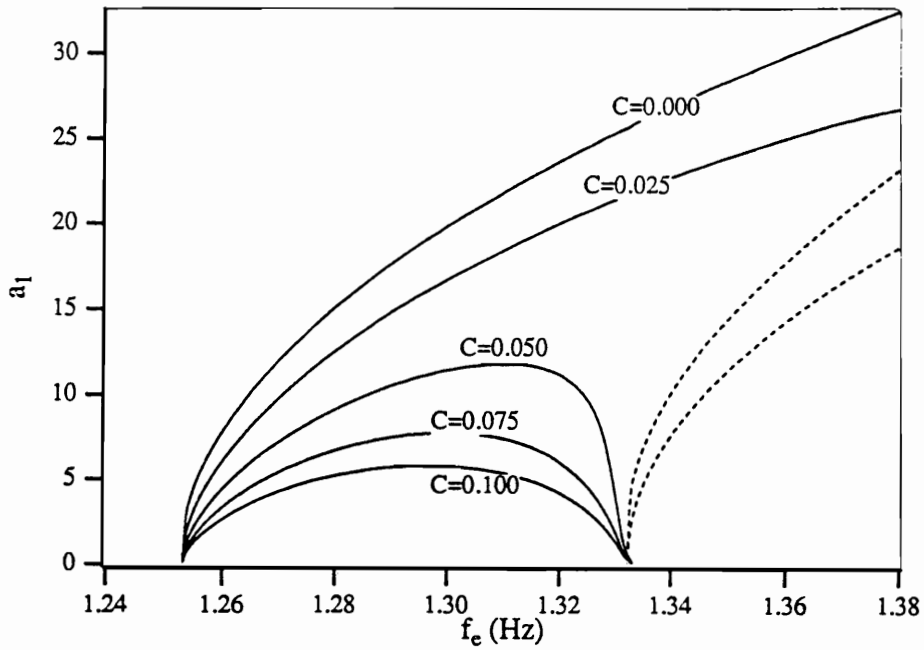

Fig. 3.3 Theoretical frequency-response curves for the first mode for a_b = 46.53 in/sec^2 and various values of C_1.

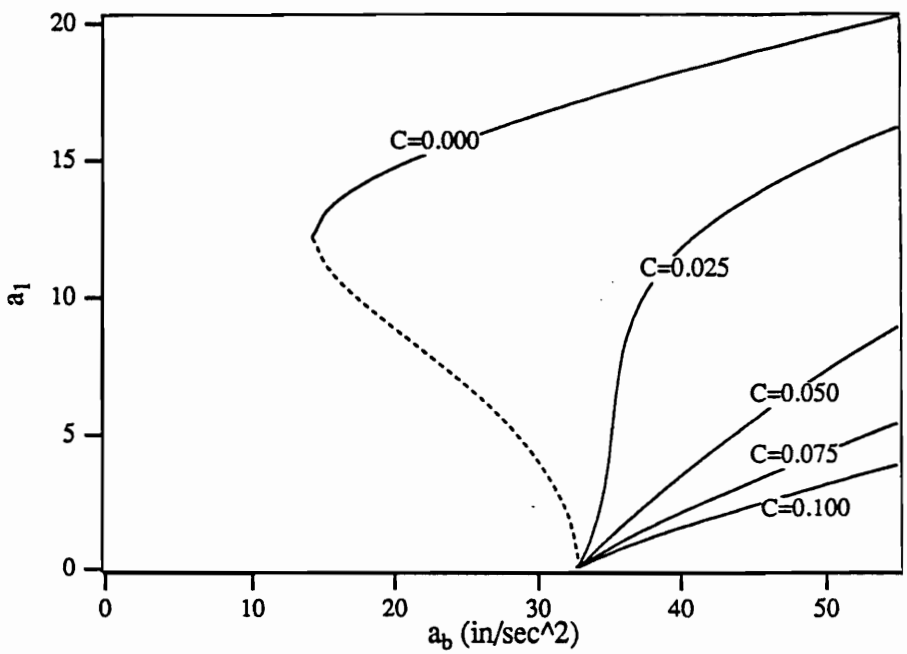

Fig. 3.4 Theoretical force-response curves for the first mode for f_e=1.253 Hz and various values of C_1.

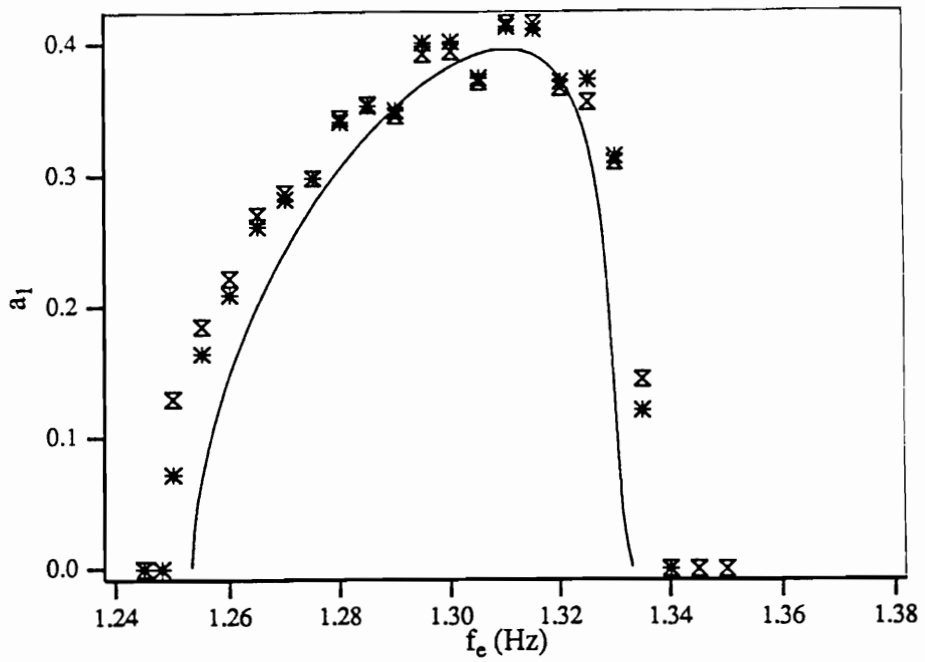

Fig. 3.5 Experimental and theoretical frequency-response curves for the first mode when C_1=0.050 and a_b = 46.53 in/sec^2.

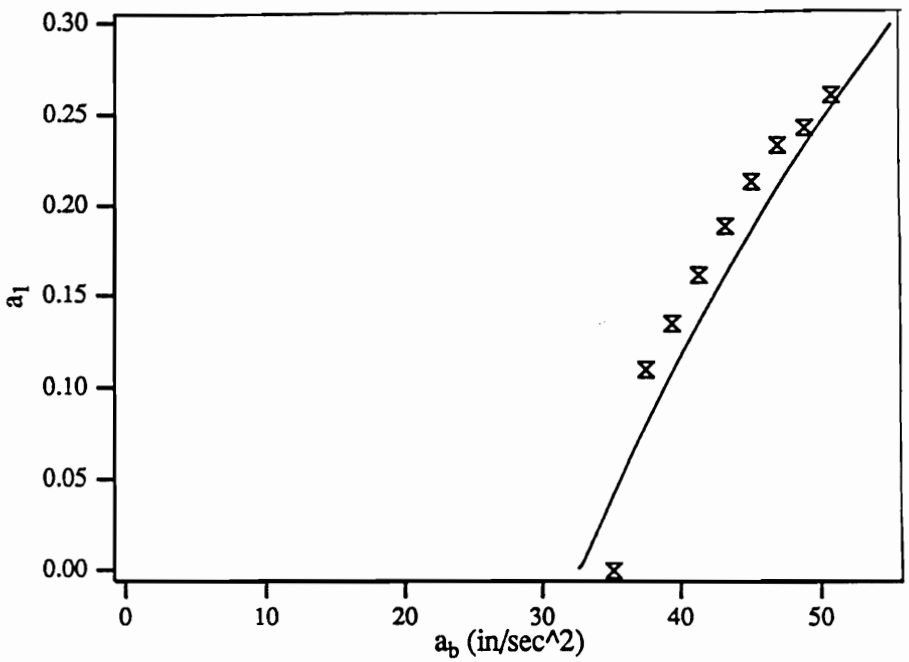

Fig. 3.6 Experimental and theoretical force-response curves for the first mode when C_1=0.050 and f_e=1.253 Hz.

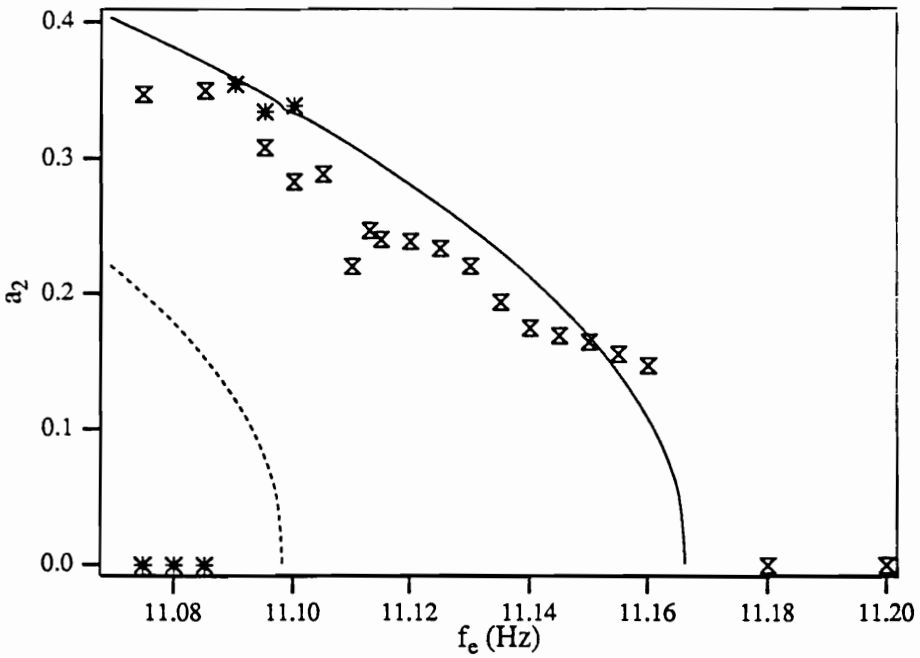

Fig. 3.7 Experimental and theoretical frequency-response curves for the second mode when C_2=0.000 and $a_b = 61.78$ in/sec^2.

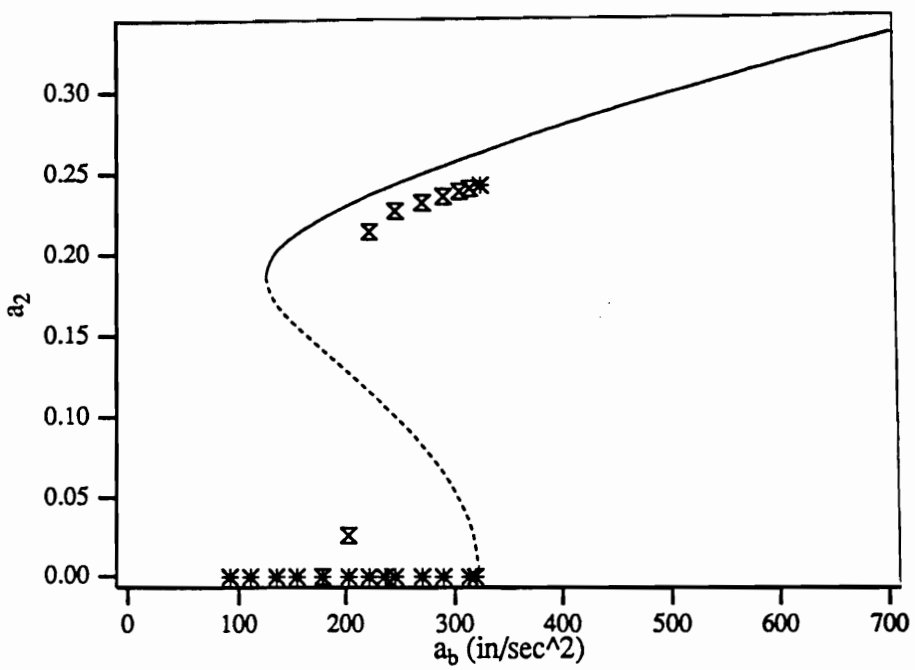

Fig. 3.8 Experimental and theoretical force-response curves for the second mode when C_2=0.000 and 11.05 Hz.

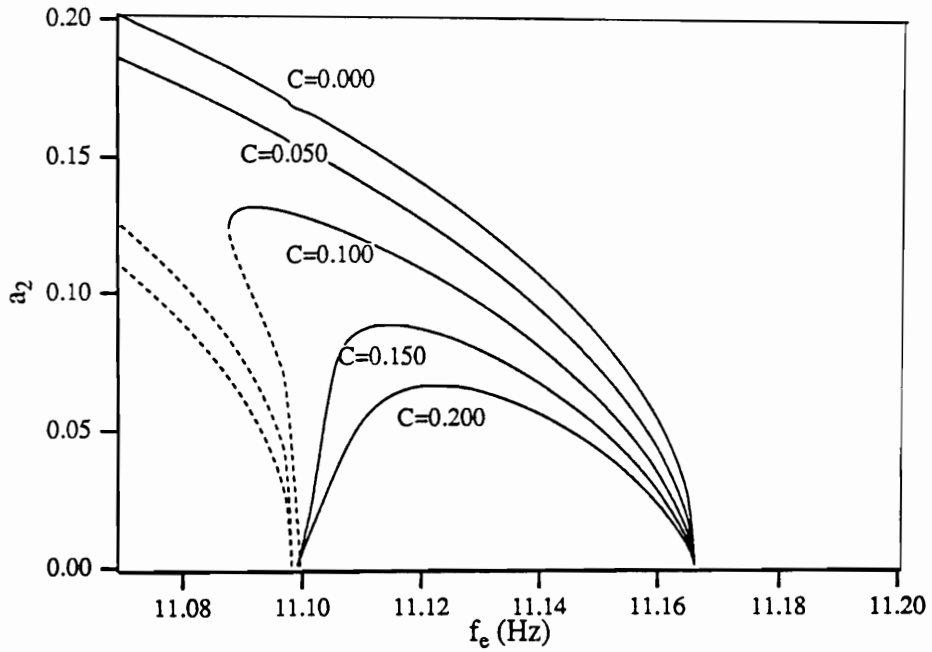

Fig. 3.9 Theoretical frequency-response curves for the second mode for $a_b = 61.78$ in/sec^2 and various values of C_2.

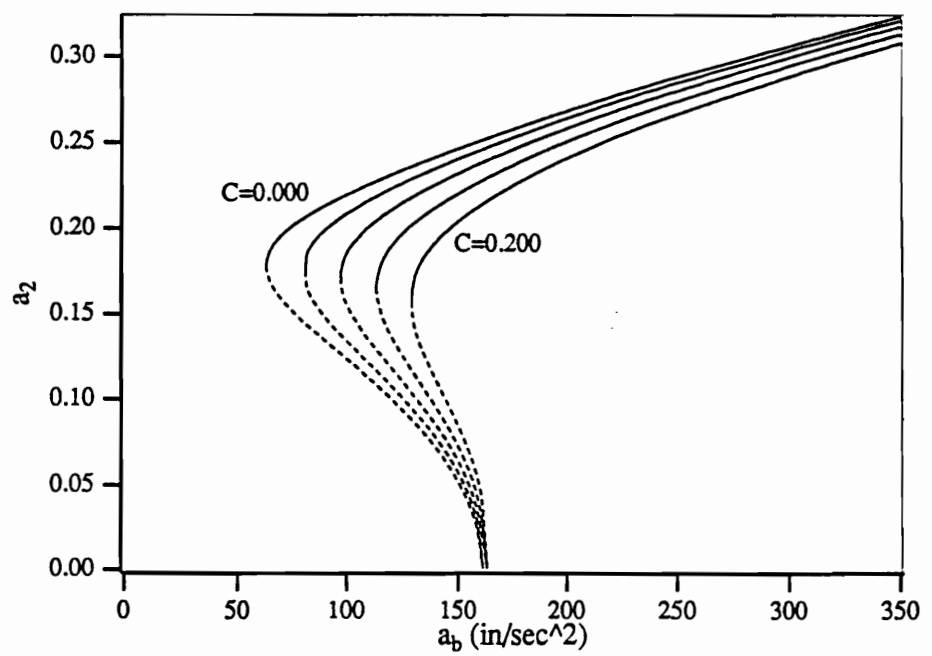

Fig. 3.10 Theoretical force-response curves for the second mode for f_e=11.05 Hz and various values of C_2.

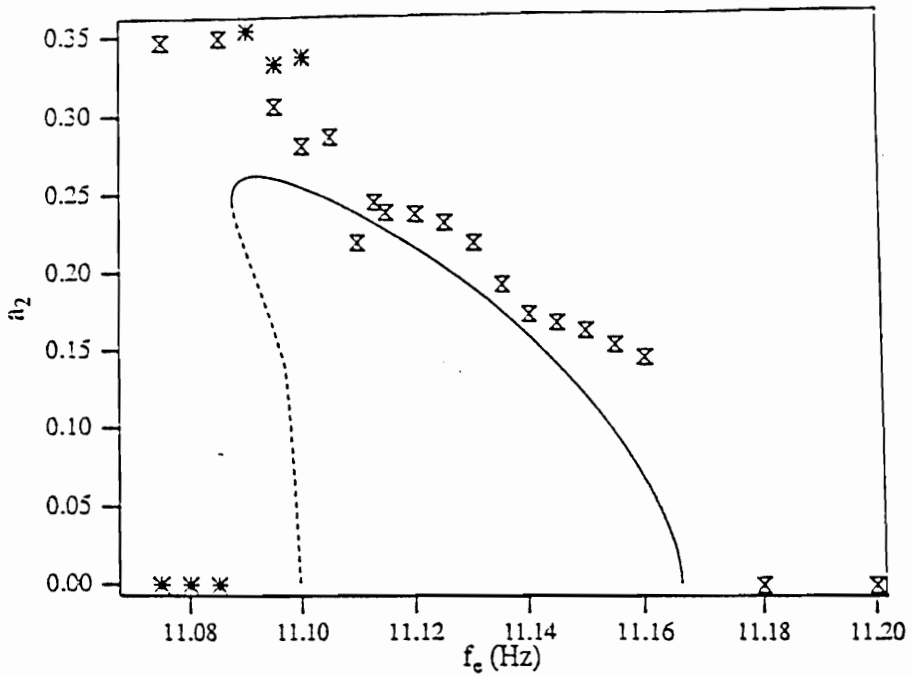

Fig. 3.11 Experimental and theoretical frequency-response curves for the second mode when C_2=0.100 and a_b = 61.78 in/sec^2.

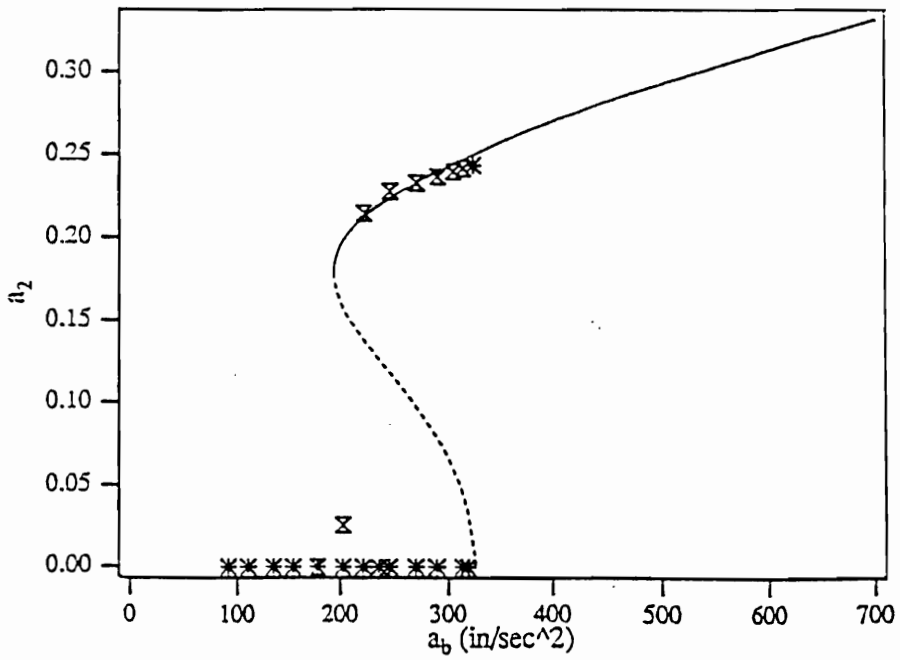

Fig. 3.12 Experimental and theoretical force-response curves for the second mode when C_2=0.100 and f_e=11.05 Hz.

4. Experimental Observations of the Transfer of Energy From High-Frequency Excitations to Low-Frequency Response Components

Aeronautical and mechanical systems often have energy inputs at frequencies much higher than many of their natural frequencies. Examples of such systems include the space station, by virtue of its very low natural frequencies, and systems with sensitive instruments isolated from high-frequency noise. If nonlinearities exist in such systems, the response can be complicated due to nonlinear (modal) interactions. We chose the flexible cantilever beam described in Chapter 2 as a convenient structure to exhibit some of these complicated phenomena in a controlled laboratory setting. In such a structure, modes with frequencies an order of magnitude higher than the frequencies of the first few modes can be excited. Energy from the directly excited high-frequency modes can be transferred to low-frequency modes through nonlinear interactions.

In this chapter, we present the results of experimental investigations into the transfer of energy from high-frequency excitations to low-frequency components in the response of the flexible cantilever beam. Four cases were considered, three with periodic base motions along the axis of the beam, and one with a band-limited random base motion transverse to the axis of the beam. A transfer of energy from high-frequency modes of the system to low-frequency modes of the system was observed in all four cases. For the three cases with periodic excitation, the frequency relationship between the excitation frequency and the lowest frequency component in the response is in the ratio of 50:1 in two cases and 25:1 in another case. When one or more of the first few modes are indirectly excited through nonlinear interactions with the directly excited modes, their motion occurs on a slow-time scale in comparison to the time scale associated with the motion of the directly excited modes.

In the first case, we excited the beam at $f_e \approx 2f_3$ with the base excitation at a_b=0.85 grms where g is the acceleration due to gravity. In this case, the response remained planar throughout the frequency sweep. During part of a frequency sweep, a large response of the first mode was observed. In the second case, we excited the beam at $f_e \approx 2f_3$ with the base excitation at a_b=1.41 grms. In this case, the planar motion of the beam lost stability and large out-of-plane motions were observed. A large response of the first mode was observed prior to the out-of-plane motion. In the third section, we present the results of two different experiments. One for f_e=138 Hz and a_b=0.52 grms, and another for f_e=144.5 Hz and a_b=0.52 grms. In these two experiments, the second mode with a natural frequency of 5.684 Hz dominated the response. It appeared that the shaker was interacting with the structure. We did not investigate the f_e=138 Hz and f_e=144.5 Hz motions in detail but, we present these results to show additional examples of the transfer of energy from a high-frequency input to low-frequency components in the response.

4.1 Test Description

The test setups used to conduct the experiments with periodic excitations are described in Chapter 2. For the $f_e \approx 2f_3$ case, we conducted stationary frequency sweeps and monitored the accelerometer and strain-gage spectra. The excitation level was held constant during the stationary sweeps. We started the experiment at a selected excitation frequency. Then, at each f_e, we waited long enough until a steady-state motion was achieved, recorded the data, incremented the frequency by a small amount, and repeated the process. We used Poincaré sections and frequency spectra to ascertain if a response had achieved a steady state. For real-time spectral analyses, we used 1280 lines of resolution in a 40 Hz baseband and a flat top window.

The test set up for the random excitation was much like that for periodic excitations except that the beam was mounted on a 100 lb shaker such that the base

motion was transverse to the axis of the beam. Also, the signal was generated using a random noise generator and band-pass filtered before it was fed to the shaker amplifier. During the random excitation, the strain-gage signals were low-pass filtered through a six-pole elliptic filter with a cut-off frequency of 50 Hz. For spectral analyses, we used 1280 lines of resolution in a 40 Hz baseband, a Hanning window, and 30 overlap averages.

For the $f_e \approx 138$ Hz case, we obtained the accelerometer and strain-gage spectra for a single excitation amplitude and frequency. For real-time spectral analyses, we used 1280 lines of resolution in a 160 Hz baseband and a flat top window.

To calculate the pointwise dimension (Moon, 1987), and high resolution FFT, we collected 72,000 points from the base strain-gage at a sampling frequency of 120.0 Hz. This was done for selected motions. The signal was low-passed filtered with a cut-off frequency of 50 Hz before data acquisition. For the dimension calculations we used 1000 reference points. For the high resolution FFT's, 65536 (2^{16}) points were used with a Kaiser window.

Throughout this discussion, we refer to the frequency component of the response near a natural frequency of a particular mode as that particular mode's contribution to the response. For large motions, this assumption may be questionable due to the possible presence of harmonics of certain frequency components and peaks at combinations of the frequency components. In the experiments, the mode shapes corresponding to the largest components of the forced response could be visually identified by the number of nodes. In addition, for the case discussed below where the third mode was initially the largest contributor to the response, the mode shape was measured. This was done by measuring the displacements optically at different locations along the beam while the excitation parameters were held constant. The amplitude of the third mode was measured from the peak near f_3 in the response spectrum. These values were plotted against the location

along the beam and compared to the linear mode shape obtained from the Euler-Bernoulli beam theory. They matched very closely. This indicates that, for this case, a peak in the spectrum near a natural frequency corresponds to that particular mode.

4.2 Planar Motion for $f_e \approx 2f_3$

The excitation frequency was varied between 33.00 Hz and 30.90 Hz while the base acceleration was held constant at 0.85 gs rms. In Fig. 4.1a, the ranges of f_e in which the different responses occur in terms of the participating modes are summarized. Note that, throughout the considered range of f_e, two different responses were found for each frequency setting except between 32.2 Hz and 32.73 Hz where only one response was found. In Fig. 4.1b, the frequency-response curve obtained during a downward sweep in frequency is presented. In Fig. 4.1c, the frequency-response curve obtained during an upward sweep in frequency is presented. In Fig. 4.1 the amplitudes correspond to the root sum squared (rms) of the signal at each modes response frequency. The scale for Fig. 4.1c was chosen to highlight the fourth mode's response. In Figs. 4.1b and 4.1c, an approximate conversion from strains to relative displacements was made by multiplying each mode's contribution to the response by f_i/f_3, where f_i is the natural frequency of the ith mode. This conversion gives a better measure of the displacements observed during the experiment.

We observed a combination resonance involving the first and fourth modes when f_e was between 33.00 Hz and 32.74 Hz during the downward sweep. A typical spectrum of this type of response is shown in Fig. 4.2a. The sum of the frequencies of the responses of the first and fourth modes is equal to the excitation frequency. A peak at the excitation frequency is also present. By using a time delay of 0.33 seconds, we calculated the pointwise dimension for this motion to be about 2.0 for n=10. The points in the Poincaré section, shown in Fig. 4.2a, form a closed loop. Both these tools indicate

that the motion is a two-period quasi-periodic motion in agreement with the spectrum. This response was difficult to obtain because very few initial conditions led to this motion. Many tries of "tapping" the beam to give different initial conditions were required to obtain this motion. The response, which most of the initial conditions would evolve to, had a single peak in the spectrum at the excitation frequency.

A response due to a principal parametric resonance of the third mode and a primary external resonance of the fourth mode was observed for f_e between 32.74 Hz and 32.40 Hz in both the downward and upward frequency sweeps. The frequency of the response of the third mode was $f_e/2$ and the frequency of the response of the fourth mode was f_e. A spectrum of this type of response is shown in Fig. 4.2b. The third mode component dominated the response, as seen in Figs. 4.1b and 4.1c. Using 72000 points, 1000 reference points, and a time delay of 0.33 seconds, we calculated the pointwise dimension for this motion to be about 1.0 for n=10. The Poincaré section, shown in Fig. 4.2b, consists of two discrete points. Both the Poincaré section and the dimension indicate a periodic motion. The two points in the Poincaré section and the spectral line at $f_e/2$ indicate that the motion had a basic period twice that of the excitation period.

A three-mode response that included the first mode was first observed at approximately 32.4 Hz during the sweep down in f_e. The three-mode response continued as the frequency was swept down until 30.10 Hz, where the first and third modes dropped out of the response, resulting in only a small peak at f_e in the spectrum. As the frequency was swept up, a transition from the single fourth-mode response to a three-mode response occurred at 32.19 Hz. A spectrum of the three-mode response, when the first mode component was large, is shown in Fig. 4.2c. When the three-mode response was observed, there were sidebands about the $f_e/2$ peak in the spectrum. The difference in frequency f_m between the $f_e/2$ peak and the sidebands varied throughout the frequency sweep. The frequency of the first-mode component of the response was equal to f_m. In

the excitation frequency range between 32.22 Hz and 32.19 Hz, f_m was approximately 0.65 Hz, which is close to the natural frequency of the first mode. This resulted in a response with a large first-mode component, as shown in Figs. 4.1b and 4.1c. The spectrum has discrete lines with f_m and f_e being the discernible incommensurate frequencies. Generating the Poincaré section for this motion, we found that the points generated two small loops, as shown in Fig. 4.2c. The length of time to collect the 512 points for the Poincaré section was about 16.0 seconds. The spectrum and the Poincaré section indicate a two-period quasi-periodic motion in the time span considered. However, the first-mode component of the spectrum never settled down to a constant value even after a long time (30 minutes). The pointwise dimension was about 2.25 for a delay of 0.33 seconds at n=10. These results indicate a basic two-period motion that is chaotically modulated. During the three-mode response, we measured a static component in the strain, which returned to zero when the three-mode response was not present. We measured the static displacement of a node of the third mode and observed that it changed as we changed f_e. The analysis of Chapter 5 helps us interpret this response as a static response of the first mode due to a dynamic response of the third and fourth modes.

A response consisting of the fourth mode alone was observed for most of the upward frequency sweep, as shown in Fig. 4.1c. A jump in the response, characteristic of a forced Duffing's oscillator with a softening spring, was observed. The Poincaré section for this motion consisted of a single point, the dimension was about 1.00, and the spectrum had a single peak. These results indicate a periodic motion with a basic frequency equal to the excitation frequency. During the downward frequency sweeps, besides the fourth mode, the third mode was present in the response. Although the fourth mode was excited by a primary resonance, the expected increase in amplitude of the fourth mode did not occur. This can be seen in Fig. 4.1b. During the upward frequency sweeps, the increase in amplitude of the fourth mode can be seen in Fig. 4.1c. When the

third mode appeared at 32.4 Hz during the upward frequency sweep, the amplitude of the fourth mode decreased as seen in Fig. 4.1c. This suggests that the presence of the third mode suppressed the fourth mode.

4.3 Out-of-Plane Motion for $f_e \approx 2f_3$

For this experiment, the excitation frequency was varied between 32.000 Hz and 31.877 Hz while the base acceleration was held constant at a_b=1.414 grms. During a downward sweep in frequency a planar three-mode motion similar to that discussed in the previous section loses stability and an out-of-plane motion occurs. In this section, we focus on the transition from the planar to out-of-plane motion and characterize the out-of-plane motion. This transition only occurred during a downward frequency sweep. Cusumano (1990) investigated similar out-of-plane motions of a flexible cantilever beam subjected to an external excitation.

A response due to a principal parametric resonance of the third mode and a primary external resonance of the fourth mode was observed at f_e=32.000 Hz in a downward frequency sweep. The frequency of the response of the third mode was $f_e/2$ and the frequency of the response of the fourth mode was f_e. Spectra of this type of response and the associated base acceleration are shown in Fig. 4.3. This spectrum of the base acceleration is typical of the rest of the experiment so the others are not shown. As the frequency was reduced to 31.880 Hz, the first mode came into the response along with sidebands about the $f_e/2$ and f_e peaks in the spectrum, as shown in Fig. 4.4. This motion has essentially the same characteristics as the three-mode motion discussed in the previous section.

As the excitation frequency was reduced to f_e=31.879 Hz, an increase in the magnitude and number of sidebands about f_e and $f_e/2$ peaks occurred, as shown in Fig. 4.5. This corresponds to an increase in the amplitude of the modulations. In addition, an

increase in the magnitude of the peak associated with the first mode occurred. A time history of a strain-gage signal for this type of motion is shown in Fig. 4.6. The oscillations of the envelope correspond to the sidebands in the spectrum.

As the excitation frequency was reduced to f_e=31.878 Hz, additional sidebands were observed. A zoom span spectrum from 10 Hz to 20 Hz around the $f_e/2$ peak with 1280 lines of resolution is shown in Fig. 4.7. The peaks appear to be spread over several lines of resolution indicating that the response may be chaotic. Unfortunately, we did not obtain a long time history for this motion for post-experiment calculation of the dimension.

As the excitation frequency was reduced to f_e=31.877 Hz, we visually observed a slow increase of the amplitude of the first mode. After some time, the planar motion lost stability and a large out-of-plane motion was observed. A spectrum of the out-of-plane motion is shown in Fig. 4.8. We note that the response has a broadband spectrum. A Poincaré section of this motion is shown in Fig. 4.9. The Poincaré section does not have a simple geometry such as a point, line, or loop; thus, the long term motion is referred to as a strange attractor. The dimension d_p was found to be about 5.26. All the tools used to characterize this motion indicate that the motion is chaotic. A time history of a strain-gage signal for this motion as the beam transitioned from a planar to an out-of-plane motion is shown in Fig. 4.10. We point out the abrupt change from a response dominated by high-frequency components to one dominated by a low-frequency component.

4.4 Band-Limited Random Base Excitation

To investigate if nonlinear interactions occur with a band-limited random base excitation, we conducted another experiment. For this case, the beam was excited by random excitation in the frequency range from 10 Hz to 50 Hz to preclude a direct excitation of the first and second modes through linear mechanisms. The excitation

signal was high-pass filtered through a six-pole elliptic filter with a cut-off frequency of 10 Hz and subsequently low-pass filtered through a six-pole elliptic filter with a cut-off frequency of 50 Hz.

The spectra of the response and the excitation are shown in Fig. 4.11 Although the beam was not provided with any input energy for frequencies less than 10 Hz, the output spectrum still contains peaks near the first and second natural frequencies besides peaks near the third and fourth natural frequencies. This observation indicates that the first and second modes are excited through nonlinear mechanisms. The first and second modes may be either indirectly excited by an energy transfer from the third and fourth modes, as in the previous case, or directly excited through combination resonances.

4.5 Periodic Base Excitation: f_e = 138 Hz and f_e=144.0 Hz

Two additional tests were conducted to determine if the transfer of energy from high-frequency modes to a low-frequency mode is an isolated phenomenon or if it occurs for a variety of conditions. The test setup used was the same as that used for the $f_e \approx 2f_3$ case. The excitation frequency f_e was 138 Hz for one test and 144 Hz for the other with a base acceleration a_b=0.52 grms for both. The 138 Hz frequency is near the eighth natural frequency of the beam, where as the 144 Hz is not near any natural frequencies of the beam.

The strain-gage and the base acceleration spectra for f_e=138 Hz are shown in Fig. 4.12. In the strain-gage spectrum, there is a large peak near 5.6 Hz and two small peaks near the excitation frequency that are separated by approximately 5.6 Hz. A visual inspection indicated that the response of the beam was clearly dominated by the second mode. The two high-frequency peaks in the response spectrum are less than a tenth of the magnitude of the low-frequency peak. Also, note that the measured response is the strain. A conversion that approximately converts from strains to relative displacements is

$f_2/f_8 \approx 0.04$, where f_8 is the natural frequency of the eighth mode. This indicates that the response of the second mode is approximately 250 times the high-frequency components in the response. Arguably, the high-frequency components in the strain-gage spectrum are negligible. The base acceleration spectrum has a main peak at 138 Hz, which is the frequency of the signal from the signal generator. There are also large sidebands around 138 Hz in the acceleration spectrum, indicating that the base acceleration is modulated. As in the first case, the frequency difference between the carrier frequency and the sidebands is near the natural frequency of a low-frequency mode of the beam. In this case, modulations are seen in the base motion.

In Fig. 4.13, we show the spectra of the base strain gage signal and the base accelerometer signal for f_e=144.0 Hz and a_b=0.52 grms. There are multiples of 60 Hz in the response spectrum that are due to line noise and should be ignored. Again, there is a large second-mode contribution to the response. As in the previous case, there are sidebands in the acceleration spectrum, indicating modulations of the base acceleration. In addition, there are small peaks in the strain-gage spectrum at the same frequencies as in the acceleration spectrum. The spacing f_m of the high-frequency peaks is equal to the response frequency of the second mode. This indicates that an interaction occurred between the complete response of the low-frequency second mode and the modulations of the high-frequency components in the experiment.

There are two interpretations of the low-frequency single-mode responses with a modulated input that were observed. One is that the response consists of essentially a single low-frequency mode excited by a modulated input. The other one is that the response consists of two modes with one being the low-frequency second bending beam mode and the other including the shaker system. This multi-mode response is driven by the periodic signal from the signal generator.

4.6 Concluding Remarks

In the experiments with $f_e \approx 2f_3$, the nonlinear mechanism responsible for exciting the first mode involved an energy exchange between the complete response of the first mode and the modulations associated with the high-frequency third and fourth modes. This resonance is a distinctly different mechanism than the combination resonance for transferring energy from a high-frequency excitation to a low-frequency mode (Dugundji and Mukhopadhyay, 1973). In the case of the cantilever beam, this type of transfer of energy was found to be robust and occurred for a variety of excitations. Such transfer of energy is expected to occur in other structures as well.

In addition, in the $f_e \approx 2f_3$ experiments, a variety of resonant responses were observed in a small range of the excitation frequency. These results highlight the richness of the response of a simple structure. They also point out some of the difficulties that can be encountered in predicting the response of a nonlinear continuous structure due to the many nonlinear resonances.

The experiments conducted on the cantilever beam were at the same time "good experiments" and "bad experiments". They were good because they revealed a previously unstudied modal interaction. The understanding of the phenomena gained from the experiments guided an analysis that captures the unusual characteristics of the observed motions. The analysis is presented in Chapter 5. The results from these studies could have applications to other flexible structures. Because of this, the experiments were part of a significant contribution to the art and science of engineering. At the same time, the experiments were "bad" because they were not very repeatable. With repeated experiments, the same type of motions would be observed but, the excitation levels and frequencies required for the various motions would change. This was due primarily to the beam yielding during the experiments. The motion that did the most damage was the

out-of-plane motion. This unfortunately was the favorite motion to show visitors. In hindsight, this type of motion should have been kept at a minimum. The result of this nonrepeatability was to make it difficult to obtain experimental results, analyze them, and go back and try and obtain more results at the same settings of the control parameter to characterize the motion further.

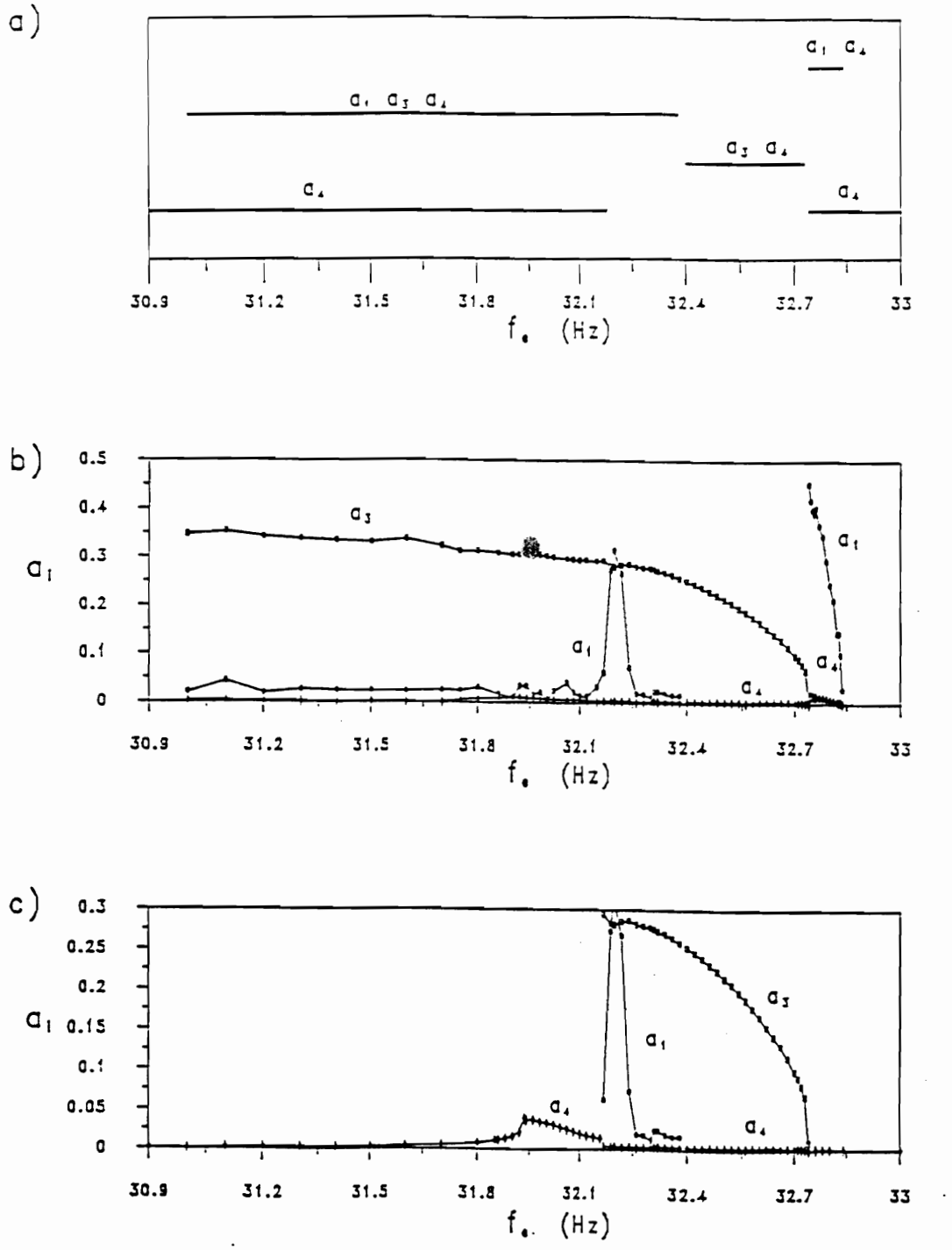

Fig. 4.1 Cantilever beam response during a steady frequency sweep: a) summary of responses observed, b) frequency response during a downward sweep in frequency, and c) frequency response during an upward sweep in frequency.

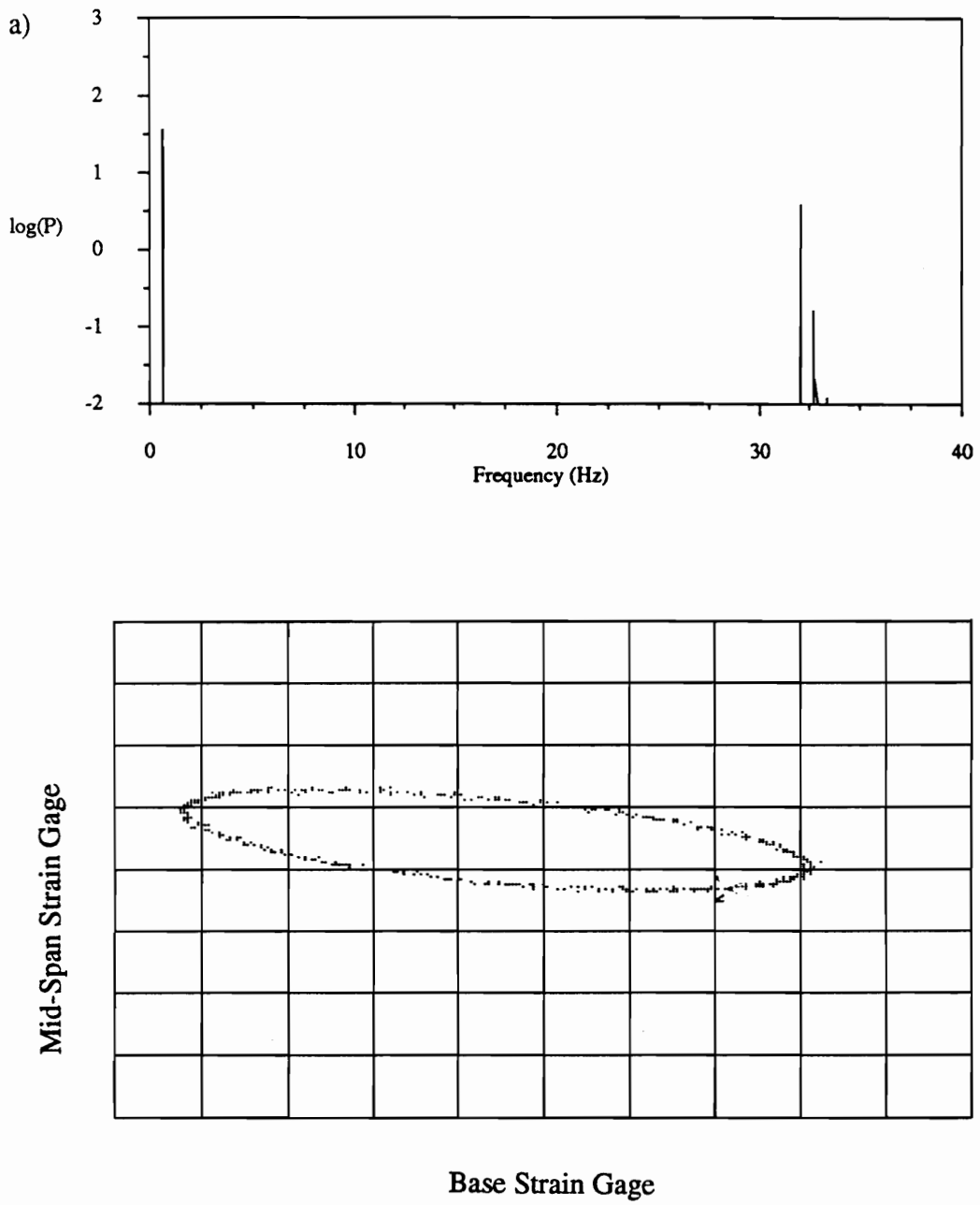

Fig. 4.2 Power spectra and Poincaré sections of the response during: a) combination resonance exciting the first and fourth modes, b) principal parametric resonance of the third mode and primary resonance of the fourth mode, and c) interaction exciting the first mode through modulations associated with the third and fourth modes.

5.1.2

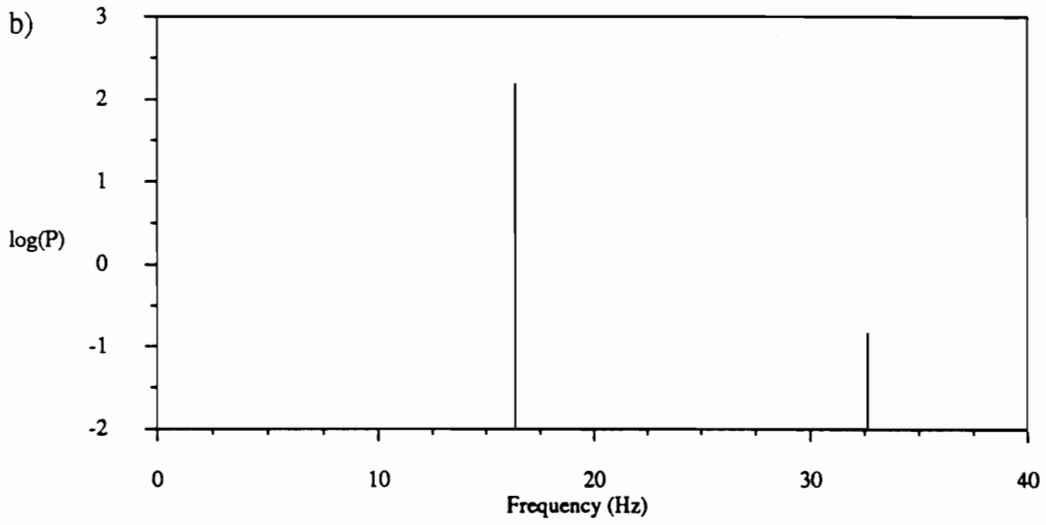

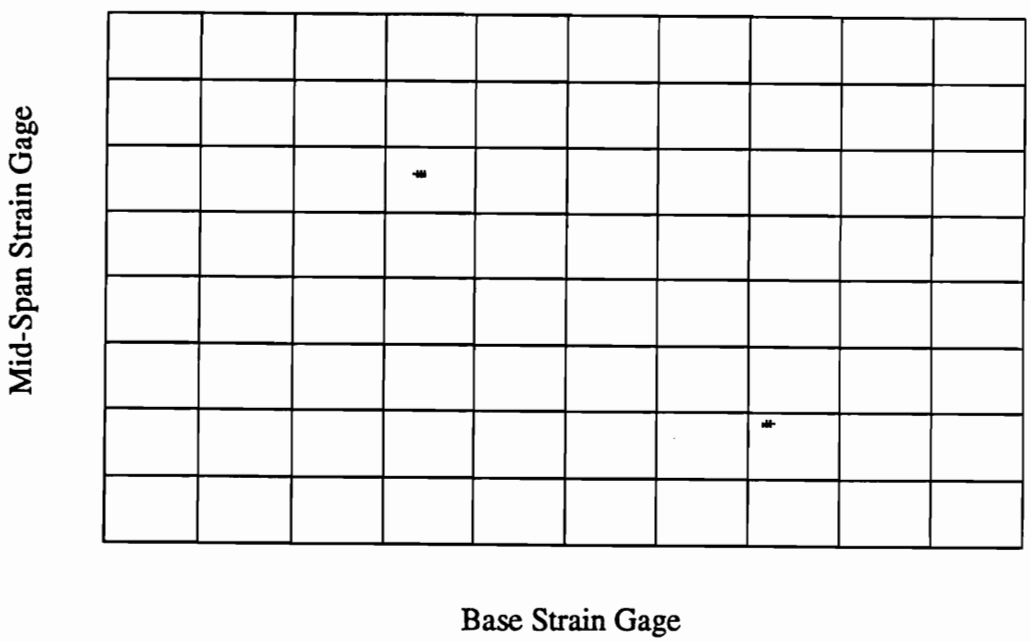

Fig. 4.2 Continued.

5.1.3

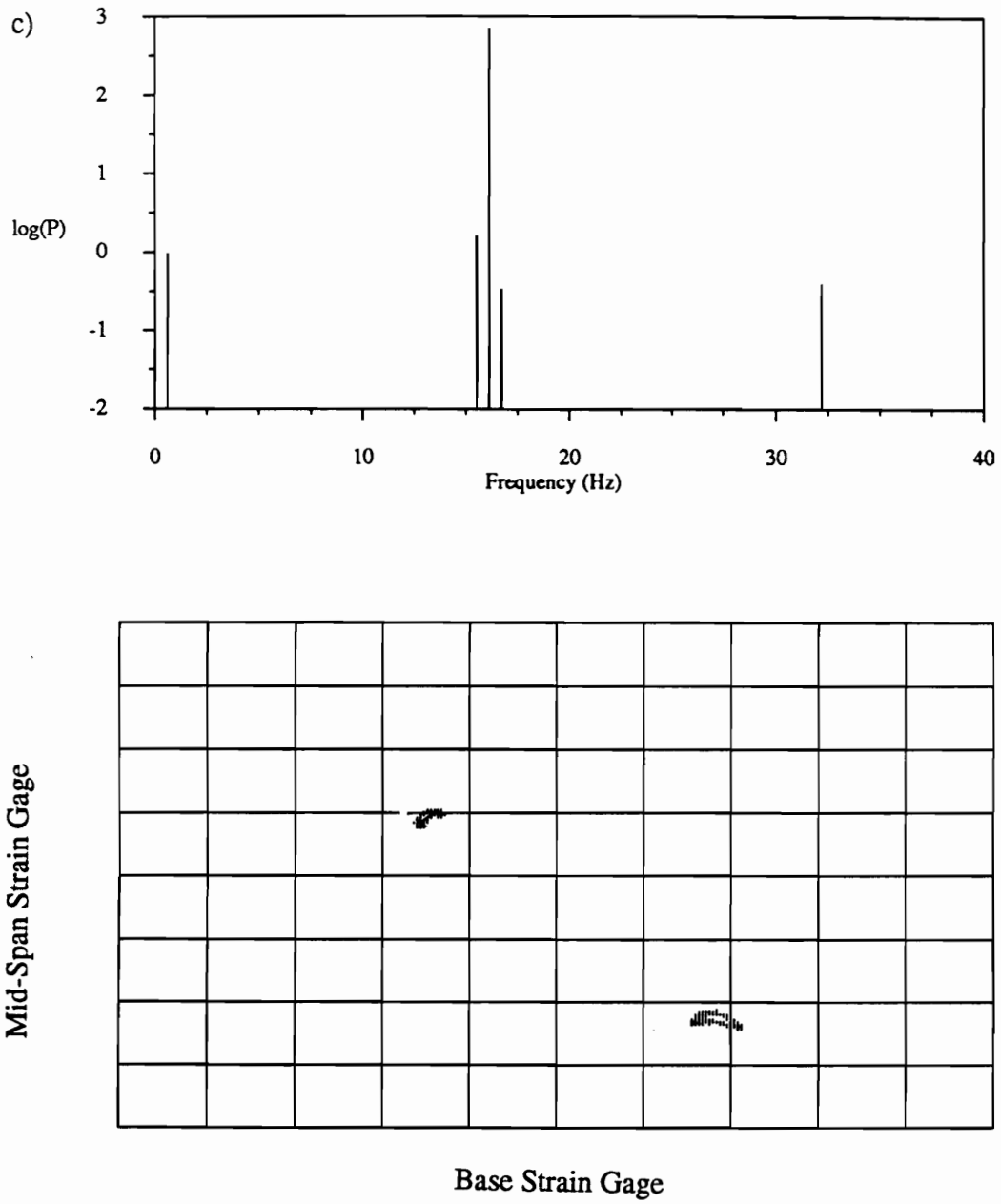

Fig. 4.2 Continued.

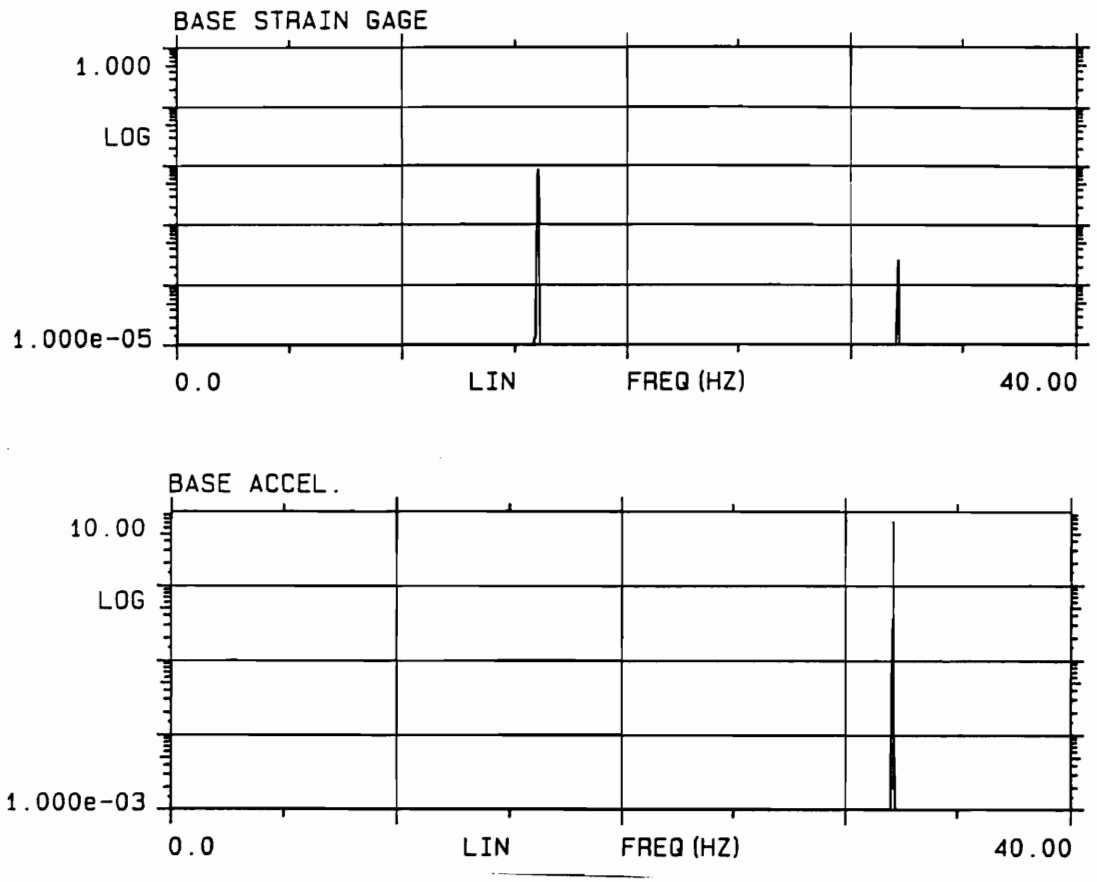

Fig. 4.3 Strain-gage and base acceleration spectra for f_e=32.00 Hz and a_b=1.414 grms.

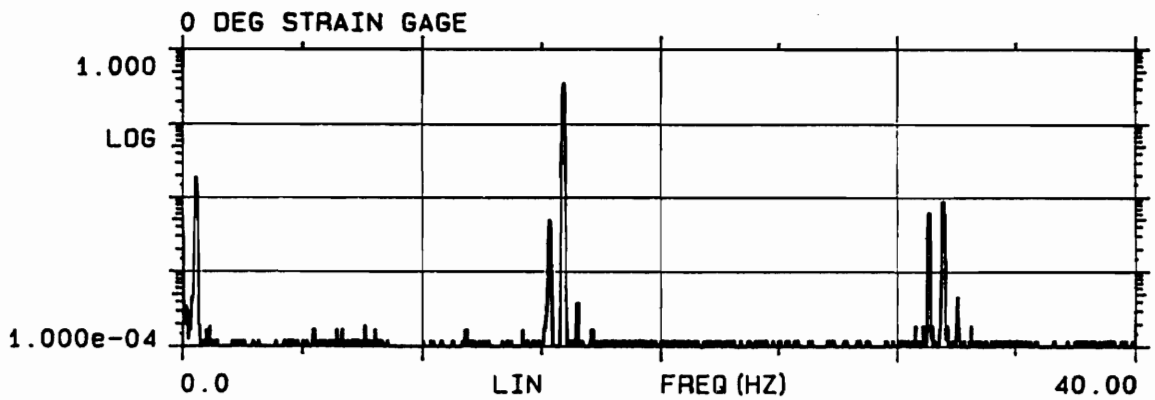

Fig. 4.4 Strain-gage spectrum for f_e=31.880 Hz and a_b=1.414 grms.

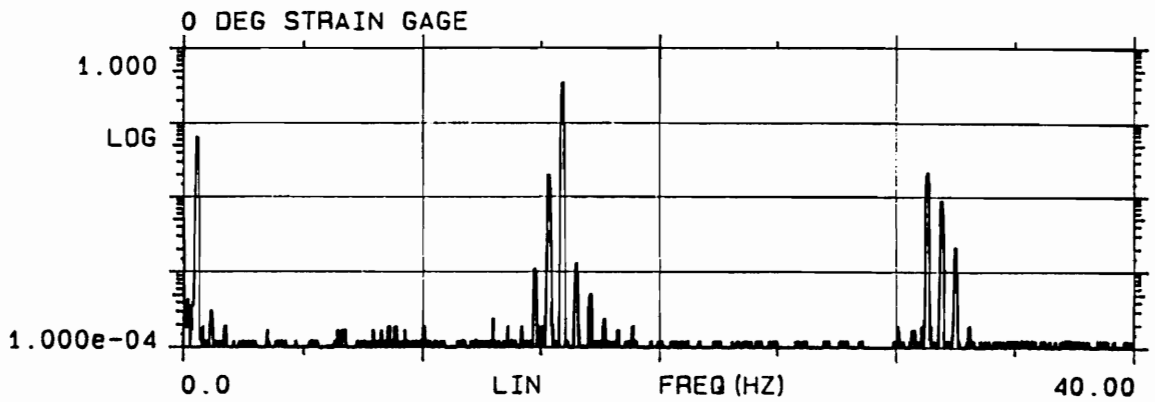

Fig. 4.5 Strain-gage spectrum for f_e=31.879 Hz and a_b=1.414 grms.

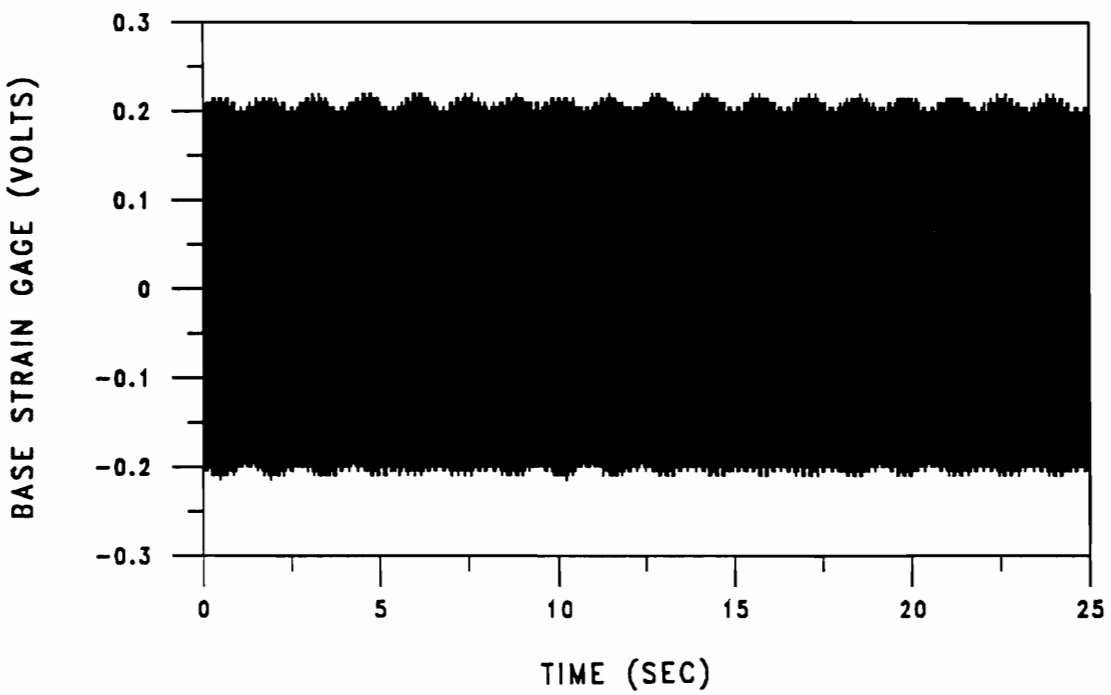

Fig. 4.6 Time trace of a quasi-periodic motion for f_e=31.879 Hz and a_b=1.414 grms.

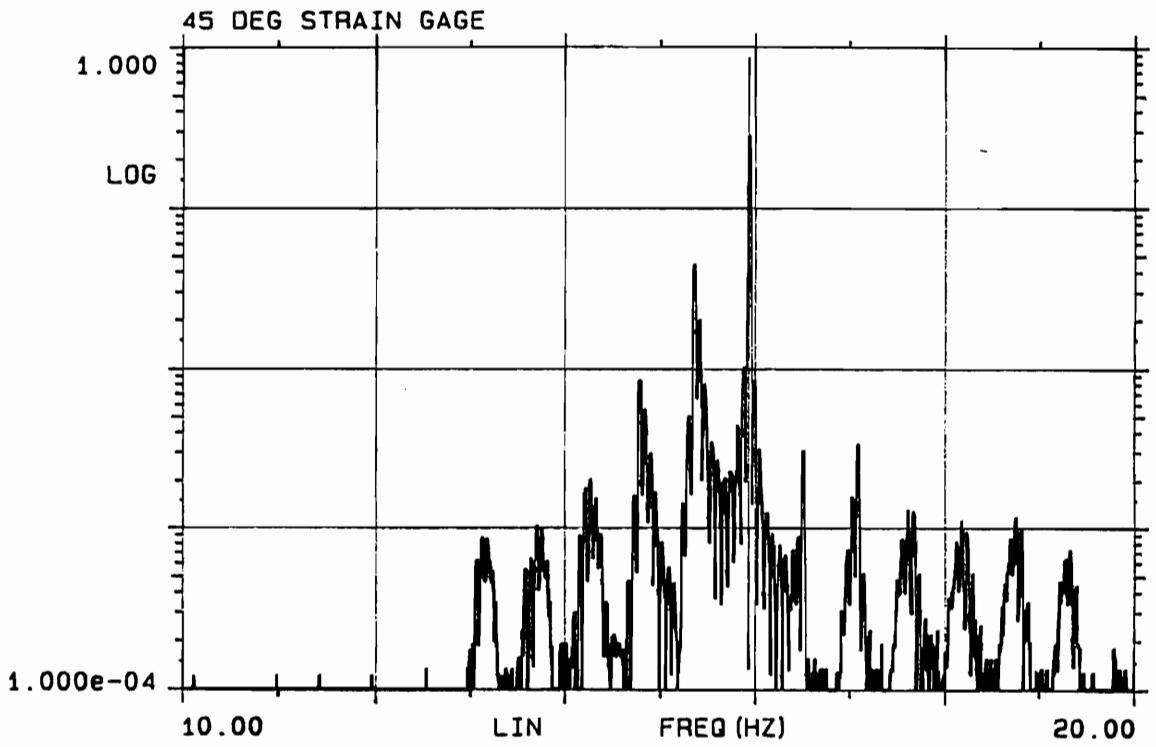

Fig. 4.7 Strain-gage zoom span spectrum for f_e=31.878 Hz and a_b=1.414 grms.

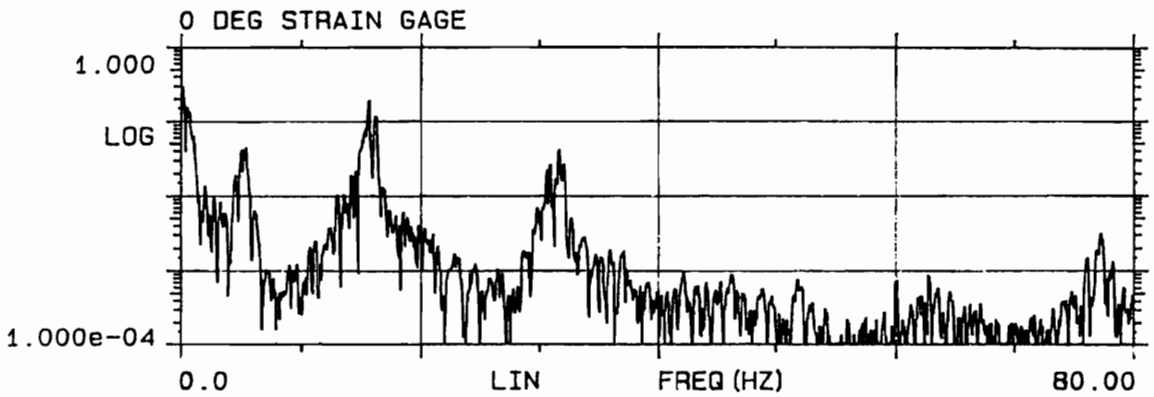

Fig. 4.8 Strain-gage spectrum for f_e=31.877 Hz and a_b=1.414 grms.

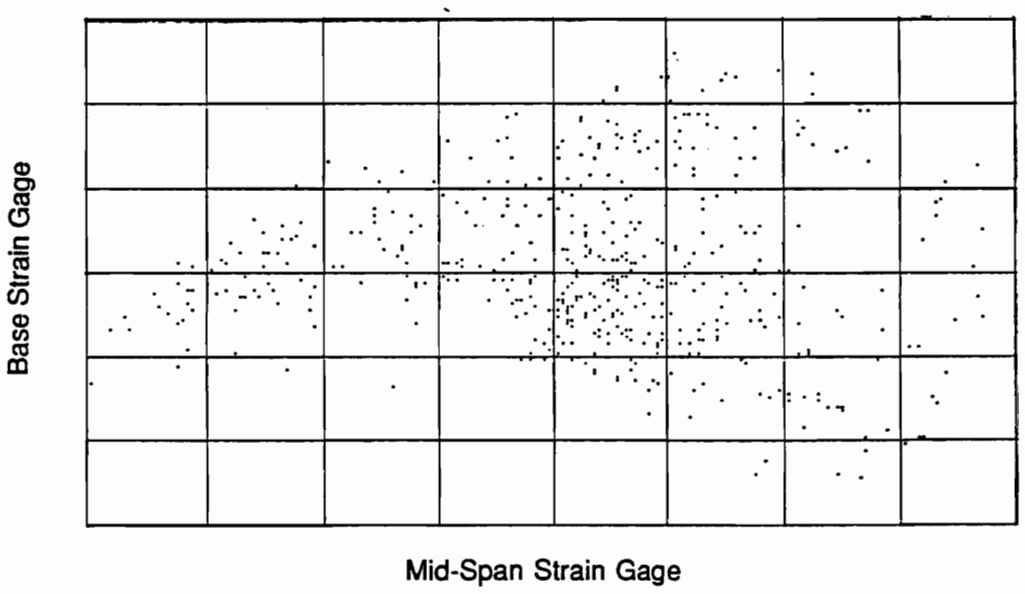

Fig. 4.9 Poincaré section for f_e=31.880 Hz and a_b=1.414 grms.

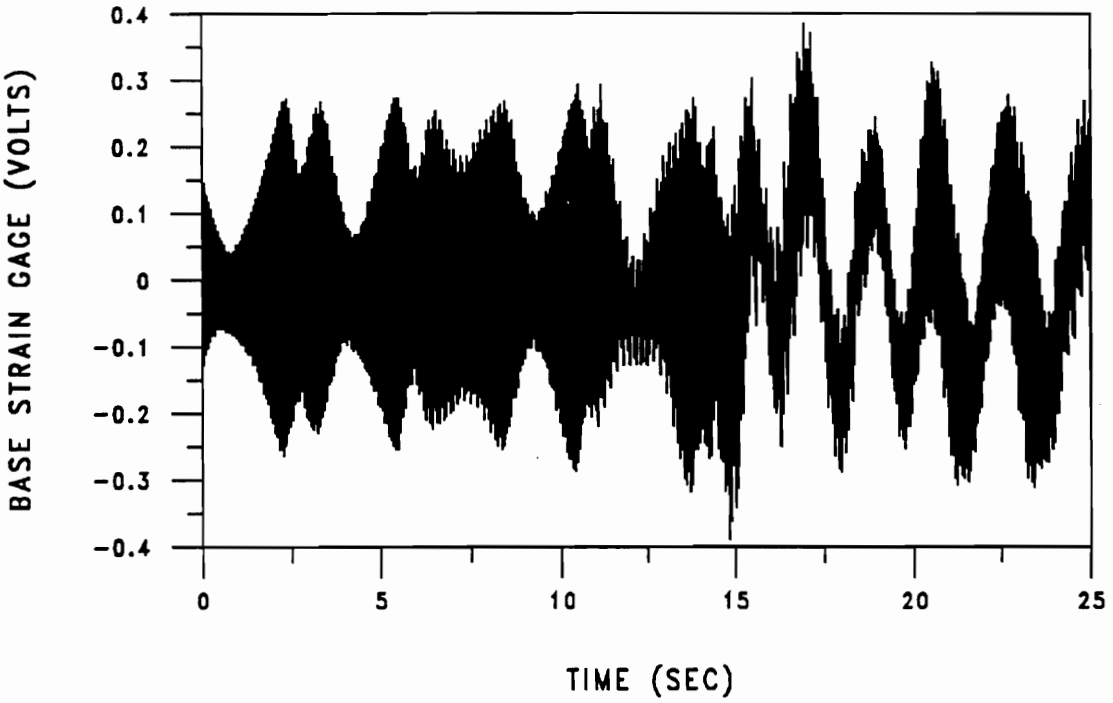

Fig. 4.10 Time trace of a transient motion for f_e=31.877 Hz and a_b=1.414 grms.

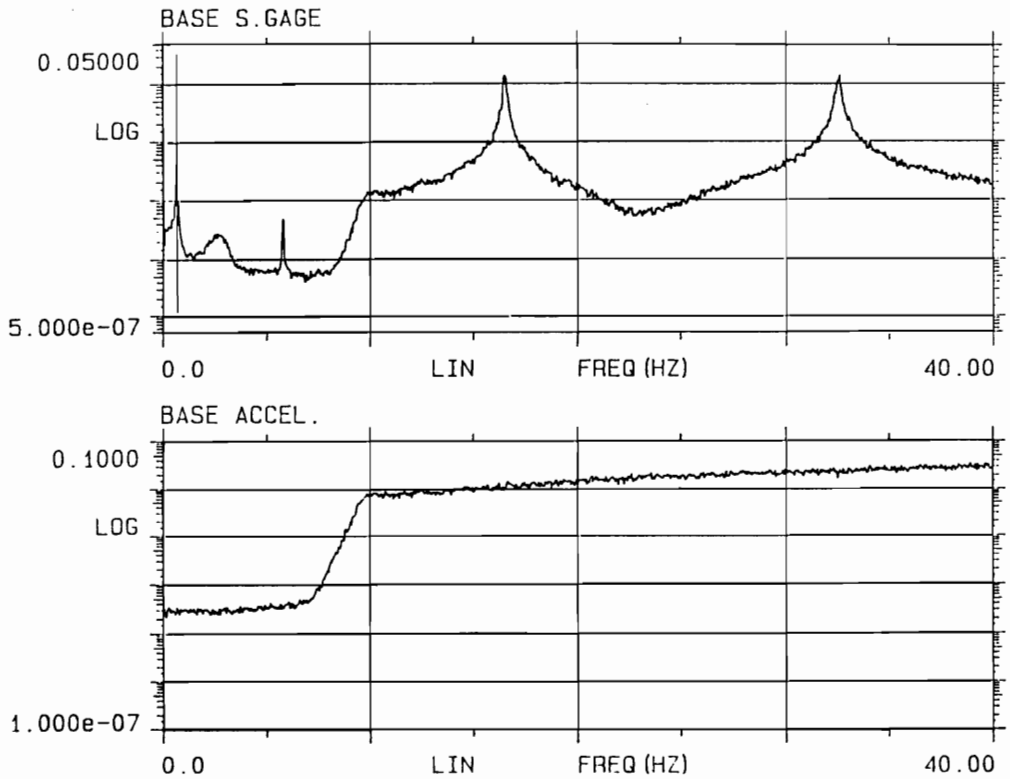

Fig. 4.11 Strain-gage and base-acceleration spectrum for band-limited random excitation.

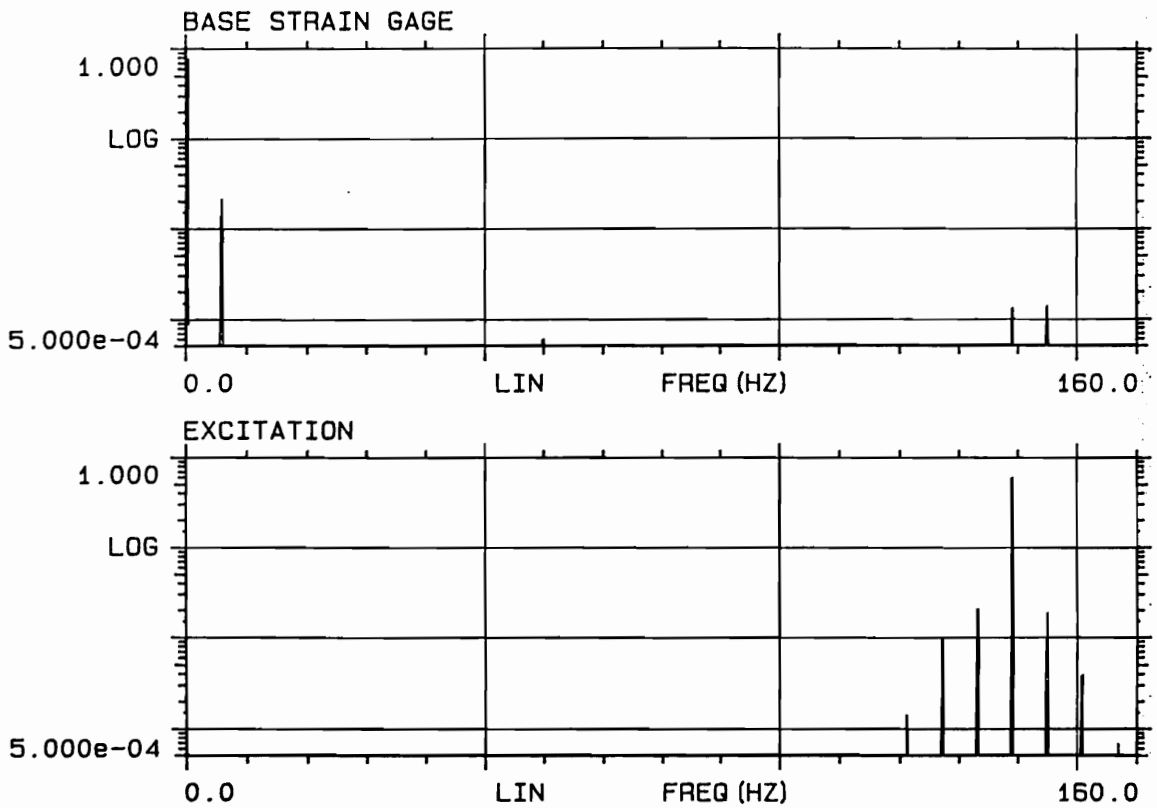

Fig. 4.12 Strain-gage and base-acceleration spectrum for f_e=138 Hz and a_b=0.52 grms.

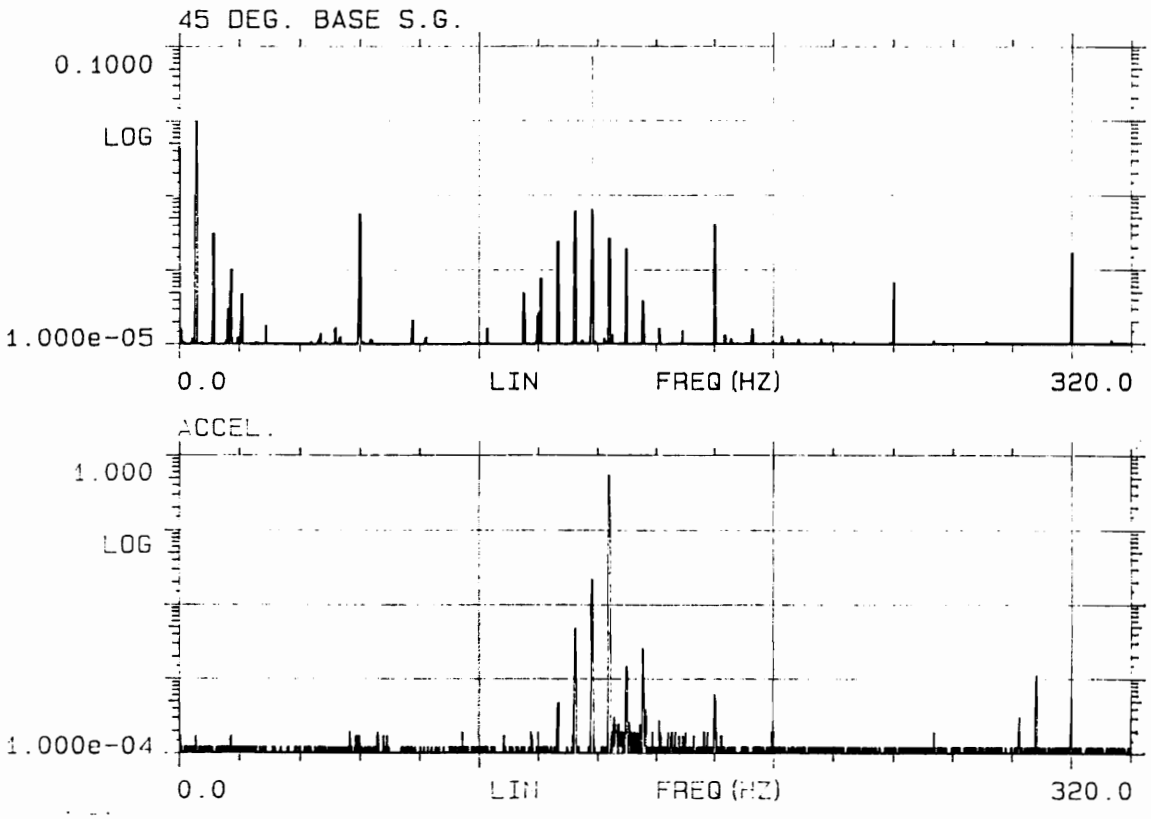

Fig. 4.13 Strain-gage and base-acceleration spectrum for f_e=144 Hz and a_b=0.52 grms.

5. Exchange of Energy Between Modes with Widely Spaced Frequencies: Theory and Experiment

In this chapter, we investigate the exchange of energy between high-frequency modes and a low-frequency mode. We present a perturbation analysis for the planar response of the cantilever beam that includes three coupled modes. Throughout the analysis, we make reference to the experimental results that guided the analysis. Then we present the theoretical results. Next, we present experimental results and compare them to the theoretical results. Also, we point out two crucial experimental observations that motivated and guided the analysis: a) the first, third, and fourth modes participated in the response and b) the response frequency of the first mode was equal to the modulation frequency associated with the third and fourth modes. An a priori knowledge of these characteristics is necessary for the analysis to capture the motions observed in the experiments. The following points regarding this study are worth noting. The choice of the Galerkin projection is dictated by the experimental observations and the analysis allows for the interaction of modes that evolve on different time scales.

5.1 Perturbation Analysis

We analyze Eqs. (2.5) and (2.6) to investigate the experimentally observed planar multi-mode vibrations of the slender cantilever beam described in Section 4.2. We repeat Eqs. (2.5) and (2.6) here for convenience

$$\begin{aligned}\ddot{v}+\mu\dot{v}+v^{iv} &= -z_n{}^2\left(v'\left(v'v''\right)'\right)' -\left(\frac{1}{2}z_n{}^2v'\int_{z_n}^{s}\frac{\partial^2}{\partial t^2}\left(\int_0^s v'^2ds\right)ds\right)' \\ &\quad -z_n\left(v''(s-z_n)+v'\right)\left(a_b\cos(\Omega t)+g\right),\end{aligned} \tag{5.1}$$

$$v=v'=0 \text{ at } s=0, \qquad (5.2)$$
$$v''=v'''=0 \text{ at } s=z_n.$$

where $(\dot{})\equiv\partial()/\partial t$ and $()'\equiv\partial()/\partial s$. Equations (5.1) and (5.2) describe the planar motion of a vertical cantilever beam with a base motion in the vertical direction. We have assumed that the beam is weakly nonlinear and retained only up to cubic nonlinearities. This assumption allows us to use the undamped, linear mode shapes to carry out the Galerkin projection for the case of forced oscillations.

The next step is to identify the modes that will be included in the analysis. This crucial step essentially determines the motions that can be predicted by the analysis. Typically, the participating modes are chosen based on frequency relationships which correspond to a particular resonance, such as, principal-parametric resonance, one-to-one internal resonance, combination resonance, etc. All other modes are assumed to decay to zero with time. Here, we use the results of the experiments conducted on a flexible cantilever beam to choose the modes which we include in the analysis. The experimentally obtained natural frequencies f_i of interest are $f_1 = 0.66$ Hz, $f_2 = 5.69$ Hz, $f_3 = 16.22$ Hz, and $f_4 = 32.06$ Hz, and we note that $f_3/f_1 \approx 25$ and $f_4/f_3 \approx 2$. We restrict our investigation to the case in which the beam is excited vertically by a harmonic motion near twice the third natural frequency of the beam. In this case, because of the levels and the frequency of excitation and the shape of the experimentally obtained frequency-response curves, we interpret the response to consist of a principal parametric resonance of the third mode and a primary resonance of the fourth mode. Also, the first mode participated in the response due to a previously unstudied modal interaction. However, if the beam were initially straight, the external excitation required for a primary resonance

of the fourth mode would not exists. Thus, we assume that the displacement $v(s,t)$ has the form

$$v(s,t) = \Phi_1(s)v_1(t) + \Phi_3(s)v_3(t) + \Phi_4(s)v_4(t) + \Phi_0(s) \tag{5.3}$$

where the $\Phi_i(s)$, i = 1,3,4, are the mode shapes for an undamped linear cantilever beam and $\Phi_0(s)$ accounts for an initial static defection of the beam that will produce an external excitation in the model. The $\Phi_i(s)$ are given Appendix 5 at the end of this chapter. However, because Eq. (5.1) was derived for an initially perfect beam, the form of the displacement implies that the beam is prestressed rather than being stress free. The distributed force needed to produce $\Phi_0(s)$ is shown in Fig. 5.1. This force is small compared with the applied load and hence may be neglected.

In the analysis, we choose $z_n = z_3$ for scaling. The $v_i(t)$ are the time-dependent parts of the solution and are called temporal amplitudes. Substituting Eq. (5.3) into Eq. (5.1) and employing the Galerkin procedure, we obtain the following three ordinary-differential equations:

$$\ddot{v}_1 + \omega_1^2 v_1 = H_1 \tag{5.4}$$

$$\ddot{v}_3 + \omega_3^2 v_3 = H_3 \tag{5.5}$$

$$\ddot{v}_4 + \omega_4^2 v_4 = H_4, \tag{5.6}$$

where $\omega_1 = (z_1/z_3)^2$, $\omega_3 = 1$, $\omega_4 = (z_4/z_3)^2$ and

$$H_i = -\left(\int_0^{z_n} \mu \Phi_i^2 ds\right) v_i - z_n \int_0^{z_n} \Phi_i \left(v'(v'v'')' \right)' ds - \frac{1}{2} z_n \int_0^{z_n} \Phi_i \left(v' \int_{z_n}^{s} \frac{\partial^2}{\partial t^2} \left(\int_0^s v'^2 ds \right) ds \right)' ds$$

$$- \int_0^{z_n} \Phi_i \left(v'(s - z_n) + v' \right) ds \left(a_b \cos(\Omega t) + g \right).$$

We mention that the Φ_i have been normalized such that $\int_0^{z_n} \Phi_i^2 ds = z_n$ and modal damping has been assumed. The natural frequencies are ω_1=0.0570, ω_3=1.000, and ω_4=1.960.

As a first-step in using the method of averaging (Nayfeh, 1981), we transform Eqs. (5.4)-(5.6) to a standard form. To this end, typically the method of variation of parameters is employed using a transformation of the form $v_i = p_i \cos(k\Omega t) + q_i \sin(k\Omega t)$, where the p_i and q_i are slowly-varying terms, Ω is the circular excitation frequency, and k is an appropriate rational number. In the experiments, we observed that the response frequency of the first mode was the same as the low frequency characterizing the modulations of the amplitudes and phases of the third and fourth modes. This led us to consider v_1 as a slowly-varying function and choose the following unconventional transformation:

$$v_1(t) = a_1(t) \tag{5.7}$$

$$v_3(t) = p_3(t)\cos\left(\frac{1}{2}\Omega t\right) + q_3(t)\sin\left(\frac{1}{2}\Omega t\right) \tag{5.8}$$

$$v_4(t) = p_4(t)\cos(\Omega t) + q_4(t)\sin(\Omega t). \tag{5.9}$$

Substituting Eqs. (5.7)-(5.9) into Eqs. (5.4)-(5.6) and using the method of variation of parameters, we obtain the following equations describing p_3, q_3, p_4, q_4, and a_1:

$$\ddot{a}_1 + \omega_1^2 a_1 = H_1 \tag{5.10}$$

$$\frac{1}{2}\Omega\dot{p}_3 = -\frac{1}{4}p_3\sigma_3\cos\left(\frac{1}{2}\Omega t\right)\sin\left(\frac{1}{2}\Omega t\right) - \frac{1}{4}q_3\sigma_3\sin^2\left(\frac{1}{2}\Omega t\right) + \sin\left(\frac{1}{2}\Omega t\right)H_3 \tag{5.11}$$

$$\frac{1}{2}\Omega\dot{q}_3 = \frac{1}{4}p_3\sigma_3\cos^2\left(\frac{1}{2}\Omega t\right) + \frac{1}{4}q_3\sigma_3\sin\left(\frac{1}{2}\Omega t\right)\cos\left(\frac{1}{2}\Omega t\right) + \cos\left(\frac{1}{2}\Omega t\right)H_3 \tag{5.12}$$

$$\Omega\dot{p}_4 = -p_4\sigma_4\cos(\Omega t)\sin(\Omega t) - q_4\sigma_4\sin^2(\Omega t) + \sin(\Omega t)H_4 \tag{5.13}$$

$$\Omega\dot{q}_4 = p_4\sigma_4\cos^2(\Omega t) + q_4\sigma_4\sin(\Omega t)\cos(\Omega t) + \cos(\Omega t)H_4, \tag{5.14}$$

where $\sigma_3 = \Omega^2 - (2\omega_3)^2$ and $\sigma_4 = \Omega^2 - \omega_4^2$ measure the detunings of the resonances.

At this point no approximation to the discretized equations has been made. Next, using trigonometric identities, we eliminate all products of $\cos(k\Omega t)$ and $\sin(k\Omega t)$, where k is a positive integer multiple or submultiple. Then we retain only the slowly-varying terms by setting the coefficients of $\cos(k\Omega t)$ and $\sin(k\Omega t)$ equal to zero. This leads to the following reduced set of equations:

$$\begin{aligned}\ddot{a}_1 + \mu_1\dot{a}_1 + (\omega_1^2 - \upsilon_1)a_1 = &-\Lambda_{1111}a_1^3 + \vartheta_2\left(p_3q_3q_4 - \frac{1}{2}q_3^2p_4 + \frac{1}{2}p_3^2p_4\right) \\ &+\vartheta_3a_1(p_3^2+q_3^2) + \vartheta_4a_1(p_4^2+q_4^2) + \vartheta_5(p_3^2+q_3^2) \\ &+\vartheta_6(p_4^2+q_4^2) - \frac{1}{2}a_{14}a_bp_4 - \Lambda_{1000} + g\alpha_{10}\end{aligned} \tag{5.15}$$

$$\begin{aligned}\frac{1}{2}\Omega\dot{p}_3 = &-\frac{1}{4}\mu_3\Omega p_3 - \frac{1}{8}(\sigma_3 + 2\alpha_{33}(2g+a_b))q_3 - \eta_2q_3(p_4^2+q_4^2) - \eta_4a_1^2q_3 \\ &-\eta_3q_3(p_3^2+q_3^2) - \eta_5a_1q_3 - \eta_6(p_3q_4 - q_3p_4) - \eta_7a_1(p_3q_4 - q_3p_4)\end{aligned} \tag{5.16}$$

$$\begin{aligned}\frac{1}{2}\Omega\dot{q}_3 = &-\frac{1}{4}\mu_3\Omega q_3 + \frac{1}{8}(\sigma_3 + 2\alpha_{33}(2g-a_b))p_3 + \eta_2p_3(p_4^2+q_4^2) + \eta_4a_1^2p_3 \\ &+\eta_3p_3(p_3^2+q_3^2) + \eta_5a_1p_3 + \eta_6(p_3p_4 + q_3q_4) + \eta_7a_1(p_3p_4 + q_3q_4)\end{aligned} \tag{5.17}$$

$$\begin{aligned}\Omega\dot{p}_4 = &-\frac{1}{2}\mu_4\Omega p_4 - \left(\frac{1}{2}\sigma_4 + \kappa_1\right)q_4 - \kappa_2q_4(p_3^2+q_3^2) \\ &-\kappa_3q_4(p_4^2+q_4^2) - \kappa_4a_1^2q_4 - \kappa_5a_1q_4 - \kappa_6p_3q_3 + \kappa_7a_1p_3q_3\end{aligned} \tag{5.18}$$

$$\begin{aligned}\Omega\dot{q}_4 = &-\frac{1}{2}\mu_4\Omega q_4 + \left(\frac{1}{2}\sigma_4 + \kappa_1\right)p_4 + \kappa_2p_4(p_3^2+q_3^2) + \kappa_3p_4(p_4^2+q_4^2) \\ &+\kappa_4a_1^2p_4 + \kappa_5a_1p_4 + \frac{1}{2}\kappa_6(p_3^2-q_3^2) + \frac{1}{2}\kappa_7a_1(p_3^2-q_3^2) - \frac{1}{2}a_1a_b\alpha_{41} - \frac{1}{2}\alpha_{40}a_b\end{aligned} \tag{5.19}$$

The definitions and typical values for the ϑ_i, η_i, κ_i, and α_{ij} are given at the end of the chapter.

Equations (5.15)-(5.19) were obtained in a rather heuristic fashion without a rigorous scaling. The slowly-varying terms were retained without regard to how "small"

they were. This approach was taken after many attempts at a rigorous scaling failed to give a set of equations that captures the characteristics of the motion observed in the experiments. In hindsight, an appropriate scaling can be

$$\omega_1 = O(\varepsilon^{1/2}); \quad a_1 = O(\varepsilon^{1/2}); \quad \dot{a}_1 = O(\varepsilon); \quad \ddot{a}_1 = O(\varepsilon^{3/2})$$
$$p_i = O(\varepsilon^{1/2}); \quad q_i = O(\varepsilon^{1/2}); \quad \dot{p}_i = O(\varepsilon^{3/2}); \quad \dot{q}_i = O(\varepsilon^{3/2})$$
$$\mu_1 = O(\varepsilon^{1/2}); \quad \mu_3 = O(\varepsilon); \quad \mu_4 = O(\varepsilon); \quad \Phi_0 = O(\varepsilon^{1/2})$$
$$\sigma_3 = O(\varepsilon); \quad \sigma_4 = O(\varepsilon),$$

where ε is a positive nondimensional parameter that is artificially introduced to gauge the different quantities. We note that μ_1 is stronger than μ_3 and μ_4 in the ordering scheme. If a_1, p_i, and q_i are chosen to be of the same order and respond with the same frequency, then $\dot{a}_1$, $\dot{p}_i$, and $\dot{q}_i$ should be of the same order. However, if $\dot{a}_1$, $\dot{p}_i$, and $\dot{q}_i$ were assumed to be of the same order, then Eqs. (5.15)-(5.19) would not have been obtained. This points out a difficulty in obtaining Eqs. (5.15)-(5.19) with a rigorous perturbation analysis.

The modal interactions predicted by Eqs. (5.15)-(5.19) have an important characteristic. A commensurate or near commensurate frequency relationship between the high-frequency and low-frequency modes is not required for the modal interactions to occur. The only requirements are a) there is nonlinear coupling between the modes and b) $\omega_i \ll \omega_j$, where ω_i is the low frequency and ω_j is the high frequency.

Equations (5.15)-(5.19) have quadratic and static terms due to a slight bend in the beam. These terms can be thought of as disturbances added to the equations governing a straight beam. The term with α_{40} in Eq. (5.19) is also due to the bend and provides the fourth mode with a small external excitation. Also, we note that $a_1(t)$ is not a modulation term but describes the complete response of the first mode. On the other hand, $p_i(t)$ and $q_i(t)$ describe the modulations associated with the ith mode.

5.2 Theoretical Results

Because we were unable to obtain closed-form solutions to Eqs. (5.15)-(5.19), we used numerical methods to investigate the solutions of these equations. The different branches of fixed points were determined by using an arc-length continuation method (Seydel, 1988). An initial point on a branch, where only one solution was expected, was obtained by numerically integrating Eqs. (5.15)(5.19) for a long time. To find a starting fixed point on the other branches, we varied the initial guesses until a fixed point on another branch was found. To determine the stability of the fixed points, we calculated the eigenvalues of the Jacobi matrix. To determine the branches of periodic solutions, we used a shooting method and a sequential continuation scheme (Seydel, 1988).

In Figs. 5.2a-5.2c, a_1 is the complete response of the first mode and a_3 and a_4, where $a_i = \sqrt{p_i^2 + q_i^2}$, are the amplitudes of the third and fourth modes. Stable fixed points are shown as solid lines and unstable fixed points are shown as broken and dotted lines. We note that a fixed point corresponds to a periodic motion of the structure. Branch ① corresponds to fixed points for which $a_1 \neq 0, p_3 = 0, q_3 = 0, p_4 \neq 0$, and $q_4 \neq 0$. Both of branches ② and ③ correspond to fixed points for which $a_1 \neq 0, p_3 \neq 0, q_3 \neq 0, p_4 \neq 0$, and $q_4 \neq 0$. However, for a given set of parameter values, the value of a_3 on branch ③ is smaller than the corresponding value of a_3 on branch ②. Also, the fixed points on branch ③ are unstable.

In the range 33.00 Hz $\geq f_e \geq$32.754 Hz, only branch ① was found and the fixed points are all stable. At the critical value $f_e \approx$32.754 Hz, a supercritical pitchfork bifurcation occurs in the response of the third mode; that is, a_3. As a result of this pitchfork bifurcation, branch ① becomes unstable for $f_e <$32.754 Hz, as seen in Figs 5.2a-5.2c. Branch ② intersects branch ① at this point. Branch ① regains stability at $f_e \approx$31.763 Hz due to a reverse pitchfork bifurcation in the response of the third

mode, as seen in Figure 5.2b. Branch ③ intersects branch ① at this point. Branch ① remains stable in the range 31.763 Hz ≥ f_e ≥ 31.669 Hz. At f_e≈31.669 Hz, a saddle-node bifurcation of branch ① occurs. On branch ① we have saddle points for 31.669 Hz>f_e>31.682 Hz. At f_e≈31.683 Hz another saddle-node bifurcation occurs on branch ① . The shape of branch ① in this region shows similarities to the frequency-response curve of a Duffing oscillator with a softening-type nonlinearity when subjected to a primary resonance excitation. Also, the peak in the frequency-response curve is near the natural frequency of the fourth mode. Based on these two observations, we attribute this peak and the two saddle-node bifurcations to a primary resonance of the fourth mode. There are no more bifurcations on branch ① in the frequency range considered.

Branch ② intersects branch ① at the pitchfork bifurcation point f_e≈32.754 Hz. For 32.754 Hz ≥ f_e ≥ 32.026 Hz, branch ② is stable. In this region, when f_e is decreased, a_3 increases rapidly with no jump, as seen in Fig. 5.2b. In addition, a_1 increases while a_4 decreases, as seen in Fig. 5.2a and 5.2c. As f_e is decreased further, we find that a supercritical Hopf bifurcation occurs at f_e≈32.026 Hz. Increasing f_e from 31.00 Hz, we find that a subcritical Hopf bifurcation occurs at f_e≈31.971 Hz. In the range 31.971 Hz<f_e<32.026 Hz, branch ② is unstable with a complex conjugate pair of eigenvalues having a positive real part. Branch ② is stable in the remainder of the region considered.

In Fig. 5.3, we show the frequency-response curves for all three modes in a small region of the control parameter that includes the Hopf bifurcation points. The solid lines in Fig. 5.3 represent stable fixed points, the dashed lines represent unstable fixed points, and the circles represent the amplitudes of the periodic solutions. During the course of the sequential continuation, the monodromy matrix associated with the periodic solution was monitored to determine if additional bifurcations occurred. No bifurcations of the

periodic solution were found. We note that the amplitudes of the periodic solution increase smoothly from the right and continue past the second Hopf bifurcation point. This indicates that the Hopf bifurcation at $f_e \approx 32.026$ Hz is supercritical and that the Hopf bifurcation at $f_e \approx 31.971$ Hz is subcritical. We have not shown the unstable branch of periodic solutions in the vicinity of the subcritical Hopf bifurcation point in Fig. 5.3. On the periodic solution branch, the magnitude of a_1 is much larger than the magnitudes of a_3 and a_4. We note that a periodic solution of Eqs. (5.15)-(5.19) corresponds to a quasiperiodic response of the cantilever beam, which was also observed in the experiments.

Branch ③ intersects branch ① at the pitchfork bifurcation point at $f_e \approx 31.763$ Hz, as shown in Figs. 5.2a-c. Branch ③ consists entirely of unstable fixed points. This branch corresponds to the lower unstable branch of a principal parametric resonance of the third mode. Turning points occur at $f_e \approx 31.525$ Hz and $f_e \approx 31.649$ Hz. In this region we see that the response curve of the first mode makes a loop. We note that the turning-points in this region are bifurcations because the number of solutions changes between one and two locally and an eigenvalue goes to zero. However, these turning-point bifurcations are not saddle-node bifurcations because the branch is unstable on both sides of the bifurcation points.

5.3 Comparison of Experimental and Theoretical Results

In Fig. 5.4, we show experimentally obtained frequency-response curves for a base acceleration of 0.85 grms. Figure 5.4a is for a downward sweep in frequency and Fig. 5.4b is for an upward sweep in frequency. There is a strong qualitative similarity between the experimental frequency-response curves and the theoretical frequency-response curves. We mention that in Fig. 5.4 an approximate conversion from strains to relative displacements was made by multiplying each mode's contribution to the response

by f_i/f_3, where f_i is the natural frequency of the ith mode. This conversion gives a better measure of the relative displacements observed during the experiment.

In the experimental downward sweep in frequency, we observed a motion with the third mode being dominant from 32.74 Hz to 31.00 Hz. Beyond f_e=31.00 Hz, the third mode dropped out of the response. The first mode was present from 32.40 Hz to 31.00 Hz with a large oscillating response between 32.24 Hz and 32.17 Hz. Part of the first-mode response consisted of a static offset. The fourth mode had a small contribution to the response throughout the experiment. This experimentally observed motion corresponds to the theoretically obtained branch ② . The large first-mode response observed in the experiments corresponds to the region between the Hopf bifurcation points in the analysis, where large periodic motions of the first mode were predicted (see Fig. 5.3).

In the experimental downward sweep in frequency, we also observed a response consisting of the first and fourth modes from f_e=32.80 Hz to f_e=32.74 Hz. This type of response was not predicted by the analysis and might be due to a combination resonance. An analysis similar to that of Dugundji and Mukhopadhyay (1973) may predict this response.

In the experimental upward sweep in frequency, we observed a motion consisting of only the fourth mode from f_e=31.00 Hz to f_e=32.17 Hz. A small increase in the magnitude of the fourth mode occurred near 31.90 Hz. The first and third modes were activated at 32.17 Hz and seemed to suppress the response of the fourth mode. The contribution of the first mode to the response was large from 32.17 Hz to 32.24 Hz and died out at 32.40 Hz. The third mode continued to contribute to the response until 32.74 Hz. For the remainder of the sweep, there was only a small response due to the fourth mode. The first part of the upward sweep in frequency corresponds to branch ① in the analysis, which corresponds to $a_1 \neq 0, p_3 = 0, q_3 = 0, p_4 \neq 0$, and $q_4 \neq 0$. The

observed increase in a_4 corresponds to the primary resonance of the fourth mode. When branch ① loses stability, one would expect the response to jump to the available stable branch ②, which corresponds to $a_1 \neq 0, p_3 \neq 0, q_3 \neq 0, p_4 \neq 0$, and $q_4 \neq 0$. On this branch, a_4 is smaller than those on branch ①, as observed in the experiment. The large a_3 component corresponds to a principal parametric resonance of the third mode. The large first-mode response observed in the experiments corresponds to the region between the Hopf bifurcation points in the analysis, where large periodic solutions of a_1 were predicted.

In the range of f_e in which the third mode was excited, the analytical results are in very good qualitative agreement with the experimental results. We show in Fig. 5.5 the spectrum and Poincaré section of an experimentally obtained three-mode response when the first-mode component was large. We show in Fig. 5.6 the spectra and phase portraits of numerically obtained responses from the averaged equations in the region between the Hopf bifurcation points. When we observed the three-mode response in the experiments, there were sidebands about the $\frac{1}{2}f_e$ and f_e peaks in the spectrum. The sideband spacing f_m varied throughout the frequency sweep. The frequency of the first-mode component of the response was equal to f_m. In the excitation frequency range between 32.22 Hz and 32.19 Hz, f_m was approximately 0.60 Hz, which is close to the natural frequency of the first mode . This resulted in a response with a large first-mode component, as shown in Figs. 5.3a and 5.3b. The spectrum has discrete lines with f_m and f_e being the discernible incommensurate frequencies. We show in Fig. 5.5 a Poincaré section of this motion; the points form two small loops. The length of time taken to collect the 512 points for the Poincaré section was about 16.0 seconds. The spectrum and the Poincaré section indicate a two-period quasi-periodic motion in the time span considered. From 600 seconds of data, the pointwise dimension was found to be about 2.25 for a delay of 0.33 seconds at n=10. The dimension calculation indicates a chaotically modulated motion when the

response of the beam is examined over a longer length of time. This chaotically modulated motion might be a result of the noise and other disturbances which may be present in the experiments but not modeled in the analysis.

Information from the experimental observations guided the theoretical development. The characteristics of the experimentally obtained three-mode response suggests that the following mechanisms were involved in the responses. A principal parametric resonance excited the third mode and a weak primary resonance excited the fourth mode, as indicated by the frequency of the main response of the third mode being at $\frac{1}{2}f_e$ and the frequency of the main response of the fourth mode being at f_e. Also, the shape of the frequency-response curve of the third mode is similar to a frequency-response curve of a nonlinear softening oscillator subjected to a principal-parametric resonance excitation. An interaction between the first mode and the modulations of the third and fourth modes resulted in an exchange of energy between the three modes, as indicated by the response frequency of the first mode being equal to the modulation frequency.

The base acceleration used in the experiments was 0.85 g rms. In the numerical simulations an acceleration of 0.85 g rms was not sufficient for exciting the first mode. So the level of excitation was increased to 1.55 g rms in order to have the first mode participate in the response. This discrepancy between the experimental and analytical results could not be accounted for.

5.4 Concluding Remarks

The interaction between the first mode and modulations associated with the third and fourth modes is a newly observed mechanism for transferring energy from a high-frequency excitation to a low-frequency mode. The analytical model developed captures

the essential characteristics of this modal interaction. Also, the analytical model predicts that a static response of a low-frequency mode can be produced due to interactions with the dynamic response of high-frequency modes. Guided by this result, further experiments revealed that this static response of the first mode was present in the response of the cantilever beam. The form of the developed equations can be used in future studies to gain insight into the behavior of flexible structures that have many modes of interest with widely separated frequencies.

Appendix 5

Definitions of the coefficients used in Chapter 5.

$$\vartheta_1 = -\left(\Lambda_{1010} + \Lambda_{1001} + \Lambda_{1100}\right) + \alpha_{11} g$$

$$\vartheta_2 = \frac{1}{2}\Omega^2\left(\Gamma_{1433} + \Gamma_{1334}\right) - \frac{1}{2}\left(\Lambda_{1334} + \Lambda_{1343} + \Lambda_{1433}\right)$$

$$\vartheta_3 = \frac{1}{4}\Omega^2\Gamma_{1313} - \frac{1}{2}\left(\Lambda_{1133} + \Lambda_{1313} + \Lambda_{1331}\right)$$

$$\vartheta_4 = \Omega^2\,\Gamma_{1414} - \frac{1}{2}\left(\Lambda_{1144} + \Lambda_{1414} + \Lambda_{1441}\right)$$

$$\vartheta_5 = \frac{1}{4}\Omega^2\Gamma_{1303} - \frac{1}{2}\left(\Lambda_{1033} + \Lambda_{1303} + \Lambda_{1330}\right)$$

$$\vartheta_6 = \Omega^2\,\Gamma_{1404} - \frac{1}{2}\left(\Lambda_{1044} + \Lambda_{1404} + \Lambda_{1440}\right)$$

$$\vartheta_7 = -\left(\Lambda_{1101} + \Lambda_{1011} + \Lambda_{1110}\right)$$

$$\eta_1 = \frac{1}{4}\Omega^2\Gamma_{3003} - \frac{1}{2}\left(\Lambda_{3003} + \Lambda_{3030} + \Lambda_{3300}\right)$$

$$\eta_2 = \frac{5}{8}\Omega^2\Gamma_{3434} - \frac{1}{4}\left(\Lambda_{3344} + \Lambda_{3434} + \Lambda_{3443}\right)$$

$$\eta_3 = \frac{1}{8}\Omega^2\Gamma_{3333} - \frac{3}{8}\Lambda_{3333}$$

$$\eta_4 = \frac{1}{8}\Omega^2\,\Gamma_{3113} - \frac{1}{2}\left(\Lambda_{3113} + \Lambda_{3311} + \Lambda_{3131}\right)$$

$$\eta_5 = \frac{1}{4}\Omega^2\left(\Gamma_{3103} + \Gamma_{3013}\right) - \left(\Lambda_{3013} + \Lambda_{3130} + \Lambda_{3301}\right)$$

$$\eta_6 = \frac{1}{8}\Omega^2\left(\Gamma_{3404} + 4\Gamma_{3340} + \Gamma_{3034}\right) - \frac{1}{2}\left(\Lambda_{3034} + \Lambda_{3340} + \Lambda_{3403}\right)$$

$$\eta_7 = \frac{1}{8}\Omega^2\left(\Gamma_{3414} + 4\Gamma_{3341} + \Gamma_{3134}\right) - \frac{1}{2}\left(\Lambda_{3134} + \Lambda_{3341} + \Lambda_{3413}\right)$$

$$\kappa_1 = \frac{1}{4}\Omega^2\Gamma_{4004} - \frac{1}{2}\left(\Lambda_{4004} + \Lambda_{4040} + \Lambda_{4400}\right) + \frac{1}{2}\alpha_{44}g$$

$$\kappa_2 = \frac{5}{8}\Omega^2\Gamma_{4334} - \frac{1}{4}\left(\Lambda_{4334} + \Lambda_{4343} + \Lambda_{4433}\right)$$

$$\kappa_3 = \frac{1}{2}\Omega^2\Gamma_{4444} - \frac{3}{8}\Lambda_{4444}$$

$$\kappa_4 = \Omega^2\Gamma_{4114} - \frac{1}{2}\left(\Lambda_{4114} + \Lambda_{4411} + \Lambda_{4141}\right)$$

$$\kappa_5 = \Omega^2\left(\Gamma_{4104} + \Gamma_{4014}\right) - \left(\Lambda_{4014} + \Lambda_{4140} + \Lambda_{4401}\right)$$

$$\kappa_6 = \frac{1}{4}\Omega^2\left(2\Gamma_{4033} + \Gamma_{4303}\right) - \frac{1}{2}\left(\Lambda_{4033} + \Lambda_{4303} + \Lambda_{4330}\right)$$

$$\kappa_7 = \frac{1}{4}\Omega^2\left(2\Gamma_{4133} + \Gamma_{4313}\right) - \frac{1}{2}\left(\Lambda_{4133} + \Lambda_{4313} + \Lambda_{4331}\right)$$

The numerical values of the coefficients when f_e=32.00 Hz are

$\vartheta_2 = -31.46431,$ $\eta_2 = 128.96815,$ $\kappa_1 = 0.02849,$
$\vartheta_3 = 0.89189,$ $\eta_3 = 213.1081,$ $\kappa_2 = 129.3159,$
$\vartheta_4 = 2.25321,$ $\eta_4 = -0.76103,$ $\kappa_3 = 3616.2123,$
$\vartheta_5 = 0.01065,$ $\eta_5 = 0.09806,$ $\kappa_4 = 2.22095,$
$\vartheta_6 = 0.02183,$ $\eta_6 = -0.16983,$ $\kappa_5 = 1.97769,$
$\eta_7 = -16.64064,$ $\kappa_6 = -0.16753,$
$\kappa_7 = -31.60610,$

$$\alpha_{ij} = \int_0^{z_n} z_n \Phi_i\left(\Phi_j''(s - z_n) + \Phi_j'\right) ds$$

$$\Gamma_{ijkl} = \frac{1}{2} z_3 \int_0^{z_3} \Phi_i \left(\Phi_j' \int_{z_3}^{s} \int_0^{s} \Phi_k' \Phi_l' \, ds ds \right)' ds$$

$$\Lambda_{ijkl} = z_3 \int_0^{z_3} \Phi_i \left(\Phi_j' \left(\Phi_k' \Phi_l'' \right)' \right)' ds$$

$$\mu_i = \int_0^{z_n} \Phi_i \mu \, ds$$

$\alpha_{40} = -0.01262848,$ $\alpha_{41} = -0.873137,$ $\alpha_{10} = 0.0000003,$ $\alpha_{10} = 0.0000006$

$$\Phi_i = \cosh(\frac{z_i s}{z_n}) - \cos(\frac{z_i s}{z_n}) + k_i\left(\sin\left(\frac{z_i s}{z_n}\right) - \sinh\left(\frac{z_i s}{z_n}\right)\right)$$

$$k_i = \frac{\cosh(z_i s) + \cos(z_i s)}{\sinh(z_i s) + \sin(z_i s)}$$

for i=1,3,4, and

$$\Phi_0 = 0.040\cosh\left(\frac{1.13s}{z_n}\right) - 0.040\cos\left(\frac{1.13s}{z_n}\right) + 0.068\sin\left(\frac{1.13s}{z_n}\right) - 0.068\sinh\left(\frac{1.13s}{z_n}\right)$$

To calculate Φ_0, we measured the static deflection along the length of the beam. Then we fit the data to a function similar to the mode shapes and used the conditions $\Phi_0(0) = \Phi_0(0) = 0$.

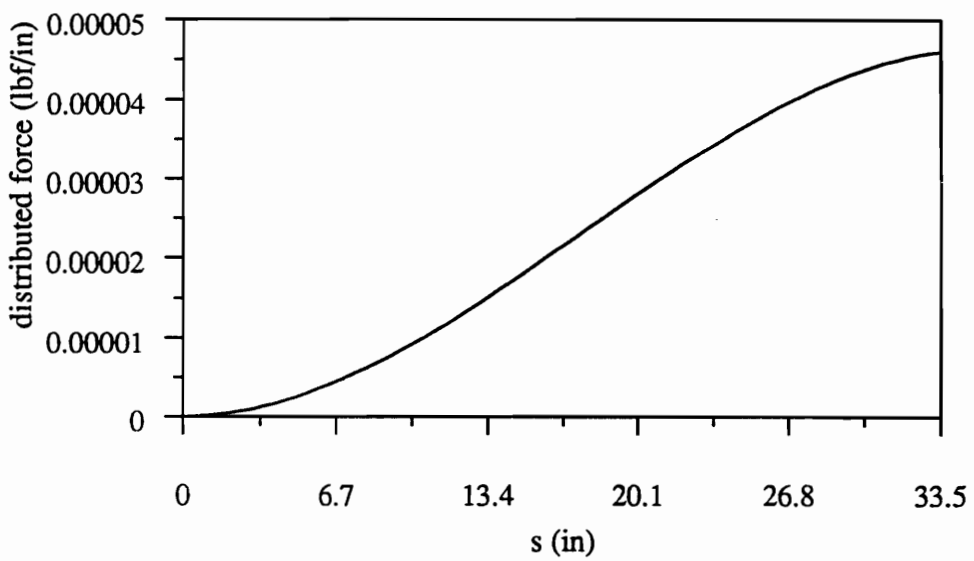

Fig. 5.1 Distribution force needed to produce the static deflection $\Phi_0(s)$

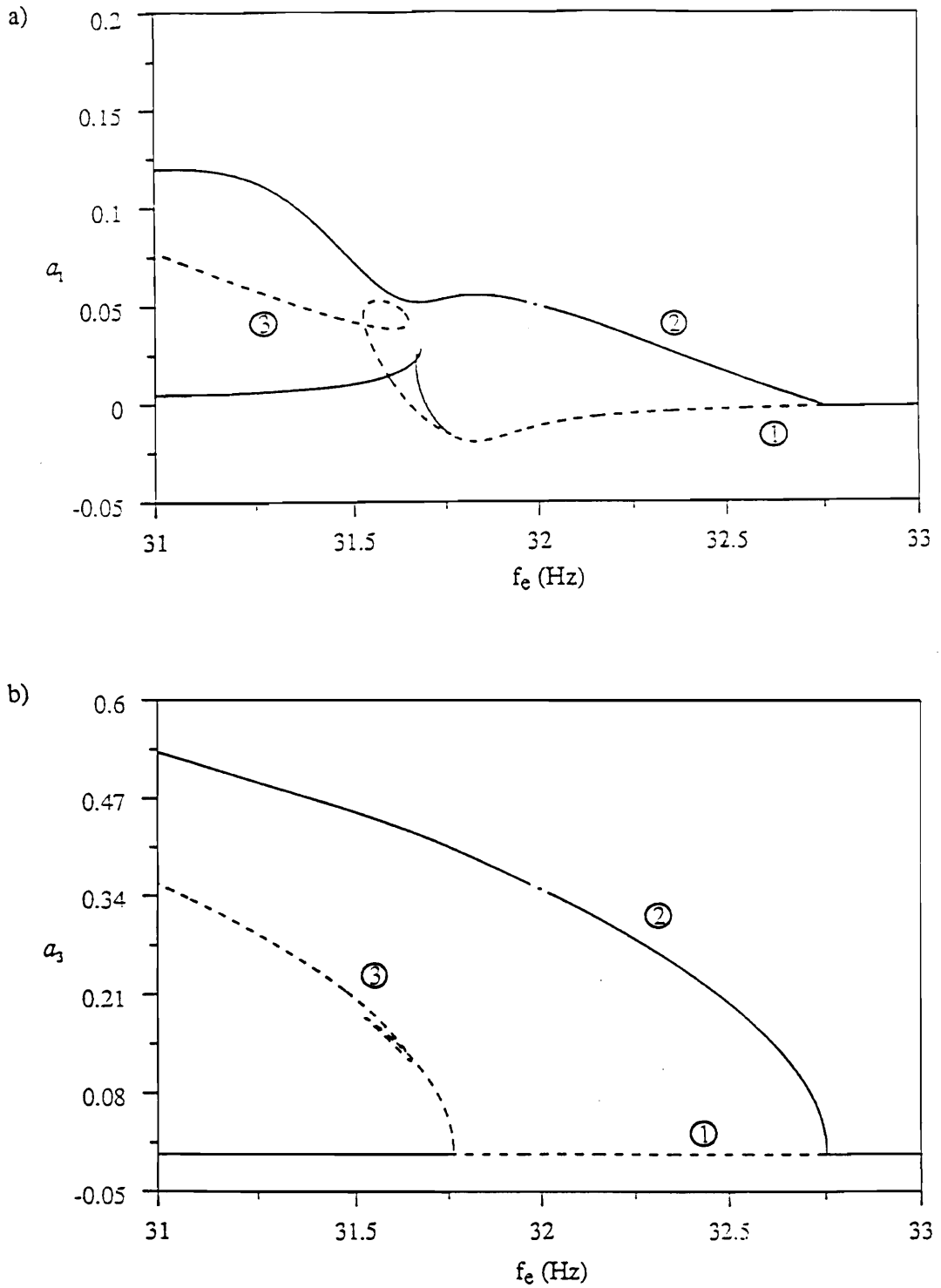

Fig. 5.2 Frequency-response curves: a) complete response of the first mode a_1, b) amplitude of the third mode a_3, and c) amplitude of the fourth mode a_4.

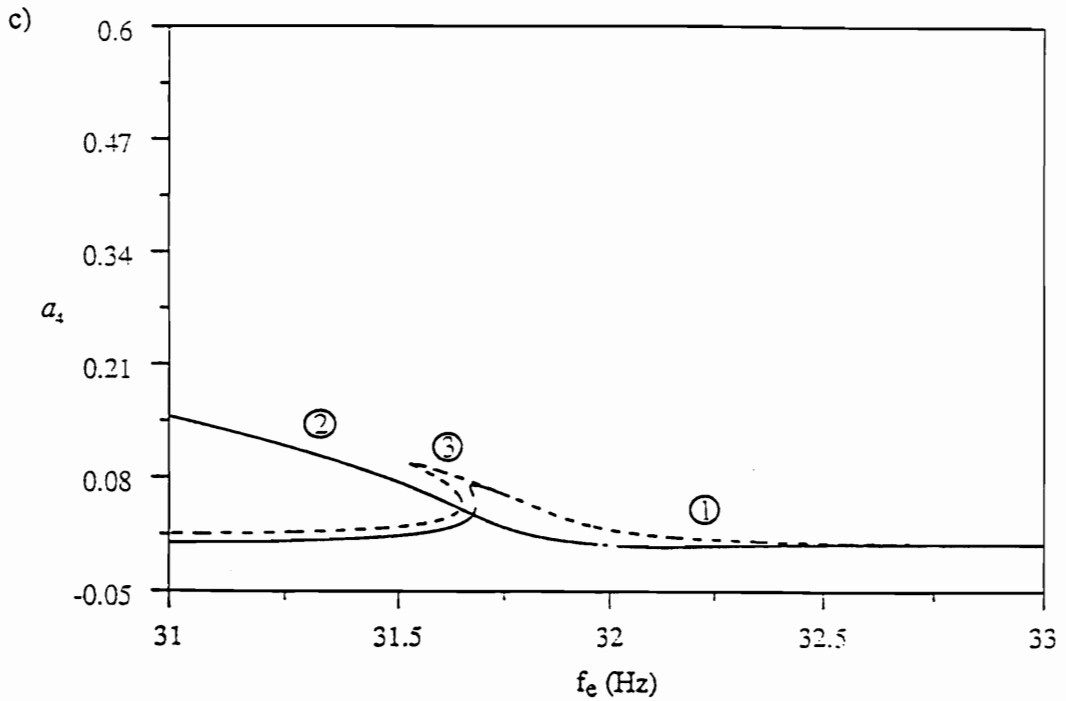

Fig. 5.2 Frequency-response curves: a) complete response of the first mode a_1, b) amplitude of the third mode a_3, and c) amplitude of the fourth mode a_4.

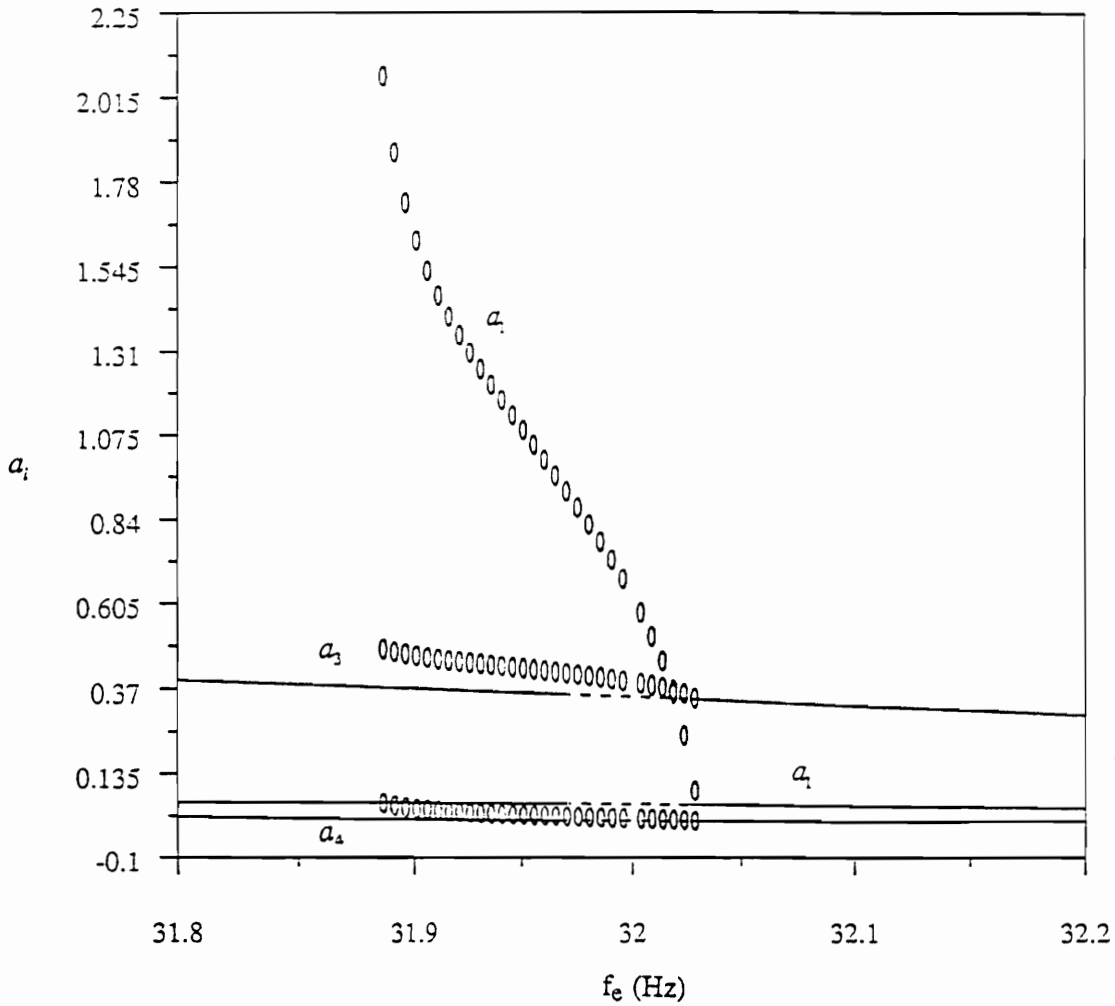

Fig. 5.3 Amplitudes of periodic solutions and magnitudes of nearby fixed points.

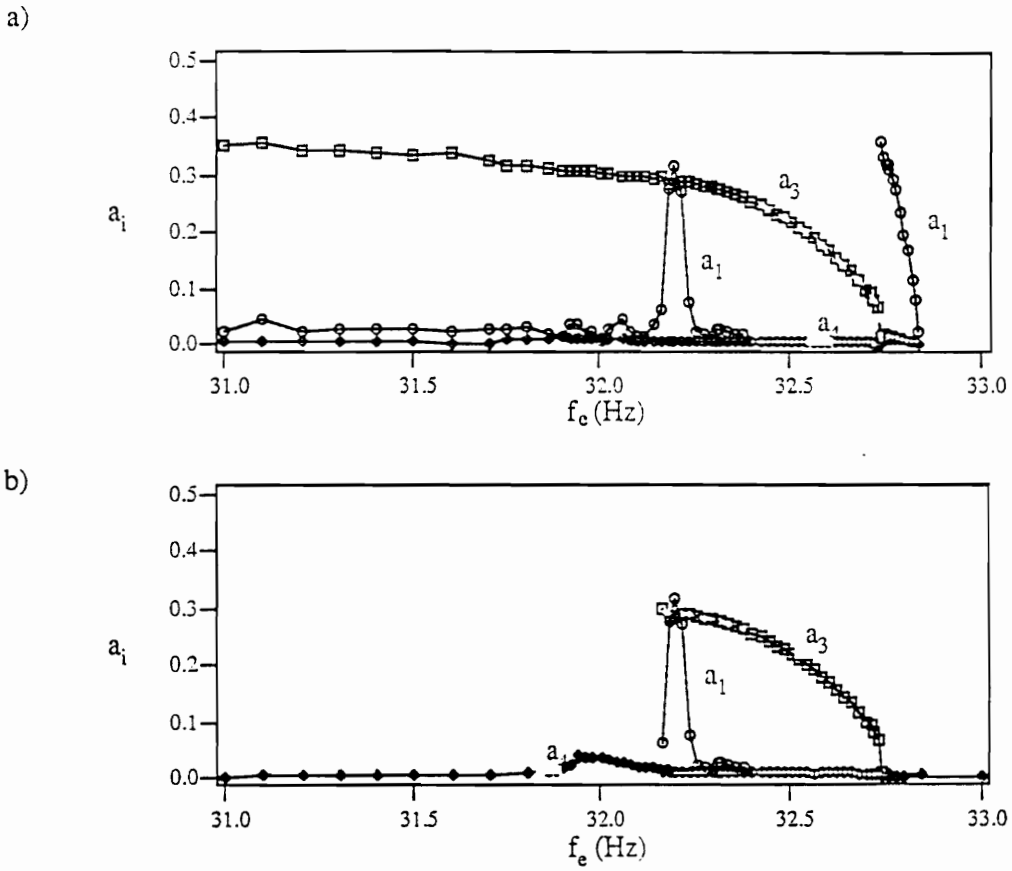

Fig. 5.4 Experimentally obtained stationary frequency-response curves: a)downward sweep and b) upward sweep.

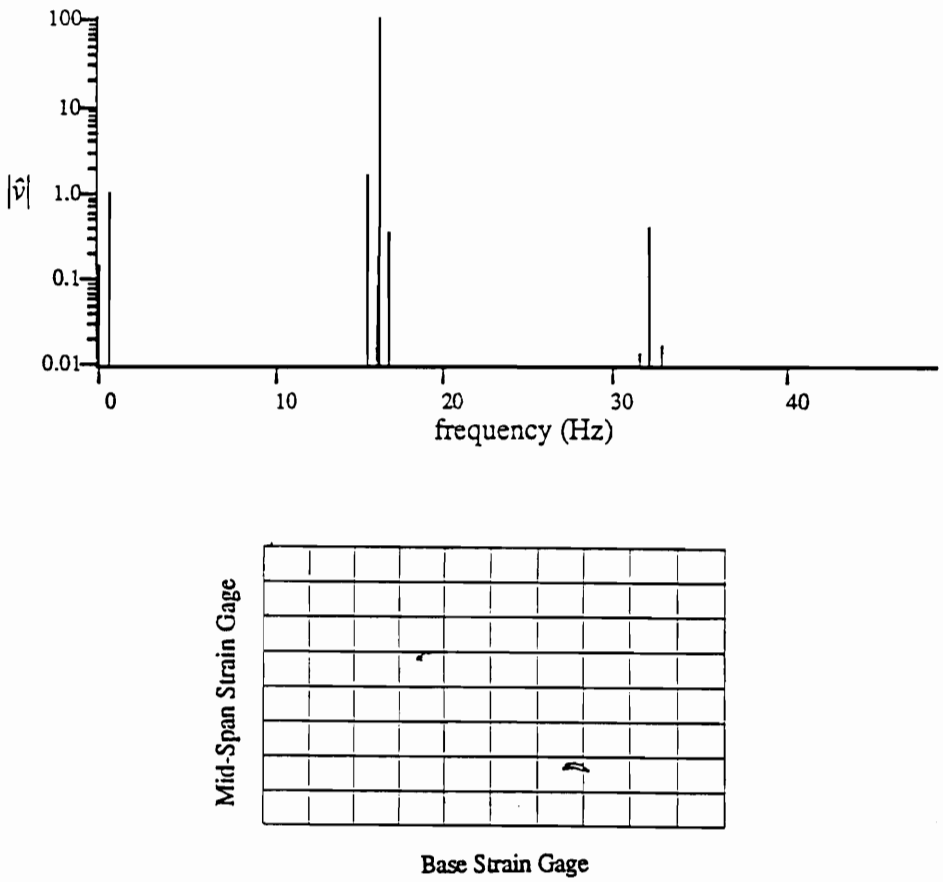

Fig. 5.5 An experimentally obtained frequency spectrum and a Poincaré section for the three-mode motion.

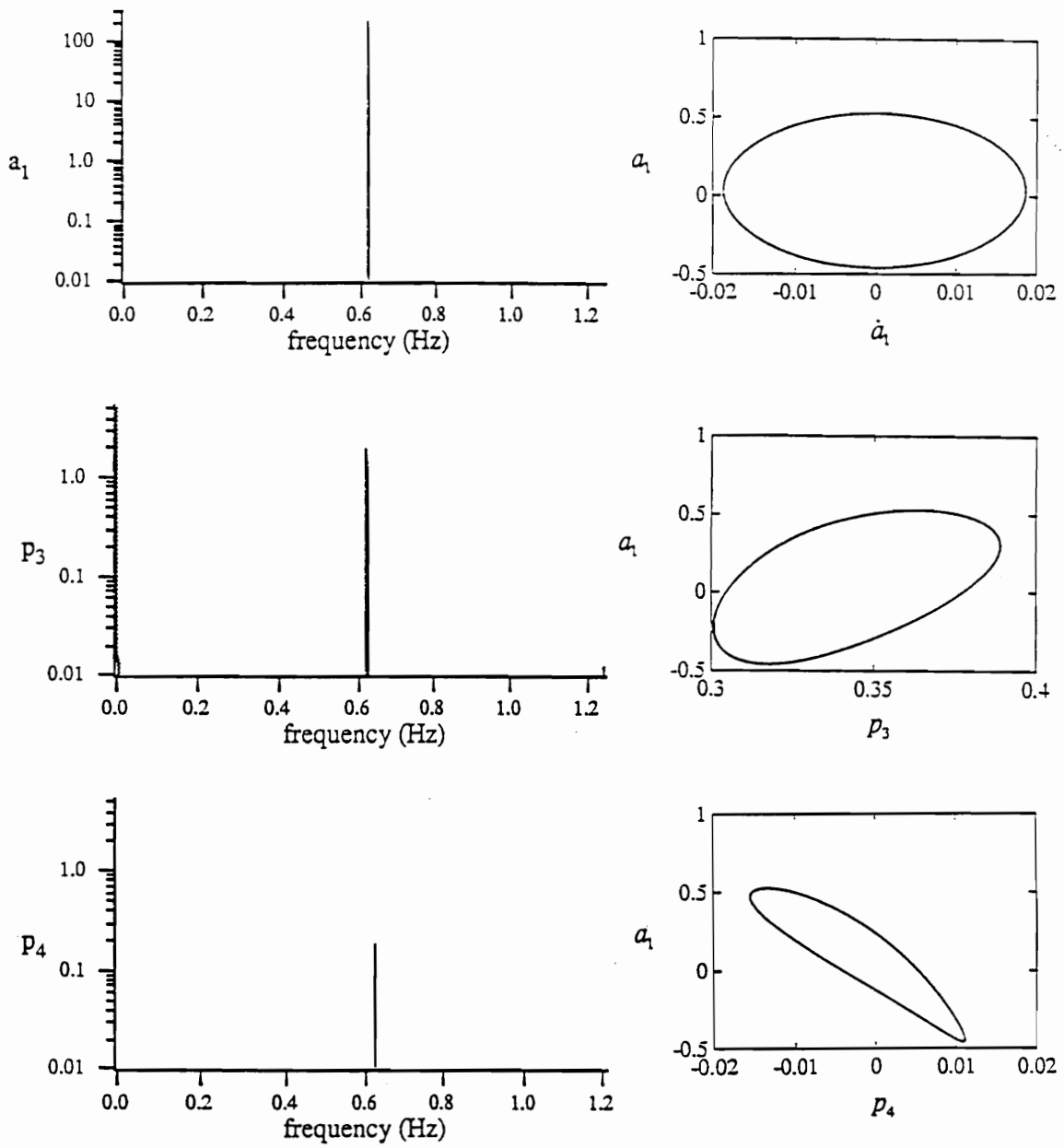

Fig. 5.6 Numerically obtained spectra and phase portraits obtained from the averaged equations.

6. Natural Frequencies and Mode Shapes of Laminated Composite Plates: Experiments and FEM

The objective of this chapter is to provide accurate experimental natural frequencies of several composite plates that can be used to validate future theoretical developments. In this study, we tried to avoid some of the problems encountered in similar previous studies, such as, mass loading the structure, using the maximum response amplitude as a measure of the natural frequency, choice of the material properties, and unknown boundary conditions.

We determined the natural frequencies and mode shapes of the four composite plates by using experimental modal-analysis techniques. We tested each plate in a free-hanging, cantilever, and fixed-fixed configuration for a total of twelve configurations. In order to eliminate mass loading of the structures, we excited them with an instrumented impact hammer and measured the response with strain gages. We also calculated the natural frequencies and mode shapes of the plates by using a finite-element analysis. To determine the elastic material properties for use in the present finite-element analysis and future theoretical analyses, we conducted tensile tests on samples made of the same material and cured with the same cure cycle. Comparing the experimental and theoretical results, we find that the difference between them is less than previously published results.

6.1 Plate Descriptions

In this section, we present the layups, dimensions, and material properties of the plates. We also describe the methods used to obtain the material properties.

For this study, we manufactured four plates with the following layups: $[-15/+15/+15/-15/+15/-15]_s$, $[-30/+30/+30/-30/+30/-30]_s$, $[90/0]_{3s}$, $[90/30/-30/-30/30/90]_s$.

We will refer to these plates as ±15°, ± 30°, cross-ply, and quasi-isotropic plates, respectively.

In Fig. 6.1 we show a sketch that defines the dimensions of the plates. The dimensions of each of the four plates are given in Table 6.1. For each plate, we used a micrometer to measure its thickness (t) at eight places. Then, we averaged the results, and listed them in Table 6.1. The thickness varied by approximately ± 0.001 inches throughout the plate. We measured the length (L) and width (W) with a measuring tape.

Table 6.1. Plate dimensions.

	t (inches)	L (inches)	W (inches)
±15°	0.139	13.44	13.88
±30°	0.138	14.09	13.31
cross ply	0.142	13.31	14.25
quasi-isotropic	0.138	13.28	13.81

The plate properties used in the finite-element analysis are given in Table 6.2. We measured the inplane properties and calculated their means and standard deviations. To obtain values for the out-of-plane properties, we multiplied the measured inplane values by correction factors. For the out-of-plane values that were calculated from measured values, only the mean values are given. The correction factors were chosen so that the ratio of the inplane to out-of-plane properties are the same as those given by Hyer (1989) for a graphite-polymer composite. Specifically, $E_3=1.25/1.30E_2$, $\nu_{13}=\nu_{12}$, $\nu_{23}=0.49/0.30\nu_1$, $G_{23}=0.90/1.03G_{12}$, and $G_{13}=G_{12}$. Varying these out-of-plane properties by 10% in the finite-element models did not make a noticeable change in the frequencies. We concluded that these values for the out-of-plane properties are reasonable for this study. This may not be the case for other applications, such as failure prediction.

To determine the inplane material properties, we made two 12" x 12" plates of the same material and cured them using the same cure cycle as the plates investigated. One plate was a uniaxial plate and the other was a symmetric cross-ply plate. A diamond saw was used to cut out specimens to ensure that the edges were not chipped and delaminated due to the cutting process. We cut the uniaxial plate into ten test specimens: five had dimensions 11.0" x 1.0" x 0.092" with the fibers being parallel to the long edges, and five had dimensions 5.0" x 2.0" x 0.092" with the fibers being perpendicular to the long edges. We cut the cross-ply plate into five test specimens with dimension 6.0" x 1.0" x 0.1". The cuts were made at 45 degrees to the plate's edges. This resulted in five $\pm 45^{\circ}$ specimens. Each of the specimen were instrumented with a biaxial strain gage and pulled in an Instrom test machine. The load cell had a 10V=10,000 lbf calibration for the 0° specimens and a 10V=2000 lbf calibration for all other specimens. The cross-head rate was 0.10 in/min for all tests. The axial and transverse strains and the forces were measured and recorded simultaneously with a PC based data acquisition system. We later plotted and curve fit the data to obtain the material properties. We used the tensile tests of the uniaxial specimens to determine the moduli of elasticity E_{11} and E_{22} and Poisson's ratios ν_{12} and ν_{21} similar to the ASTM D 3039-76 test procedure for inplane tensile properties. We used the tensile tests of the cross-ply specimens to determine the inplane shear modulus G_{12} similar to the ASTM D 3518-76 test procedure for inplane shear properties. Because we were not interested in the strength information, we did not test the specimens to failure.

To determine the density, we divided the weight by the measured volume. This was then converted to the appropriate units for mass and volume.

Table 6.2 Plate material properties.

	Mean Value	Standard Deviation (5 samples)
E_{11}	22.14 $*10^6$ lbf/in^2	0.485 $*10^6$ lbf/in^2
E_{22}	1.281 $*10^6$ lbf/in^2	0.060 $*10^6$ lbf/in^2
E_{33}	1.165 $*10^6$ lbf/in^2	
ν_{12}	0.297	0.0136
ν_{23}	0.485	
ν_{13}	0.297	
G_{12}	0.765 $*10^6$ lbf/in^2	0.031 $*10^6$ lbf/in^2
G_{23}	0.668 $*10^6$ lbf/in^2	
G_{13}	0.765 $*10^6$ lbf/in^2	
ρ	1.46 $*10^{-4}$ lbf$*$s^2/in^4	0.031 $*10^{-4}$ lbf$*$s^2/in^4 (4 samples)

The selected plates gave a large variation in the degree of anisotropy as can be observed by comparing the elements of the A and D matrices of the classical laminate theory (CLT), which are given in Table 6.3. For example, $D_{11}/D_{22}=13.44$ for the $\pm 15^\circ$ angle ply plate and $D_{11}/D_{22}=1.355$ for the quasi-isotropic plate. Because the plates are symmetric, there is no bending stretching coupling and hence all of the elements of the B matrix are zero for all plates. For comparison purposes, the A and D matrices were calculated using the average ply thickness and not the actual thickness of each plate.

Table 6.3 CLT stiffness matrices for the four plates calculated using the average ply thickness of 0.0116 in.

	A ($*10^{-6}$ lbf/in)			D ($*10^{-3}$ lbf*in)		
±15°	2.732	0.225	0.000	4.414	0.363	-0.0297
	0.225	0.203	0.000	0.363	0.328	-0.0030
	0.000	0.000	0.278	-0.0297	-0.0030	0.449
±30°	1.854	0.568	0.000	2.996	0.918	-0.0417
	0.568	0.394	0.000	0.918	0.637	-0.0150
	0.000	0.000	0.621	-0.0417	-0.0150	1.004
cross-ply	1.639	0.0533	0.000	2.059	0.086	0.000
	0.0533	1.639	0.000	0.086	3.238	0.000
	0.000	0.000	0.107	0.000	0.000	0.172
quasi-isotropic	1.296	0.396	0.000	1.843	0.564	0.083
	0.396	1.296	0.000	0.564	2.498	0.030
	0.000	0.000	0.450	0.083	0.030	0.650

6.2 Test Setup and Analysis

Each plate was tested in three configurations: free-hanging, cantilever, and fixed-fixed for a total of twelve test configurations. We show schematics of the free-hanging, cantilever, and fixed-fixed configurations, in Figs. 6.1-6.3 respectively. In Fig. 6.4, we show the dimensions of the fixture used for the cantilever and fixed-fixed configurations. This fixture was bolted to a 20" x 16" x 4" block of aluminum, which in

turn was effectively attached to a rigid ground. In Table 6.4, we give the effective plate dimensions for each of the twelve configurations.

Table 6.4 Effective plate dimensions of the twelve configurations.

Description	t (in.)	L (inches)	W (inches)
±15°			
free-hanging	0.139	13.88	13.44
cantilever	0.139	12.55	13.44
fixed-fixed	0.139	10.00	13.44
±30°			
free-hanging	0.138	13.31	14.09
cantilever	0.138	12.31	14.09
fixed-fixed	0.138	10.00	14.09
cross ply			
free-hanging	0.142	14.25	13.31
cantilever	0.142	12.31	13.31
fixed-fixed	0.142	10.00	13.31
quasi-isotropic			
free hanging	0.138	13.28	13.84
cantilever	0.138	11.28	13.84
fixed-fixed	0.138	10.00	13.84

In Fig. 6.5, we show a schematic of the instrumentation used. We used a GenRad 2515 to acquire the data and calculate the strain frequency-response functions (SFRF). We also used the GenRad 2515 to perform the modal analyses with the SDRC

Modal-Plus software. To minimize the mass loading of the plates, we chose to excite the structures with an instrumented impact hammer and measure the responses with strain gages.

In calculating the SFRFs we used 512 lines of resolution. We chose this resolution because the analyzer is built in such a way that 512 lines of resolution are the most convenient for modal analysis. For the free-hanging and cantilever configurations the tested frequency range was 0-512 Hz. For the fixed-fixed configuration, the tested frequency range was 0-1024 Hz. To obtain the natural frequencies, mode shapes, and damping coefficients, we used a polyreference technique available in the SDRC MODAL-PLUS software (1985). For the free-hanging and cantilever configurations, we obtained 6 X 6 grids of SFRFs. For the fixed-fixed configurations, we obtained 5 X 5 grids of SFRFs

When using an impact hammer to excite a structure, one must exercise care to ensure the quality of the obtained data. Corelli and Brown (1984) reviewed some problems associated with impact testing and means for dealing with them. With these problems in mind, we took a number of steps to ensure the quality of the obtained data. We monitored the hammer impulse and a small part of the strain-gage response on an oscilloscope that was set to trigger by the impulse and freeze the screen. The oscilloscope had a much higher sampling rate than that used with the signal analyzer. The use of the oscilloscope enabled us to perform several checks. Based on the peak value observed on the oscilloscope, we set the full range value of the analyzer to prevent overloads. Also, we checked for double hits. We often observed double hits and manually discarded the data if it was not discarded by the signal analyzer. In addition, we checked the hammer impulse width to ensure that the analyzer acquired at least 6 samples during the hammer impulse. If the analyzer acquired fewer samples during the impulse, then either the sample period or the hammer tip was changed for that test. Additionally,

we checked the autospectrum of the impulse to make sure that there was less that 20 db roll off of the signal in the measurement frequency range. We used an appropriate force window for the hammer signal from the windows available on the signal analyzer. In addition, we used an exponential window for both the hammer and strain-gage signals.

When using strain gages to measure the response of a structure, one can obtain the natural frequencies and modal damping factors with conventional modal-analysis techniques. In addition, if one gage is used and different SFRFs are obtained by moving the force (hammer impact location), then mode shapes proportional to the displacement mode shapes are obtained (Bernasconi and Ewins, 1989). We used thin foil strain gages. Typically the coherence is good only around the peaks for SFRF. This is sufficient to extract the modal constants with good precision (Bernasconi and Ewins, 1989).

For the finite-element analysis (FEA), we used the commercial FEA code ABAQUS. We used the eight noded quadrilateral element S8R with five integration points through the thickness (ABAQUS User's Manual, 1989). For all the cases, we used a uniform 20 X 20 grid of elements. To determine this pattern, we calculated FEA results with a 10 X 10 mesh. We then refined the mesh until there were no significant changes in the calculated natural frequencies. For the free-hanging configurations, we added soft springs between the plate and ground to prevent the rigid-body modes from having zero natural frequencies. It is interesting to note that the free-hanging configurations required a finer element mesh than the cantilever or the fixed-fixed configurations for the natural frequencies to converge.

6.3 Results and Comparisons

In Tables 6.5-6.16, we present the experimental natural frequencies, experimental damping coefficients, FEA natural frequencies, and the percent difference between the experimental and FEA natural frequencies. In Figs. 6.6-6.17, we show contour plots of

the experimentally obtained mode shapes. In Figs. 6.18-6.29, we show displacement plots of the calculated modes shapes. We present the experimental contour plots to show the symmetry or asymmetry of the modes. Because of the coarseness of the experimental grids, one cannot easily use them to identify the modes, so we did not include them. To identify the experimental modes and compare them with the FEA results, we observed the animated mode shapes on the signal analyzer. For the FEA mode shapes, we show displacement plots with fine meshes so that the type of modes can be easily identified. Using both the experimental contour and FEA displacement plots, one can identify each mode. By comparing the experimental and FEA mode shapes, we found that, in all cases, the order of the modes by frequency was the same for the experiments and the FEA.

In Tables 6.5-6.8, we show the results for the four free-hanging configurations. The boundary conditions in this case are well known because there are no clamps. The clamps tend not to be rigid, as was assumed in the analysis, but to have some finite stiffness. The agreement between the experimental and FEM results is very good for the $\pm 15^{\circ}$ and $\pm 30^{\circ}$ plates. For the $\pm 15^{\circ}$ plate, the worst case is the second mode with a 3.5% discrepancy and an average percent absolute discrepancy of only 1.74%. For the $\pm 30^{\circ}$ plate, the worst case is the third mode with a -3.6% discrepancy and an average percent absolute discrepancy of 1.69 The agreement between the experimental and FEM results for the cross-ply plate is good with the worst case having 5.8% discrepancy and an average percent discrepancy of 2.42. The agreement between the experimental and FEM results for the quasi-isotropic plate is not as good as the others with the worst case having a discrepancy of -8.9% and an average percent absolute discrepancy of 4.38.

In Tables 6.9-6.12, we show the results for the four cantilever configurations. For the $\pm 15^{\circ}$ plate, the agreement between the experimental and FEM results is slightly better for the cantilever plate than for the free-hanging plate. For the $\pm 15^{\circ}$ plate, the worst case is the second mode with a 3.3% discrepancy and an average percent absolute discrepancy

of only 1.51. The agreement between the experimental and FEM results is slightly worse for the ±30° cantilever plate compared to the ±30° free-hanging plate. For the ±30° plate, the worst case is the third mode with a 3.8% discrepancy and an average percent absolute discrepancy of 1.88. The agreement between the experimental and FEM results for the cantilever cross-ply plate is much worse than that for the free-hanging cross-ply plate with the worst case having a 10.0% discrepancy and an average percent absolute discrepancy of 5.72. The agreement between the experimental and FEM results for the quasi-isotropic plate is better for the cantilever configuration than for the free-hanging configuration with the worst case having a 3.8% discrepancy and an average percent absolute discrepancy of 1.58.

In Tables 6.13-6.16, we show the results for the four fixed-fixed configurations. The fixed-fixed configurations have the most uncertainty boundary conditions compared with the other two configurations. We do not know how close the clamps were to ideal rigid clamps. With the fixed-fixed configuration, there is a potential for a slippage of the plate between the clamps due to midplane stretching. Also the length of the plates were shorter for the fixed-fixed configurations than for the other two configurations. The shorter length and the fixed-fixed boundary conditions resulted in natural frequencies that are higher than those for the other two configurations. We speculate that plate modes with higher natural frequencies tend to interact more with the clamp motions as the frequencies approach those of the clamps. The agreement between the experimental and FEM results is much worse for the fixed-fixed configurations compared to the other two configurations. For the ±15° plate the worst case is the first mode with a 10.9% discrepancy and an average percent absolute discrepancy of 4.41. For the ±30° plate, the worst case is the first mode with a 14.0% discrepancy and an average percent absolute discrepancy of 6.31. For the cross-ply plate, the worst case is the fourth mode with a 7.9% discrepancy and an average percent absolute discrepancy of 3.58. For the quasi-

isotropic plate, the worst case is the fifth mode with a 6.9% discrepancy and an average percent absolute discrepancy of 4.88.

Table 6.5 Modal analysis results and comparison with finite-element results for the free-hanging ±15° plate.

Finite-Element Frequencies (Hz)	Experimental Frequencies (Hz)	Percent Difference	Experimental Damping Coef.
71.84	72.40	-0.8	0.0020
90.31	87.26	+3.5	0.0015
196.09	193.58	-1.3	0.0016
197.72	201.69	-2.0	0.0023
284.97	291.19	-2.1	0.0005
338.07	338.49	-0.1	0.0017
339.77	345.04	-1.5	0.0004
393.35	404.00	-2.6	0.0023
475.11	483.87	-1.8	0.0010

Table 6.6 Modal analysis results and comparison with finite-element results for the free-hanging ±30° plate.

Finite-Element Frequencies (Hz)	Experimental Frequencies (Hz)	Percent Difference	Experimental Damping Coef.
84.92	82.77	+2.6	0.0025
130.74	130.97	-0.2	0.0006
209.32	217.23	-3.6	0.0009
260.69	263.56	-1.1	0.0026
280.11	281.50	-0.5	0.0012
353.18	361.49	-2.2	0.0009
474.71	478.97	-0.9	0.0017

Table 6.7 Modal analysis results and comparison with finite-element results for the free-hanging cross-ply plate.

Finite-Element Frequencies (Hz)	Experimental Frequencies (Hz)	Percent Difference	Experimental Damping Coef.
58.47	55.28	+5.8	0.0060
203.60	206.98	-1.6	0.0016
233.67	227.60	+2.7	0.0026
235.21	236.00	+0.1	0.0033
261.18	252.27	+3.5	0.0023
391.34	388.19	+0.8	0.0019

Table 6.8 Modal analysis results and comparison with finite-element results for the free-hanging quasi-isotropic plate.

Finite-Element Frequencies (Hz)	Experimental Frequencies (Hz)	Percent Difference	Experimental Damping Coef.
116.02	110.17	+5.3	0.00052
169.08	168.52	-0.3	0.00058
213.19	233.94	-8.9	0.0004
295.68	282.50	-4.7	0.0006
304.34	313.47	-2.9	0.00059
510.78	490.12	+4.2	0.0011

Table 6.9 Modal analysis results and comparison with finite-element results for the ±15° cantilever plate.

Finite-Element Frequencies (Hz)	Experimental Frequencies (Hz)	Percent Difference	Experimental Damping Coef.
13.96	14.00	-0.5	0.0023
55.73	53.94	+3.3	0.0017
86.89	85.99	+1.0	0.0022
182.69	177.79	+2.8	0.0015
242.77	240.82	+0.8	0.0028
307.14	312.98	-1.9	0.0006
356.02	350.58	+1.6	0.0021
436.01	437.10	-0.2	0.0087
485.35	489.42	-0.8	0.0081

Table 6.10 Modal analysis results and comparison with finite-element results for the ±30° cantilever plate.

Finite-Element Frequencies (Hz)	Experimental Frequencies (Hz)	Percent Difference	Experimental Damping Coef.
18.93	18.24	+3.8	0.0009
79.61	78.06	+2.0	0.0007
113.15	108.61	+4.2	0.0022
248.39	249.71	-0.5	0.0023
256.89	253.58	+1.3	0.0009
345.23	341.25	+1.2	0.0028
488.93	482.20	+1.4	0.0024

Table 6.11 Modal analysis results and comparison with finite-element results for the cross-ply cantilever plate.

Finite-Element Frequencies (Hz)	Experimental Frequencies (Hz)	Percent Difference	Experimental Damping Coef.
40.84	37.48	+9.0	0.0114
57.09	58.93	-3.1	0.0035
246.61	224.29	+10.0	0.0101
255.58	245.12	+4.3	0.0541
276.64	292.68	-5.4	0.0067
407.53	397.57	+2.5	0.01716

Table 6.12 Modal analysis results and comparison with finite-element results for the quasi-isotropic cantilever plate.

Finite-Element Frequencies (Hz)	Experimental Frequencies (Hz)	Percent Difference	Experimental Damping Coef.
43.69	43.78	-0.2	0.0067
91.28	87.96	+3.8	0.0020
235.50	229.18	+2.8	0.0064
279.33	278.23	+0.4	0.0115
349.93	347.53	+0.7	0.0027

Table 6.13 Modal analysis results and comparison with finite-element results for the ±15° fixed-fixed plate.

Finite-Element Frequencies (Hz)	Experimental Frequencies (Hz)	Percent Difference	Experimental Damping Coef.
138.26	124.69	+10.9	0.0118
191.82	184.24	+4.1	0.0040
381.42	354.18	+7.7	0.0167
422.60	422.12	+0.1	0.0073
460.40	447.45	+2.9	0.0031
720.07	675.13	+6.7	0.0291
750.21	726.44	+3.3	0.0077
839.14	817.05	+2.7	0.0057
904.94	917.32	-1.3	0.0026

Table 6.14 Modal analysis results and comparison with finite-element results for the ±30° fixed-fixed plate.

Finite-Element Frequencies (Hz)	Experimental Frequencies (Hz)	Percent Difference	Experimental Damping Coef.
189.15	165.91	+14.0	0.0091
265.56	251.61	+5.5	0.0034
483.18	465.75	+3.7	0.0139
522.88	481.48	+8.6	0.0055
632.49	602.12	+5.0	0.0034
851.65	841.03	+1.3	0.0047
944.99	907.08	+4.2	0.0087
1027.4	949.84	8.2	0.0251

Table 6.15 Modal analysis results and comparison with finite-element results for the cross-ply fixed-fixed plate.

Finite-Element Frequencies (Hz)	Experimental Frequencies (Hz)	Percent Difference	Experimental Damping Coef.
410.98	404.30	+1.7	0.0181
419.61	414.89	+1.1	0.00224
504.43	487.04	+3.6	0.0052
806.54	747.49	+7.9	0.00203

Table 6.16 Modal analysis results and comparison with finite-element results for the quasi-isotropic fixed-fixed plate.

Finite-Element Frequencies (Hz)	Experimental Frequencies (Hz)	Percent Difference	Experimental Damping Coef.
353.21	341.03	+3.6	0.0312
388.59	381.59	+1.8	0.0034
525.97	495.69	+6.1	0.0056
809.32	763.23	+6.0	0.0026
967.81	905.72	+6.9	0.0183

6.4 Summary and Discussion

We presented experimental modal-analysis results for twelve different configurations of laminated composite plates. We compared these results with FEA results obtained with a commercial FEA program. We presented material properties that were obtained experimentally from the same materials with the same cure cycle. These properties were used in the FEA. Comparisons between the experimental and FEA results for the free-hanging and cantilever configurations are very good except for the free-hanging quasi-isotropic and cantilever cross-ply cases. Comparisons between the experimental and FEA results for the fixed-fixed configurations are not as good. We believe that the increase in the percent difference between the experimental and FEA results for the fixed-fixed configuration is due to the non-ideal boundary conditions.

In this study, we tried to avoid some of the problems encountered by similar previous studies, such as mass loading the structure, using the maximum amplitude as a measure of the natural frequency, choice of the material properties, and unknown boundary conditions. Moreover, experimentally obtained properties for the material are

included. The results of the free-hanging configuration provide accurate experimental natural frequencies for several composite plates, these results can be used to validate future theoretical developments. The results of the fixed-fixed configuration can be used to provide possible explanations for the discrepancies between the measured and calculated natural frequencies previously reported in the literature.

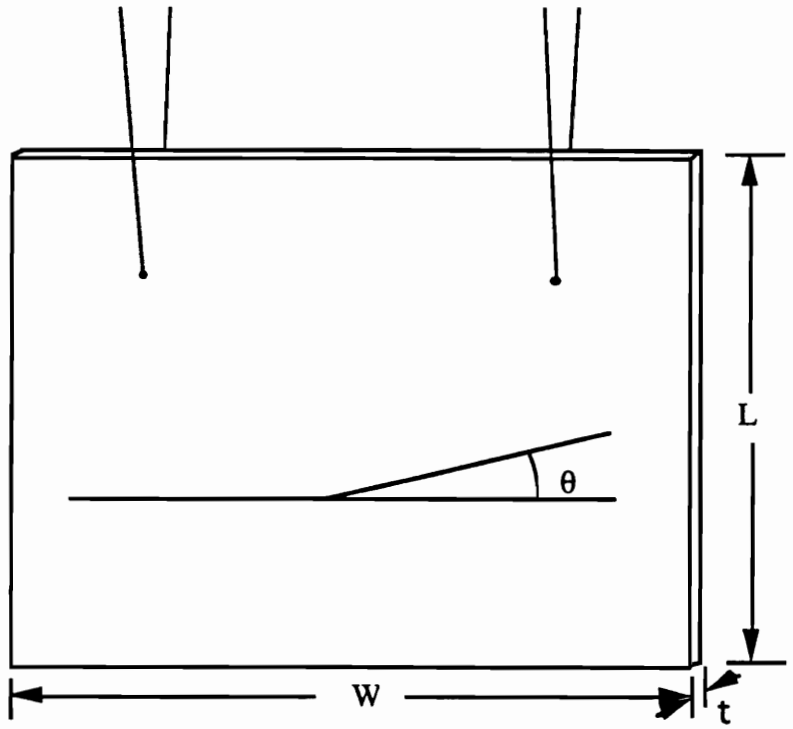

Fig. 6.1 Free-hanging plate description and plate dimension definitions.

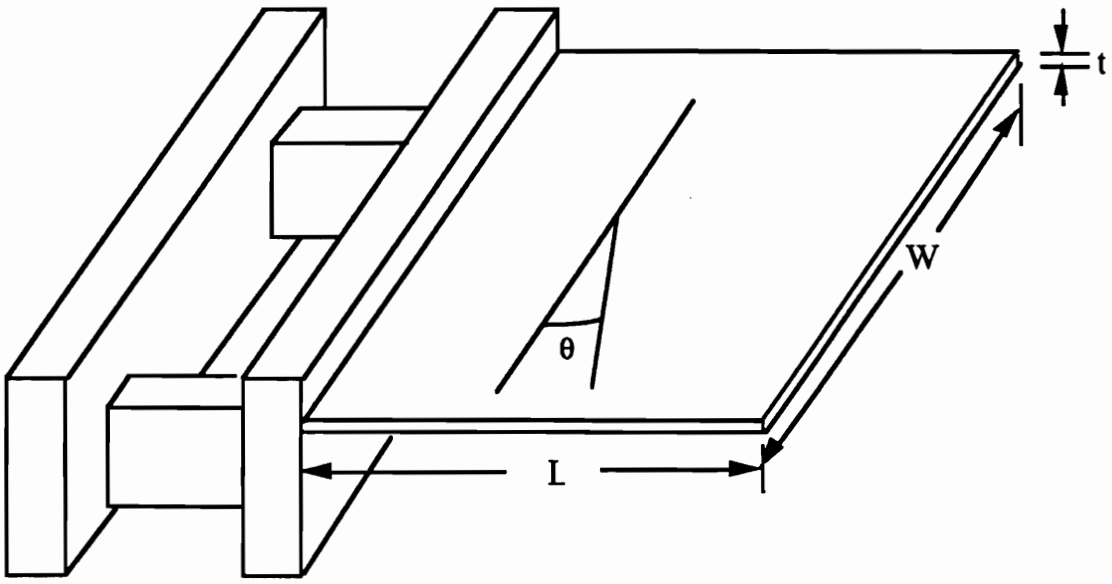

Fig. 6.2 Cantilever plate configuration.

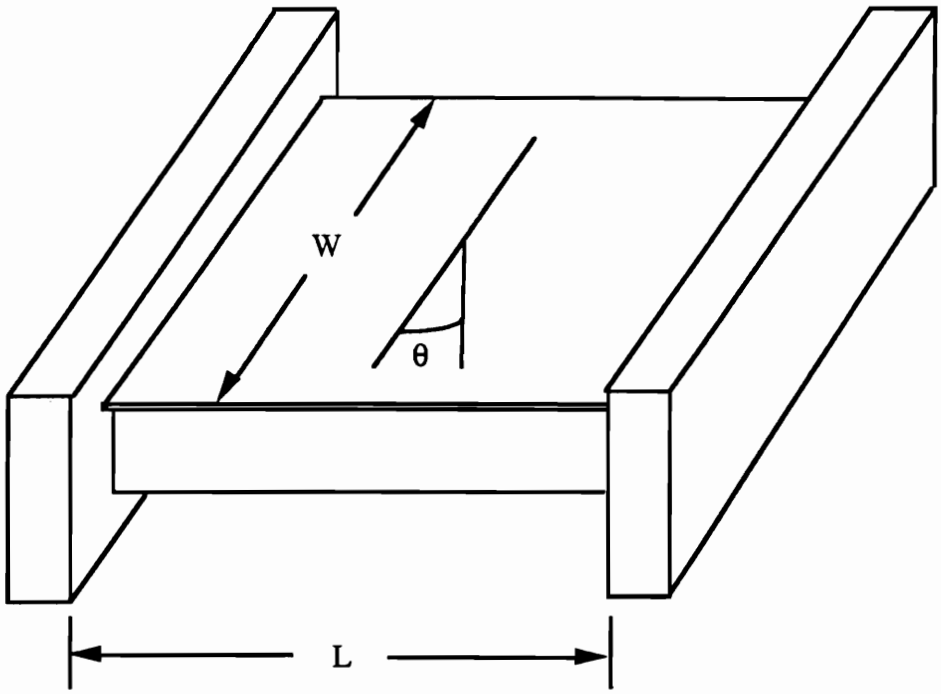

Fig. 6.3 Fixed-fixed plate configuration.

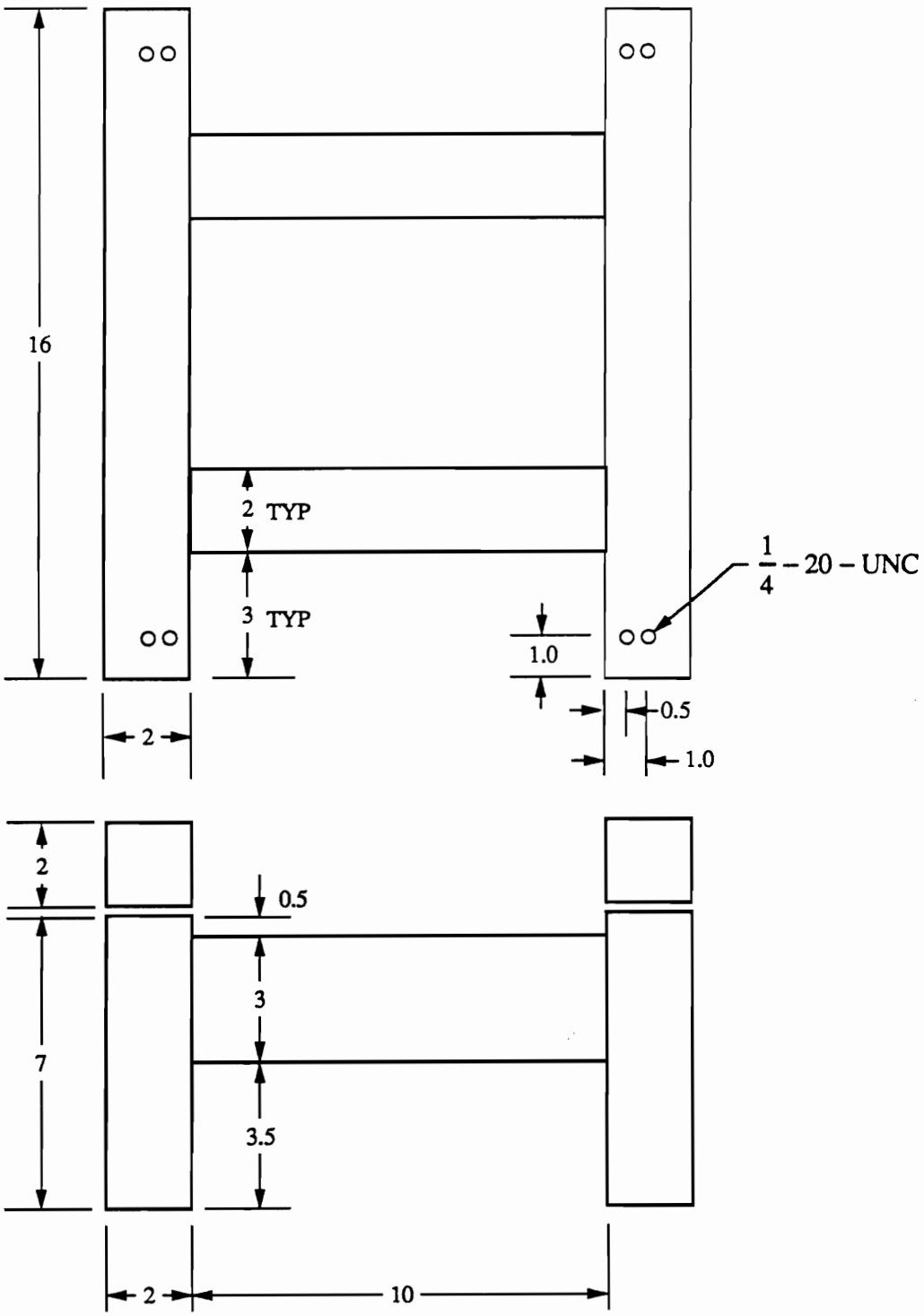

Fig. 6.4 Details of the clamp used for the cantilever and fixed-fixed configurations.

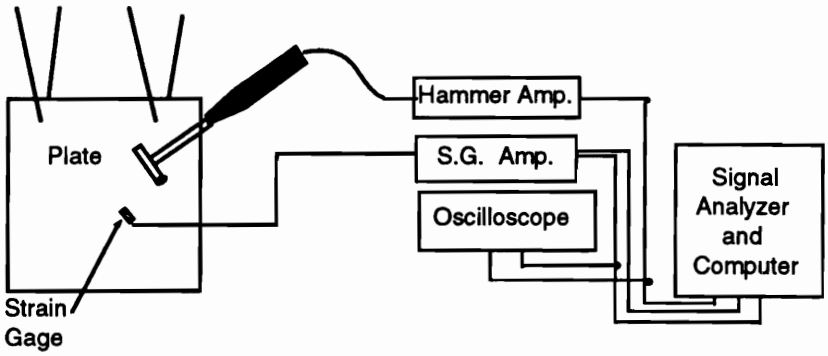

Fig. 6.5 Schematic of the modal analysis test setup.

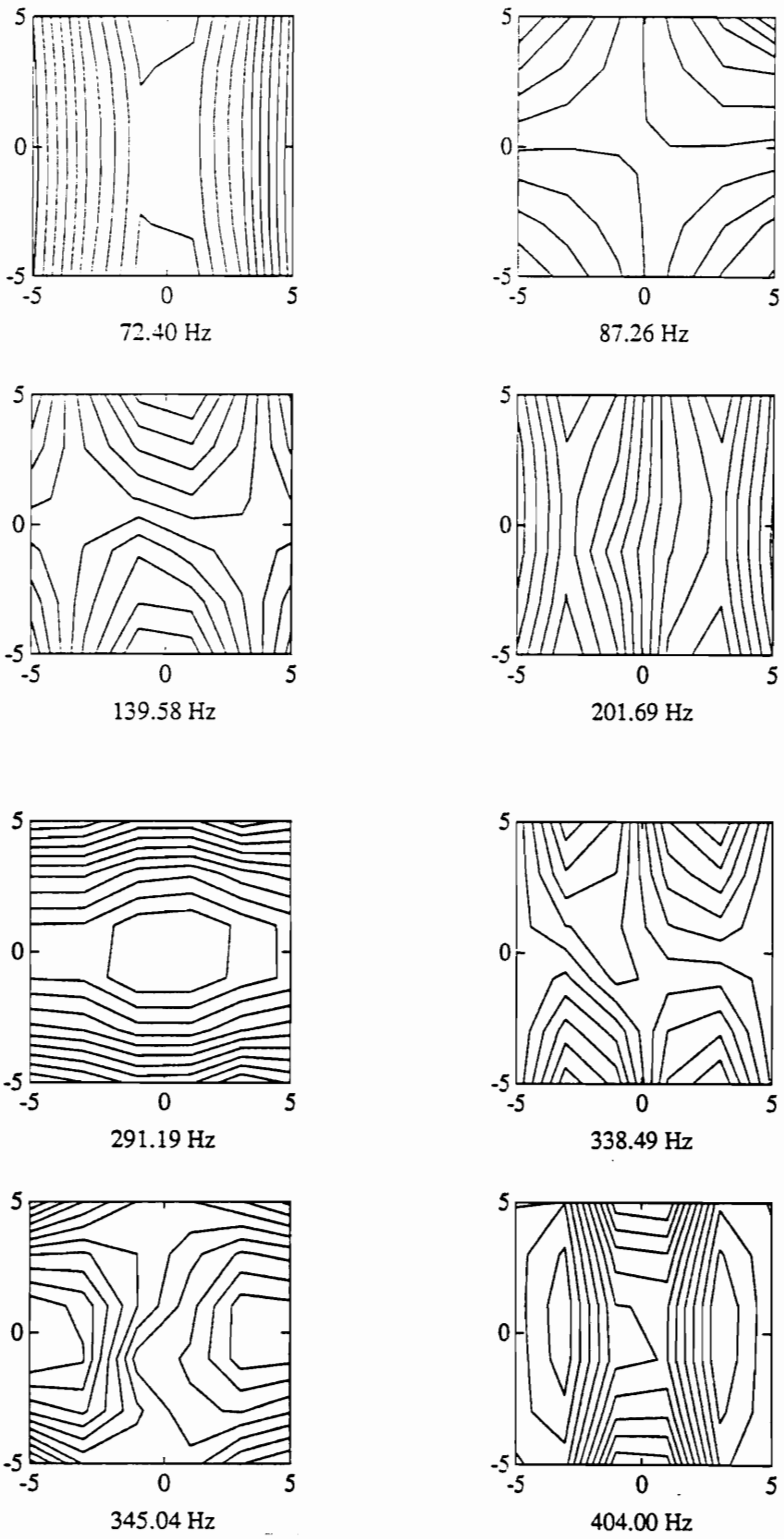

Fig. 6.6 Contour plots of experimentally obtained mode shapes for the free-hanging ±15° plate configuration.

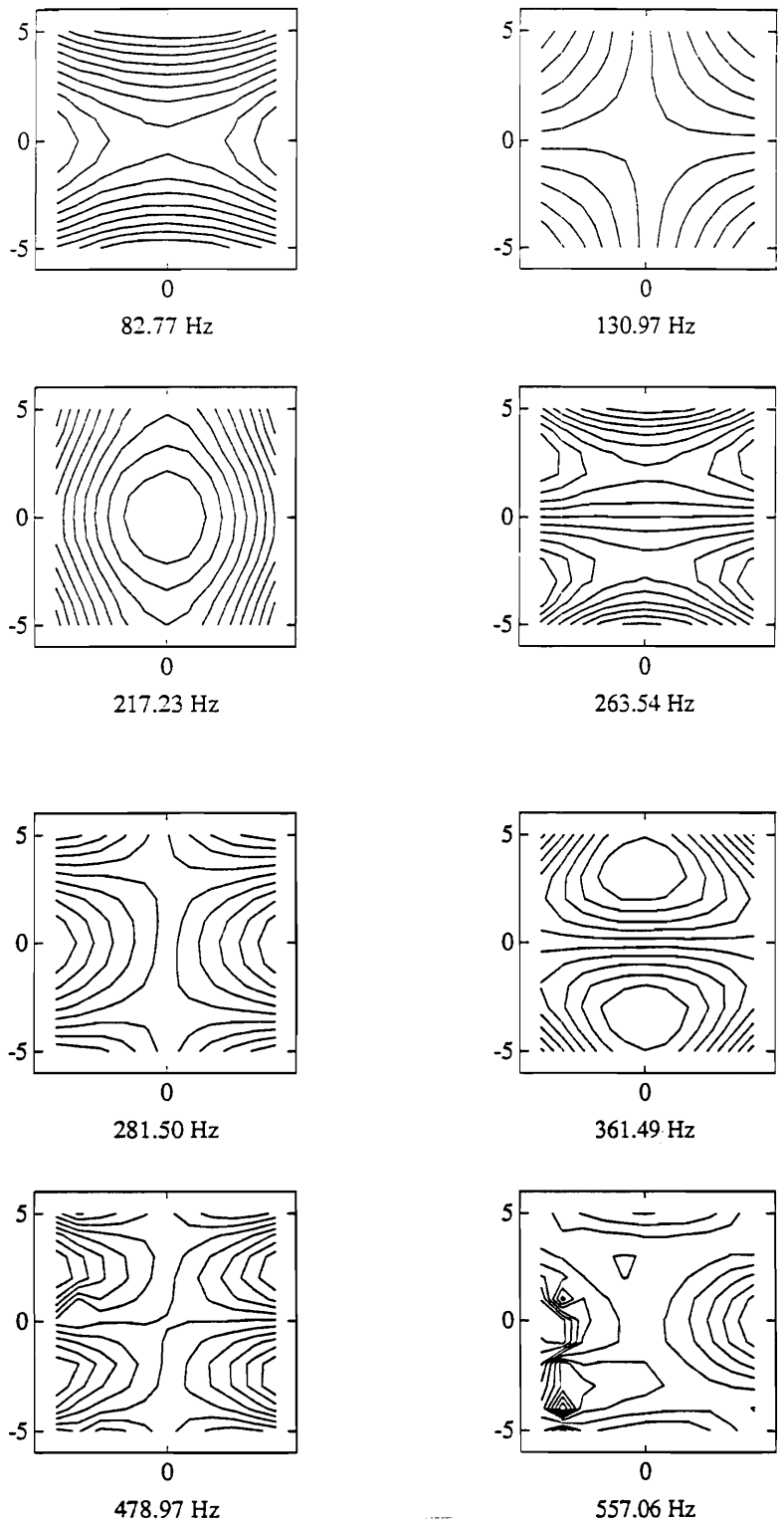

Fig. 6.7 Contour plots of experimentally obtained mode shapes for the free-hanging ±30° plate configuration.

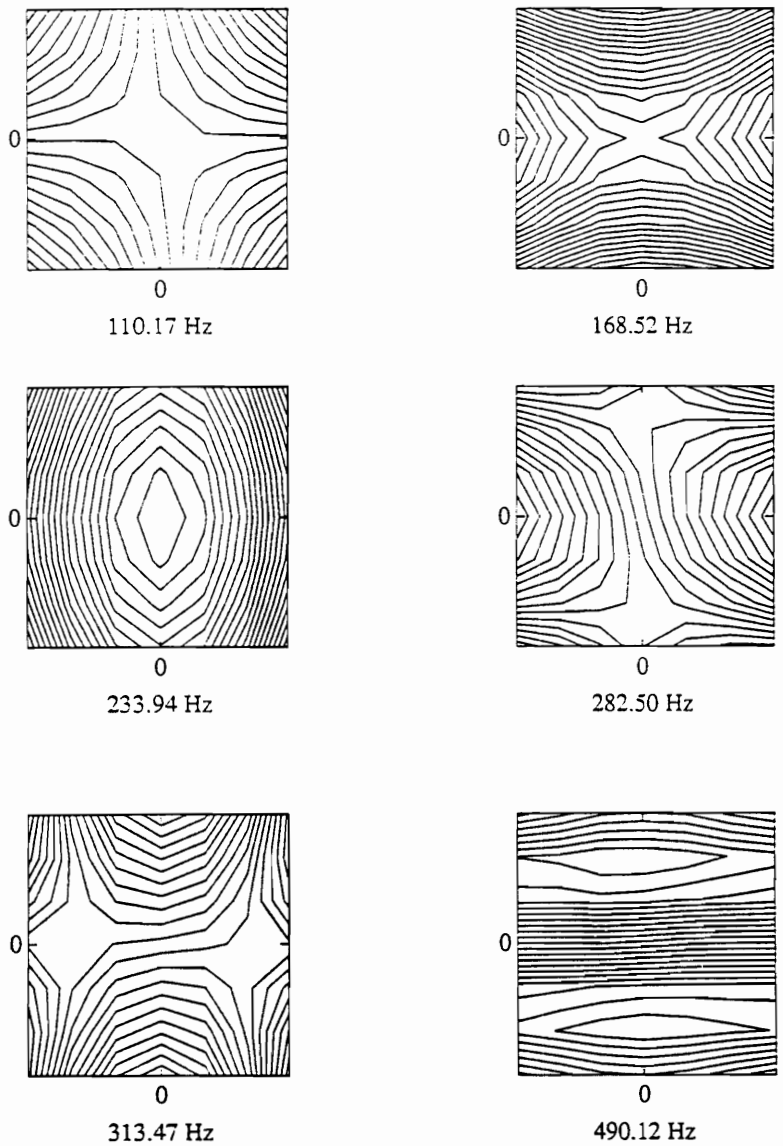

Fig. 6.8 Contour plots of experimentally obtained mode shapes for the free-hanging cross-ply plate configuration.

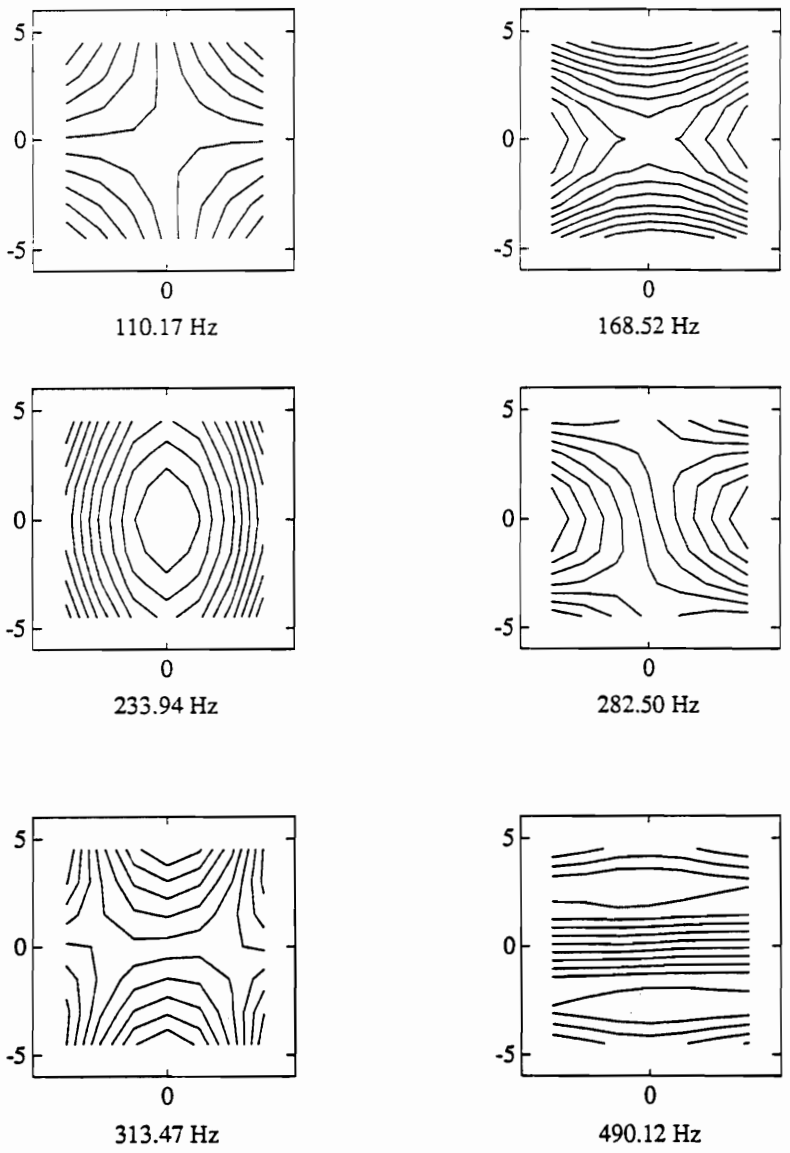

Fig. 6.9 Contour plots of experimentally obtained mode shapes for the free-hanging quasi-isotropic plate configuration.

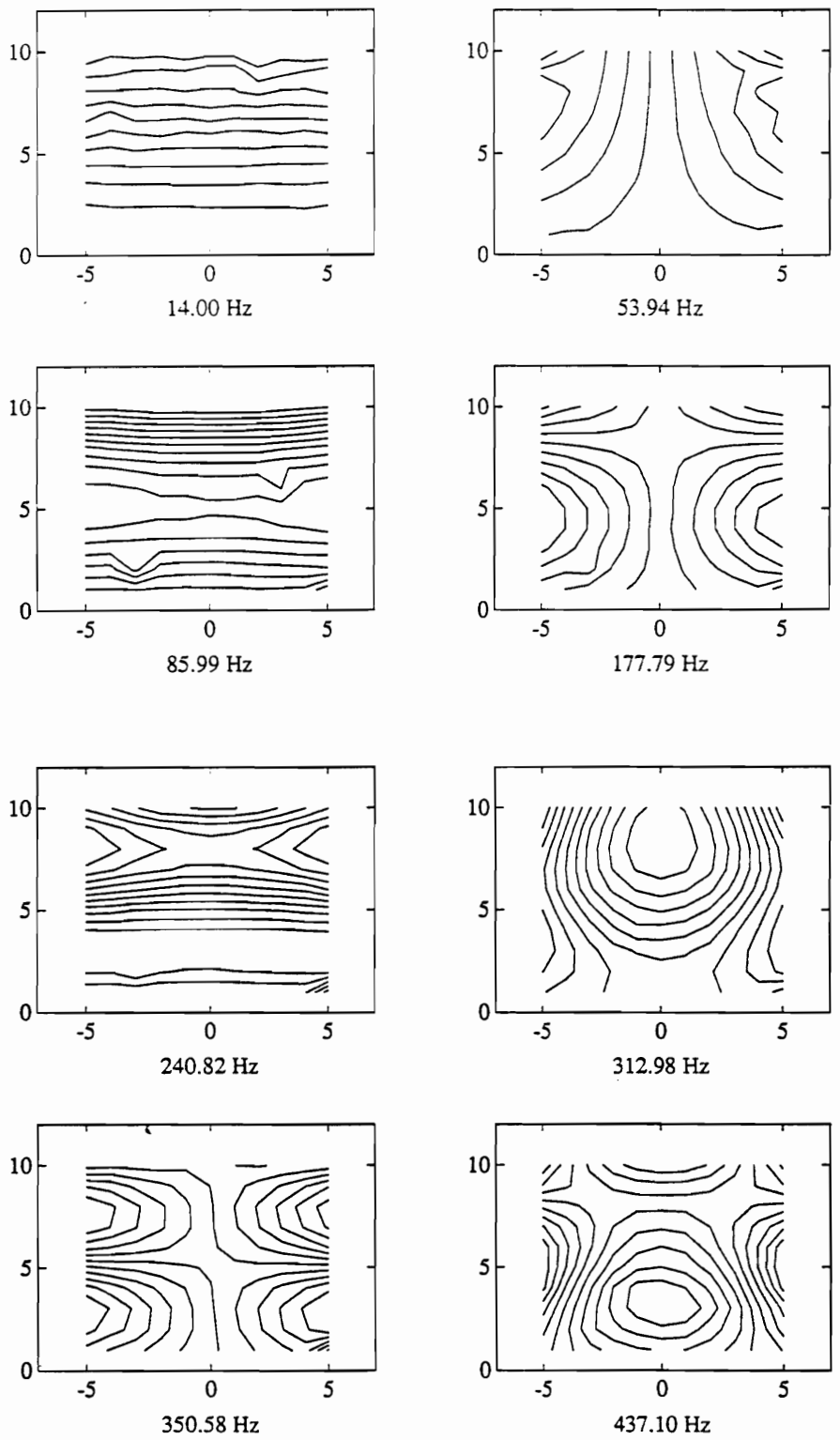

Fig. 6.10 Contour plots of experimentally obtained mode shapes for the cantilevered ±15° plate configuration.

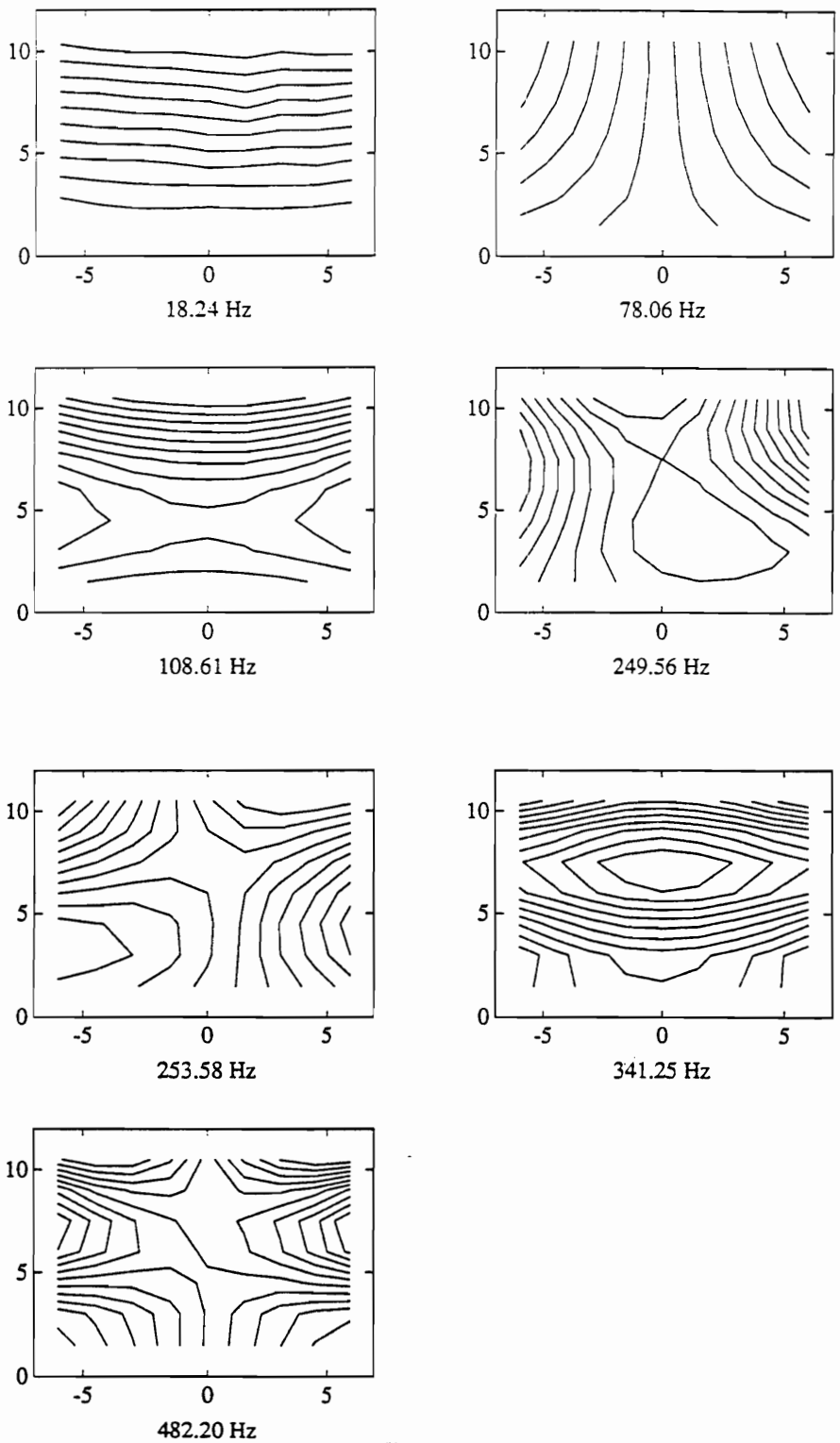

Fig. 6.11 Contour plots of experimentally obtained mode shapes for the cantilevered ±30° plate configuration.

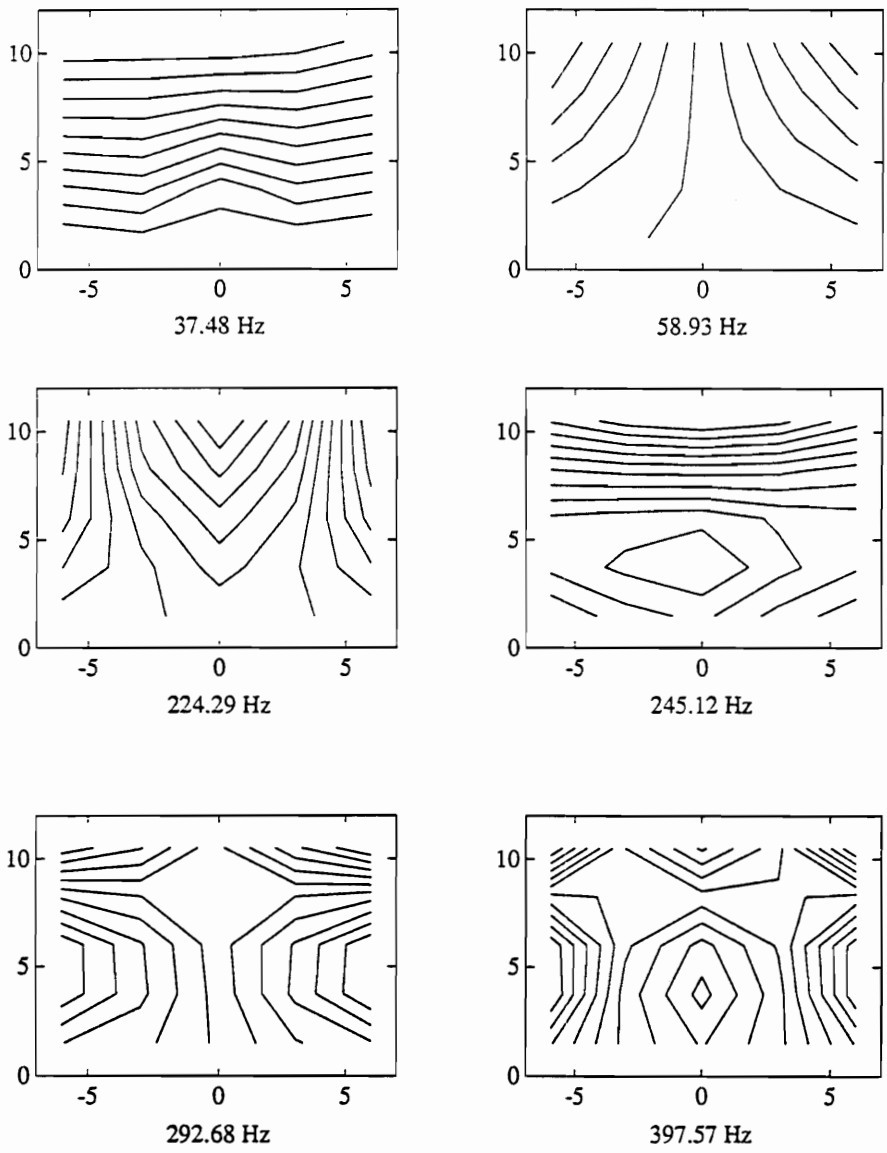

Fig. 6.12 Contour plots of experimentally obtained mode shapes for the cantilevered cross-ply plate configuration.

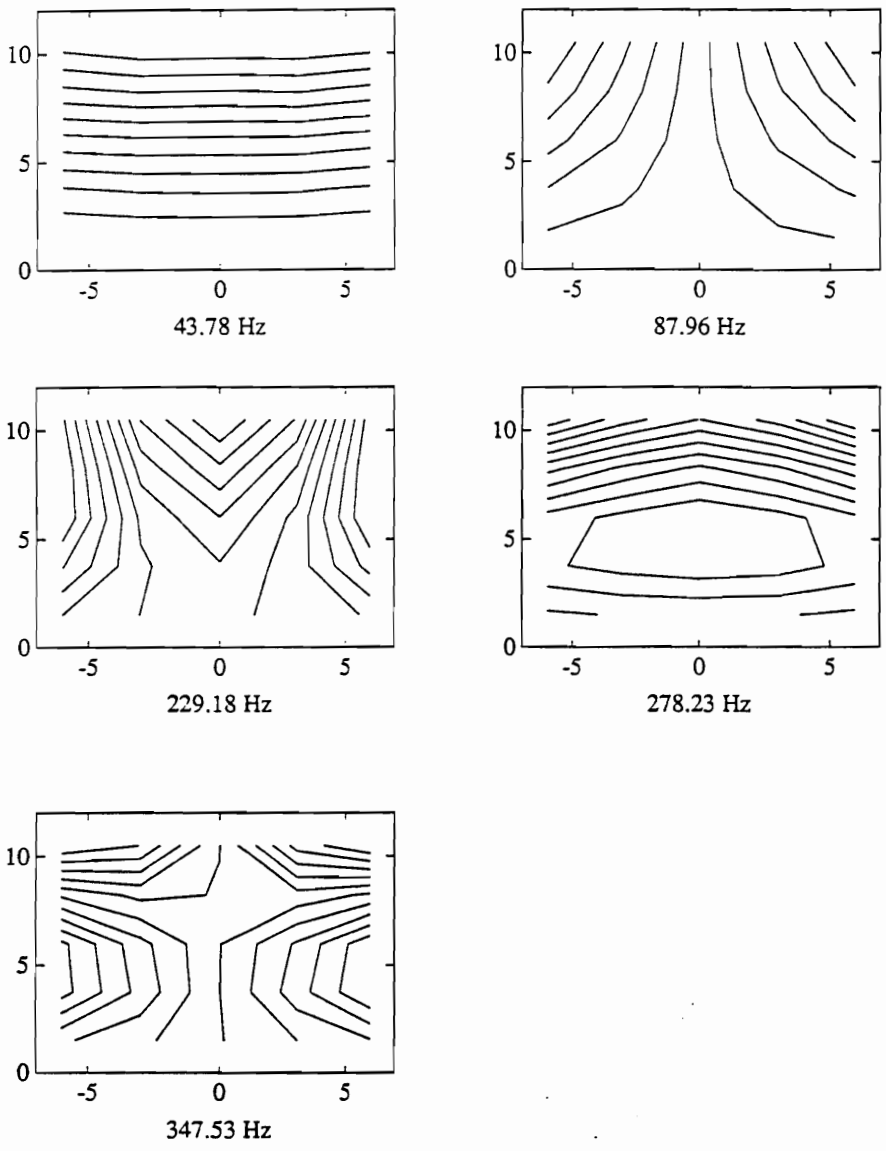

Fig. 6.13 Contour plots of experimentally obtained mode shapes for the cantilevered quasi-isotropic plate configuration.

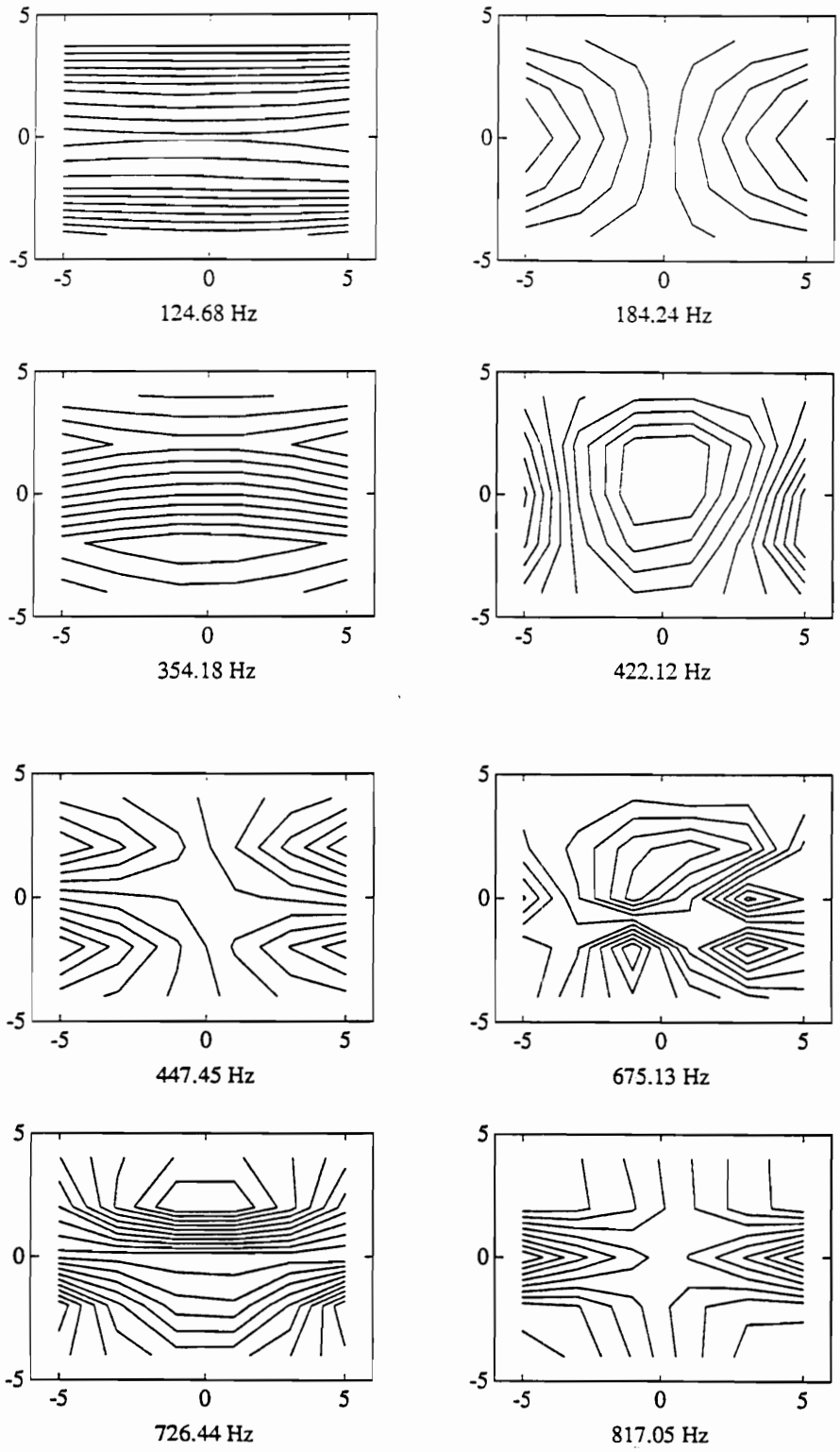

Fig. 6.14 Contour plots of experimentally obtained mode shapes for the fixed-fixed ±15° plate configuration.

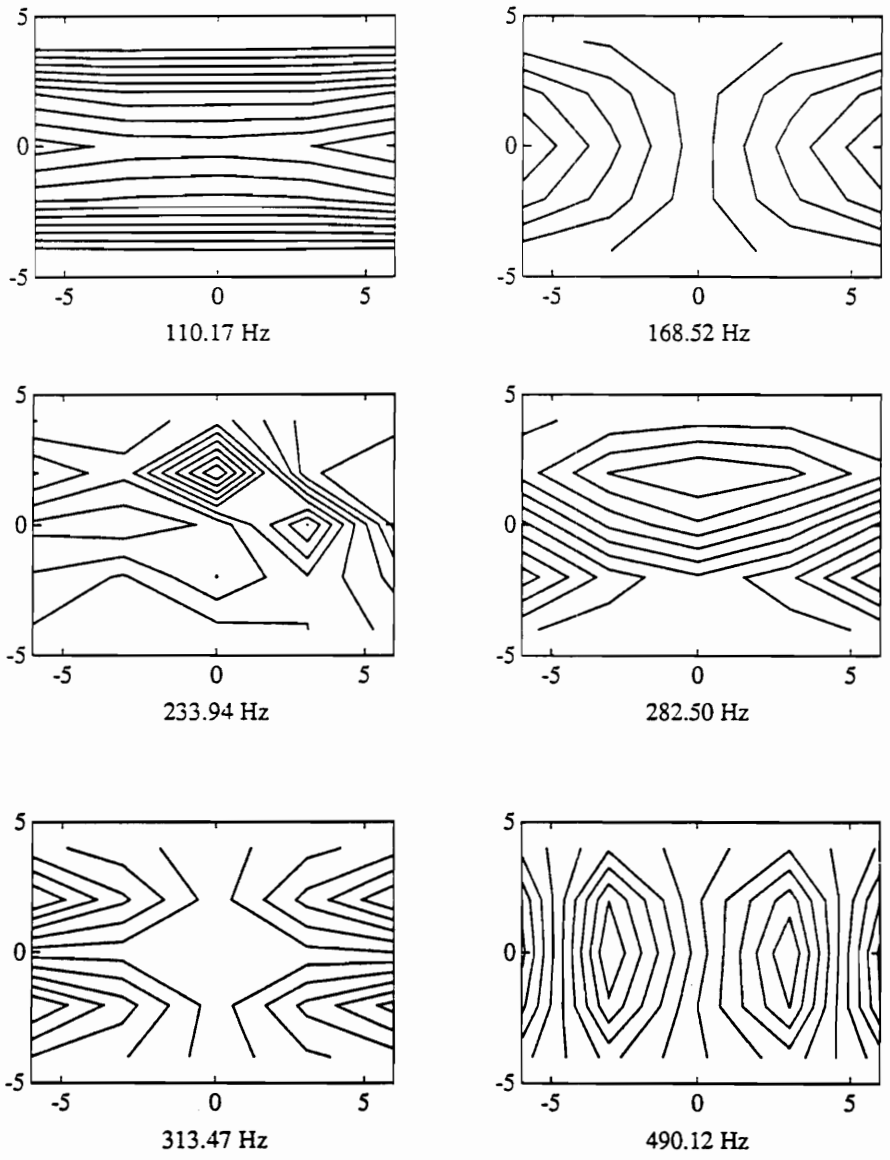

Fig. 6.15 Contour plots of experimentally obtained mode shapes for the fixed-fixed ±30° plate configuration.

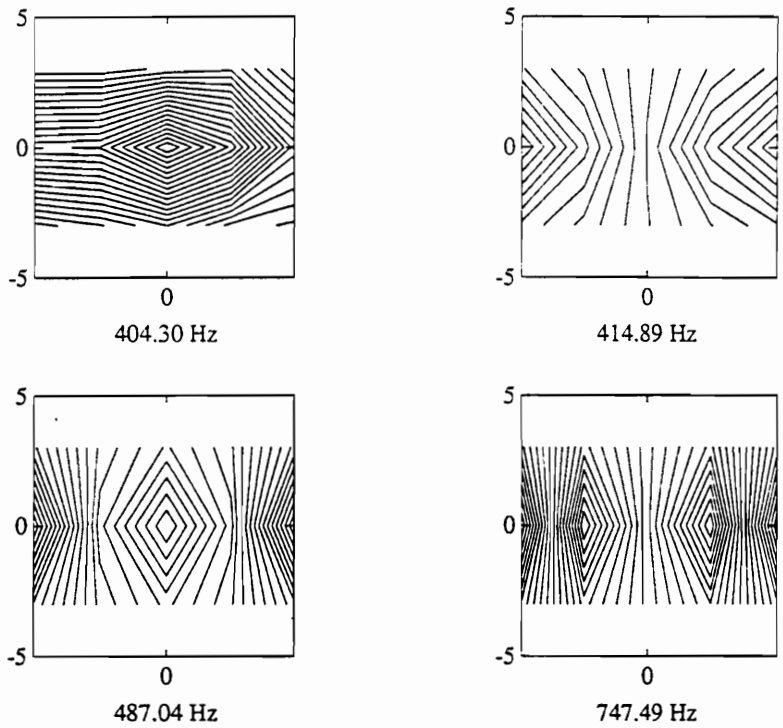

Fig. 6.16 Contour plots of experimentally obtained mode shapes for the fixed-fixed cross-ply plate configuration.

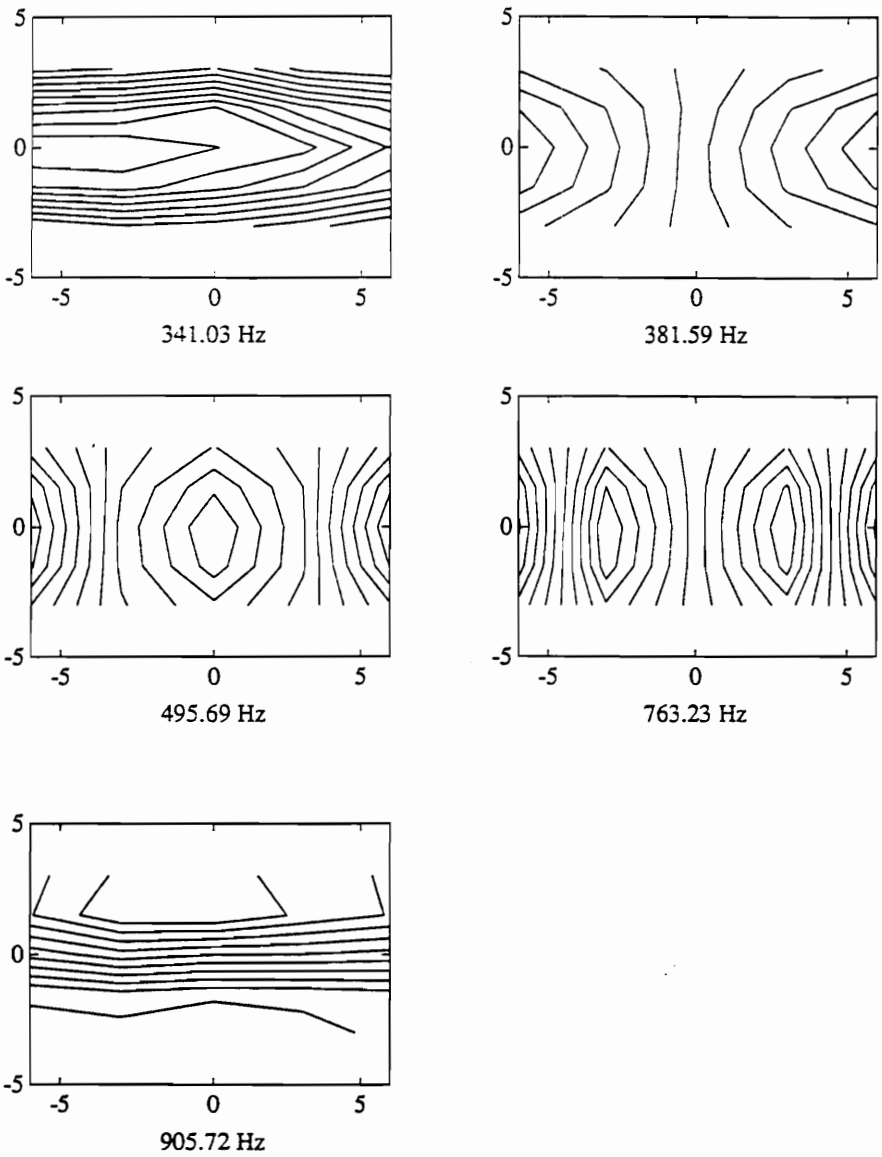

Fig. 6.17 Contour plots of experimentally obtained mode shapes for the fixed-fixed quasi-isotropic plate configuration.

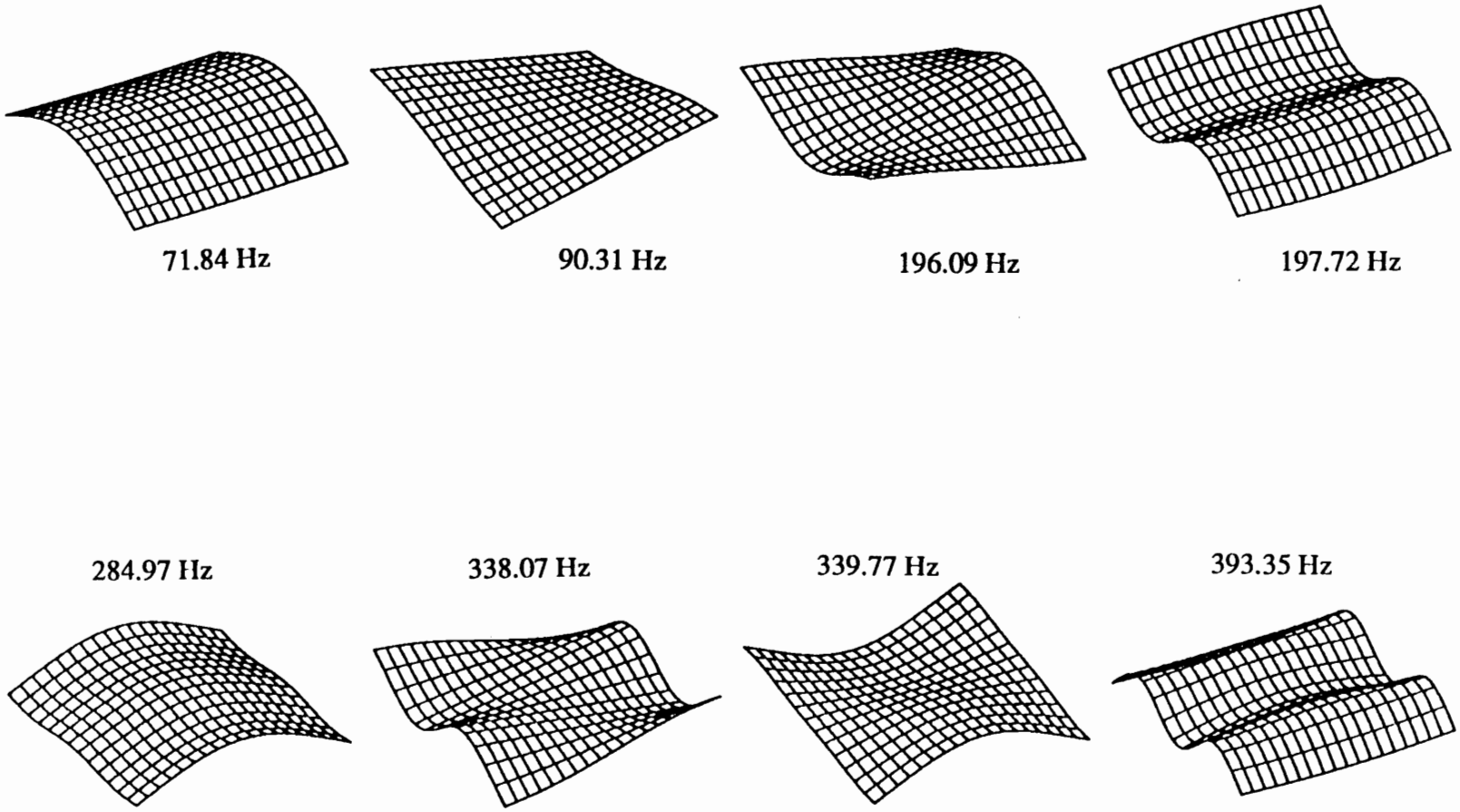

Fig. 6.18 Displacement plots of theoretically obtained mode shapes for the free-hanging ±15° plate configuration.

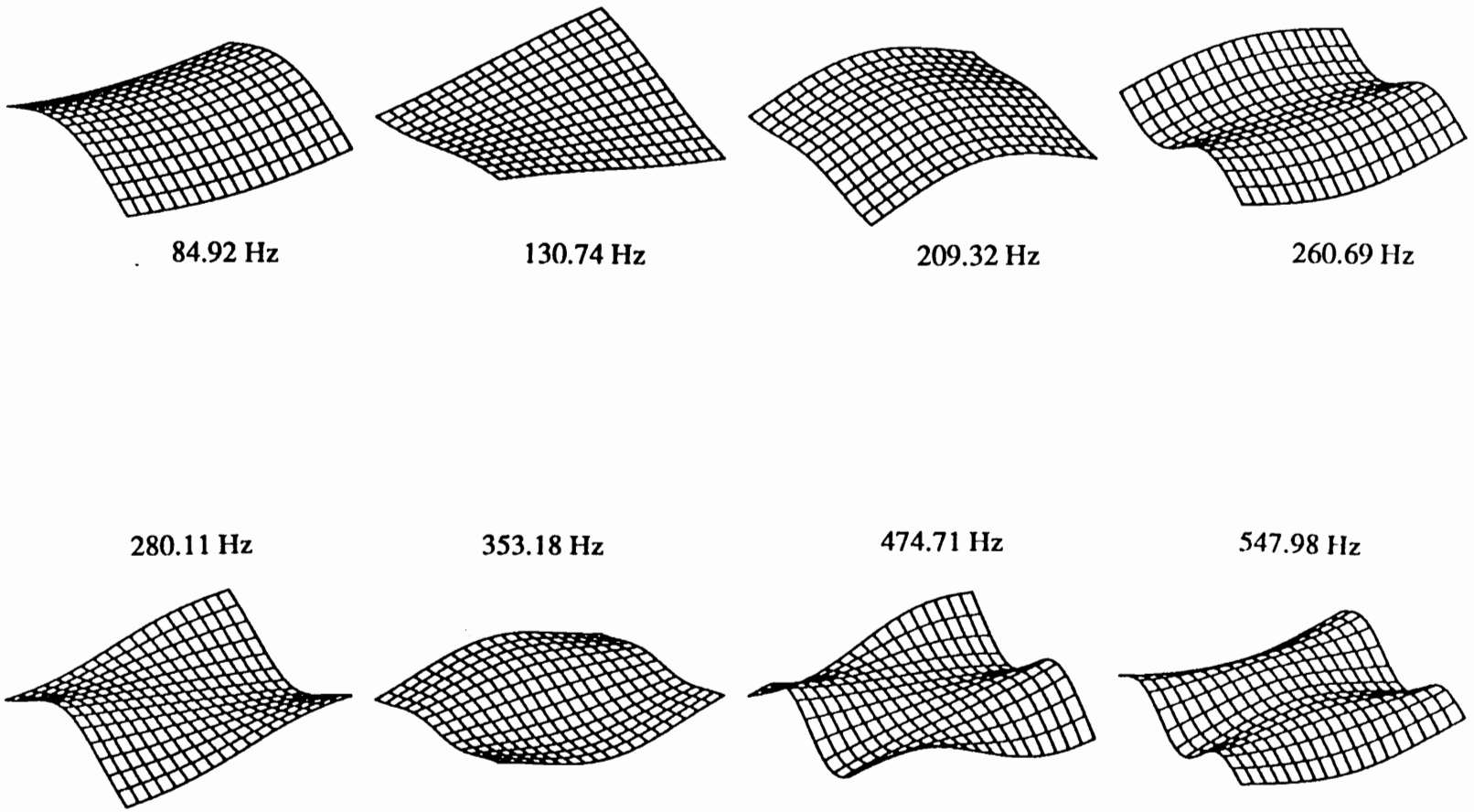

Fig. 6.19 Displacement plots of theoretically obtained mode shapes for the free-hanging ±30° plate configuration.

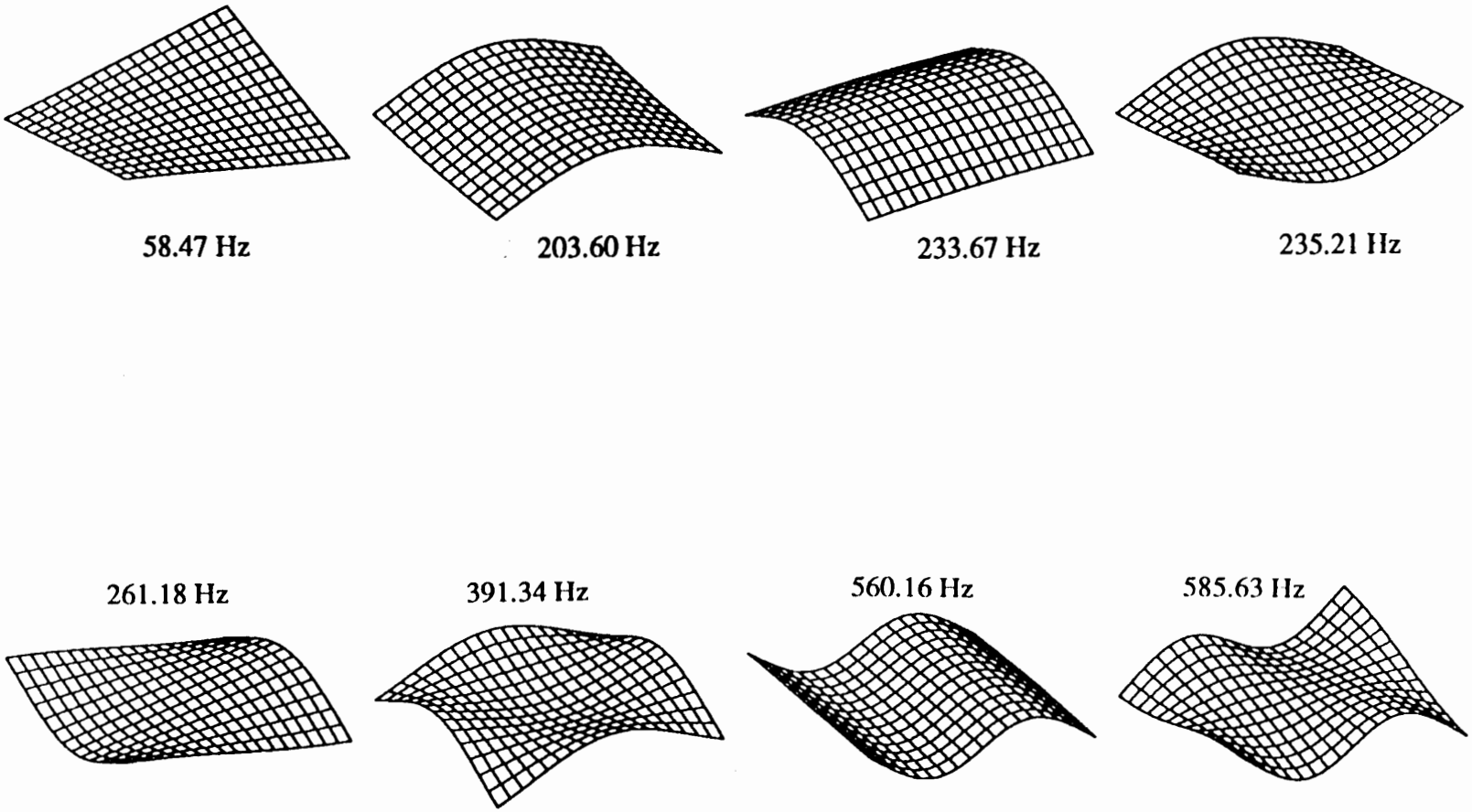

Fig. 6.20 Displacement plots of theoretically obtained mode shapes for the free-hanging cross-ply plate configuration.

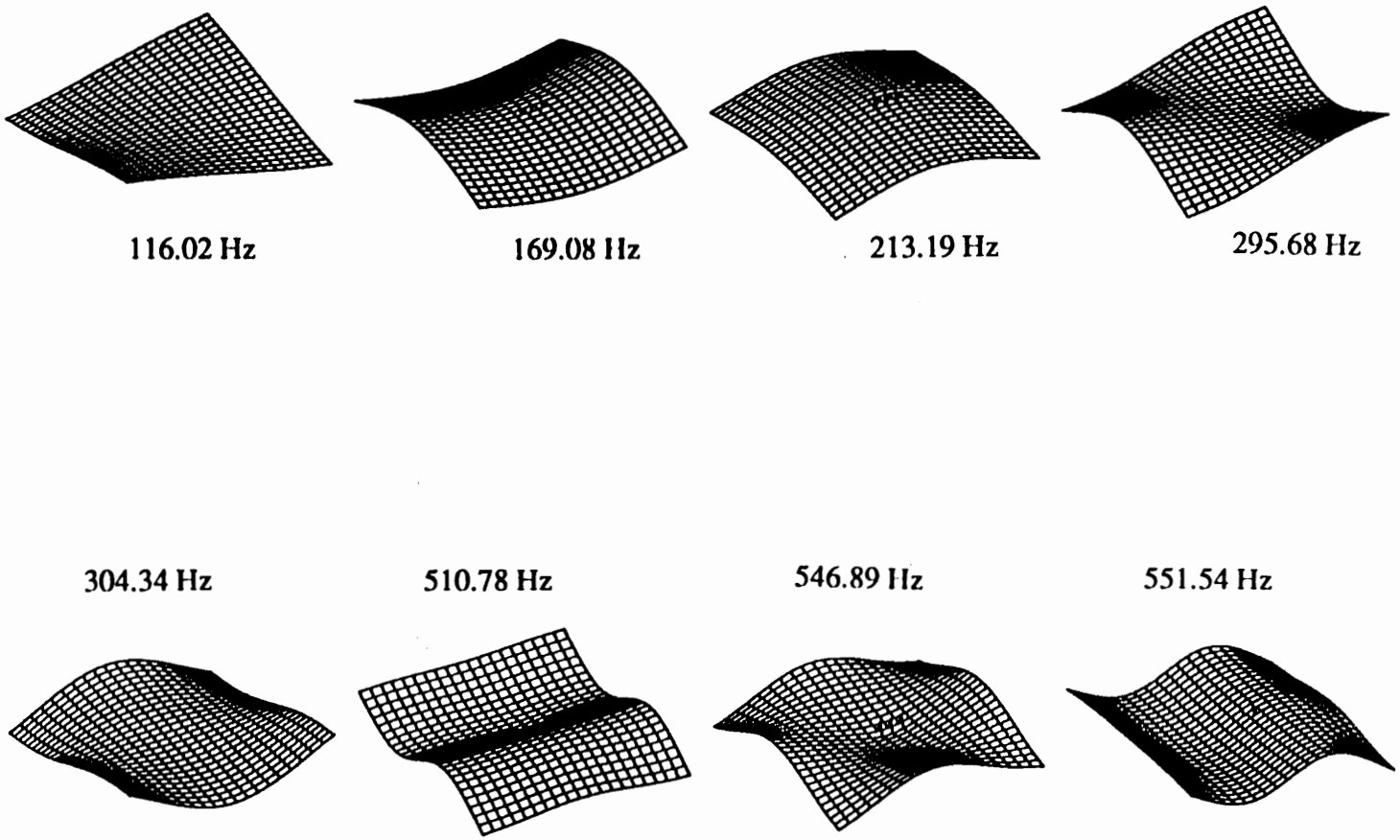

Fig. 6.21 Displacement plots of theoretically obtained mode shapes for the free-hanging quasi-isotropic plate configuration.

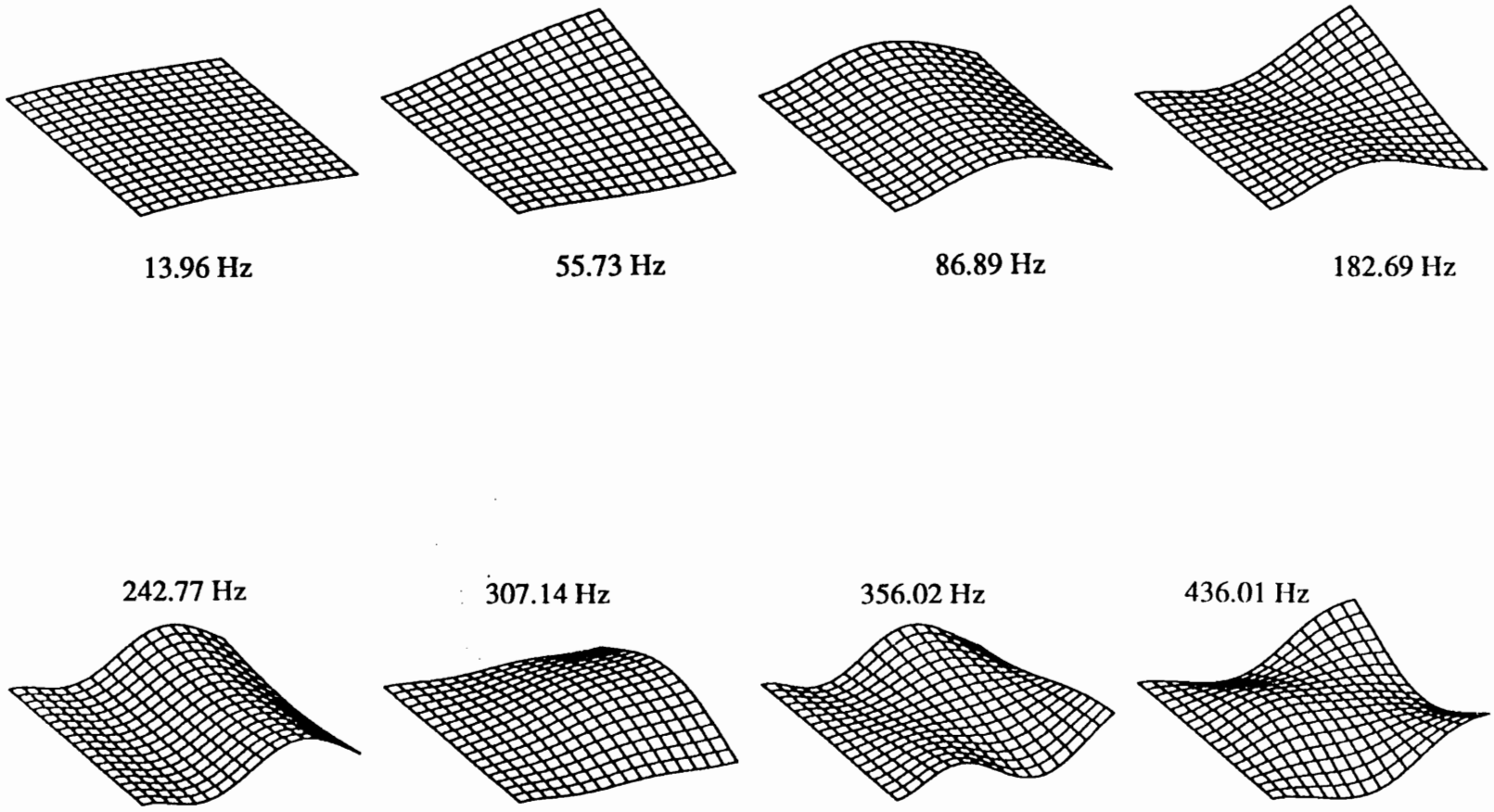

Fig. 6.22 Displacement plots of theoretically obtained mode shapes for the cantilevered ±15° plate configuration.

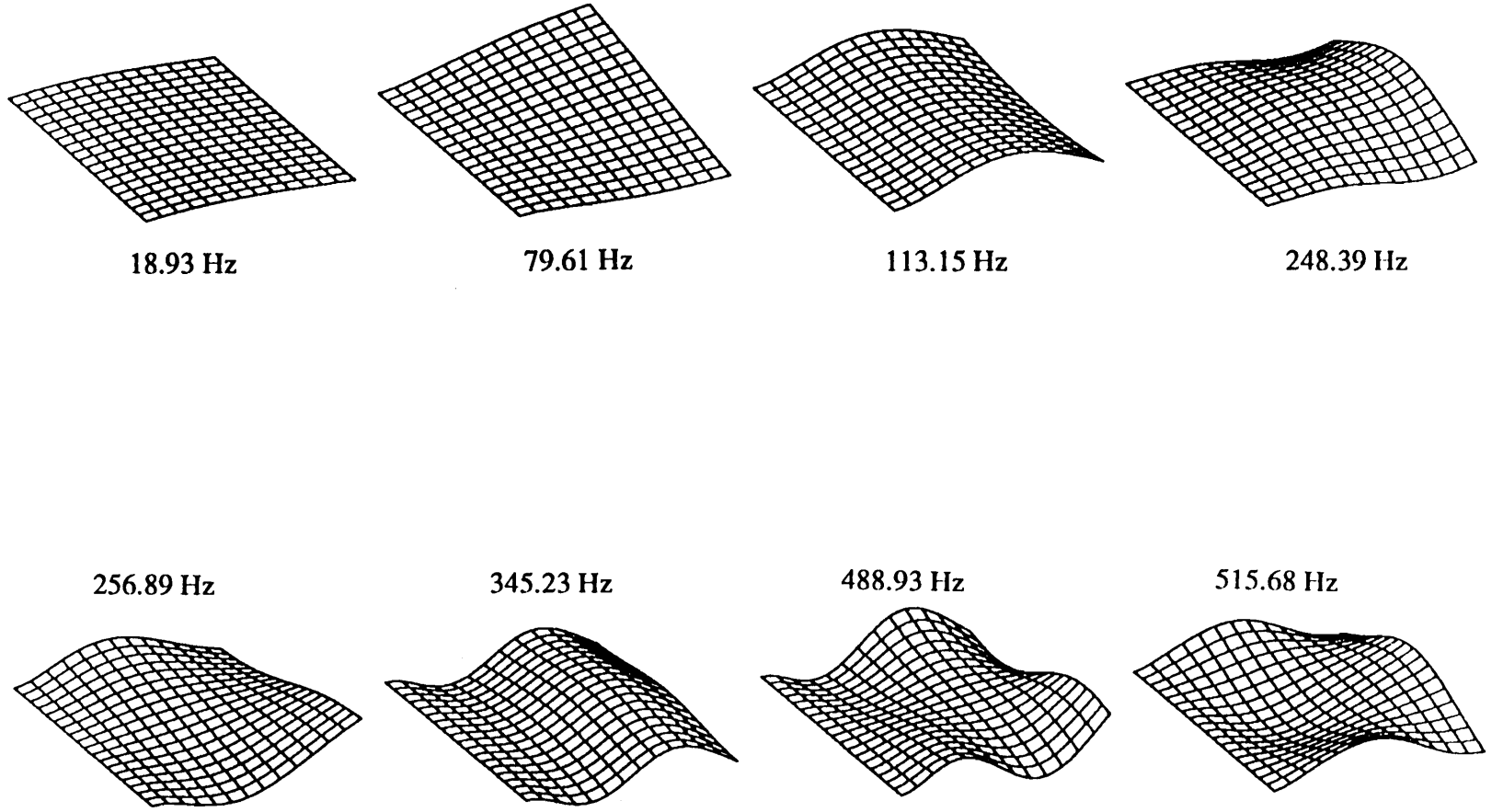

Fig. 6.23 Displacement plots of theoretically obtained mode shapes for the cantilevered ±30° plate configuration.

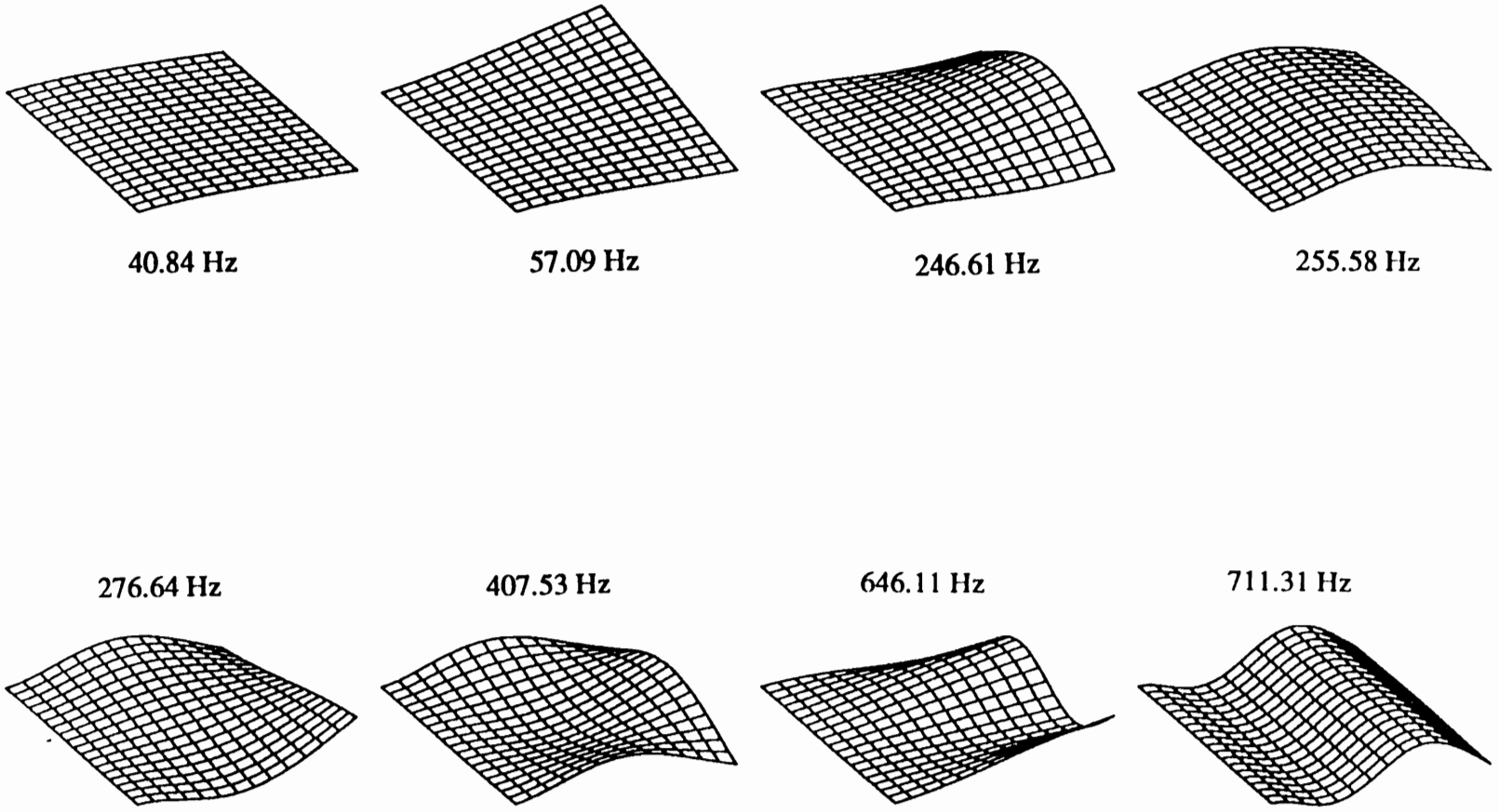

Fig. 6.24 Displacement plots of theoretically obtained mode shapes for the cantilevered cross-ply plate configuration.

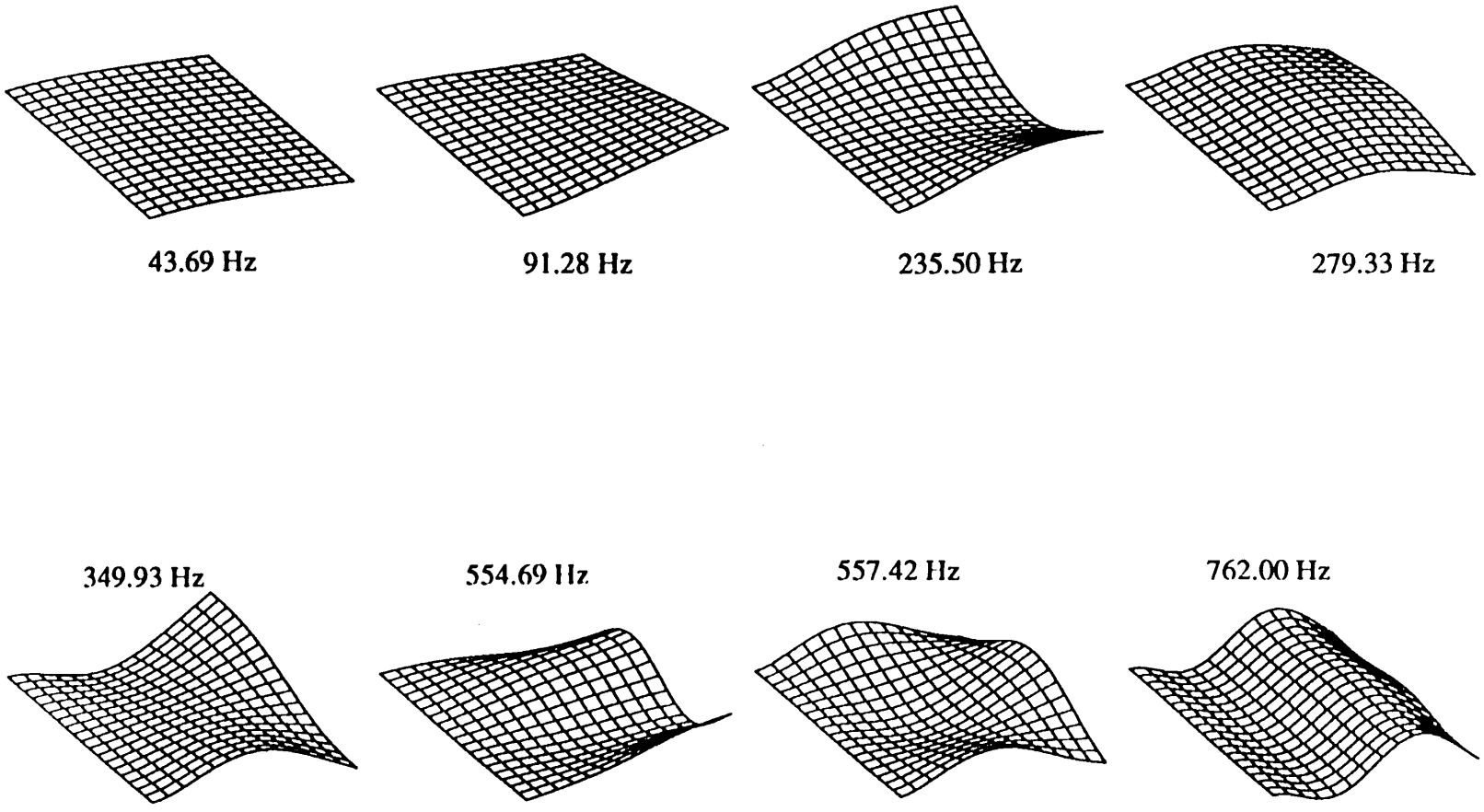

Fig. 6.25 Displacement plots of theoretically obtained mode shapes for the cantilevered quasi-isotropic plate configuration.

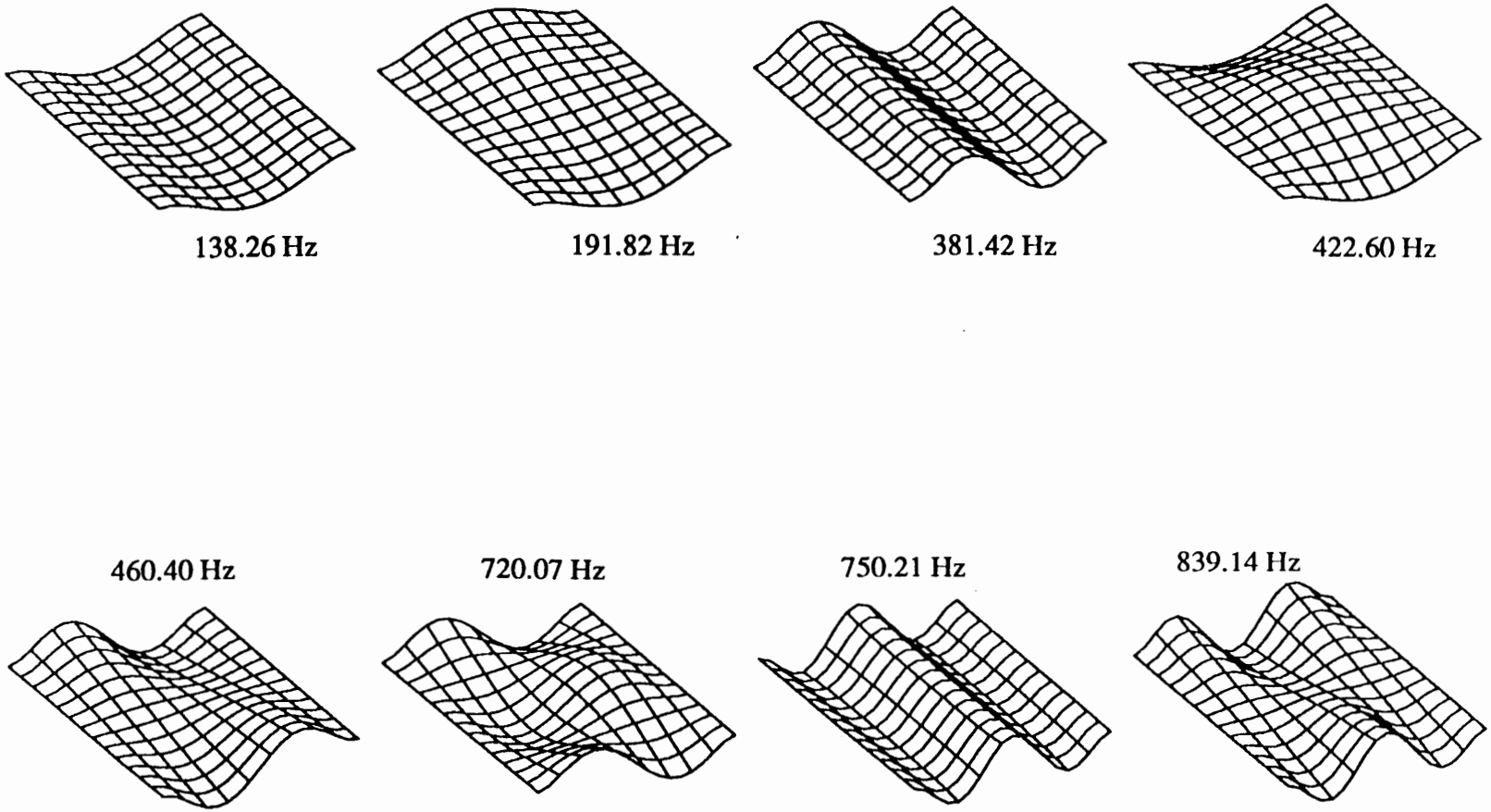

Fig. 6.26 Displacement plots of theoretically obtained mode shapes for the fixed-fixed ±15° plate configuration.

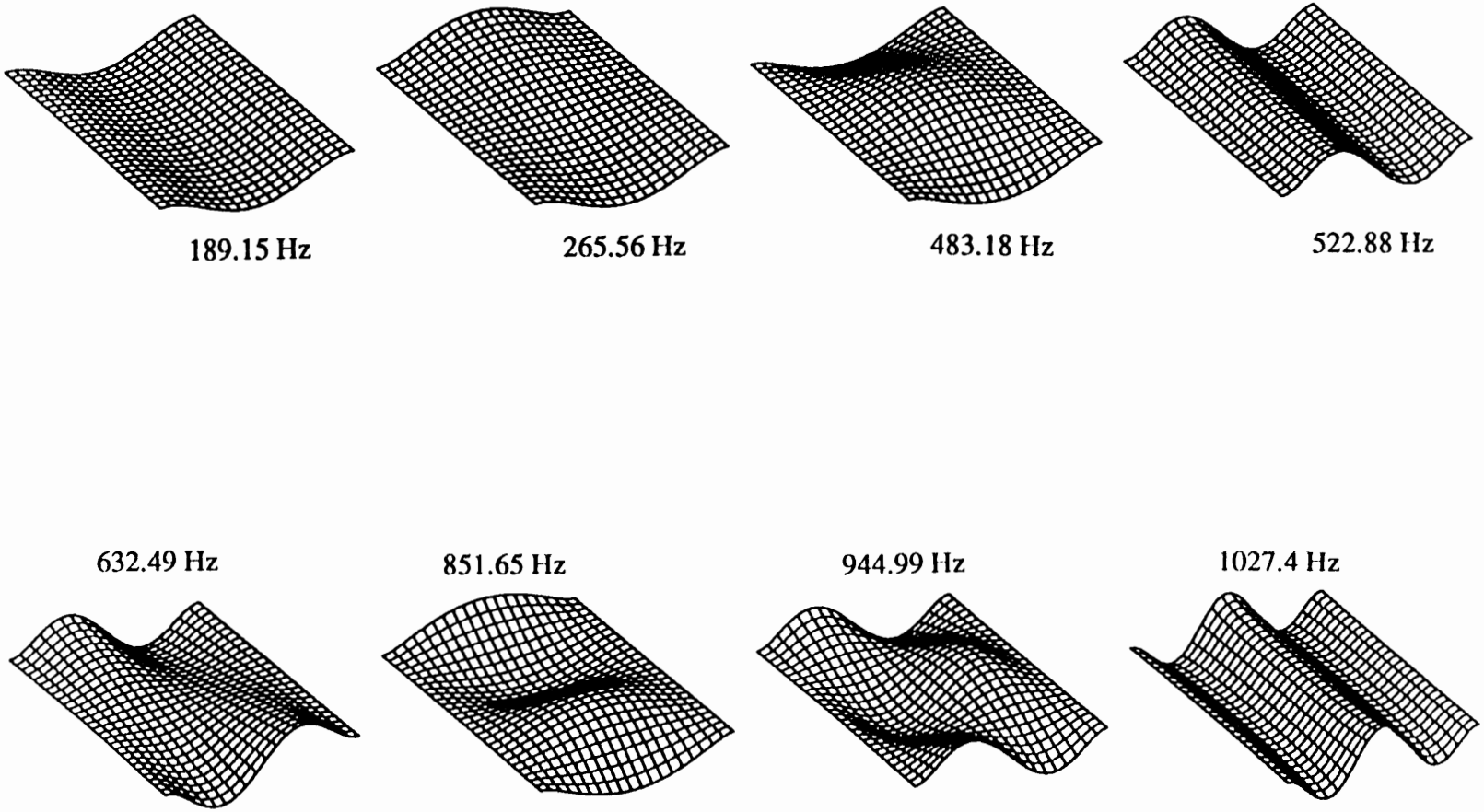

Fig. 6.27 Displacement plots of theoretically obtained mode shapes for the fixed-fixed ±30° plate configuration.

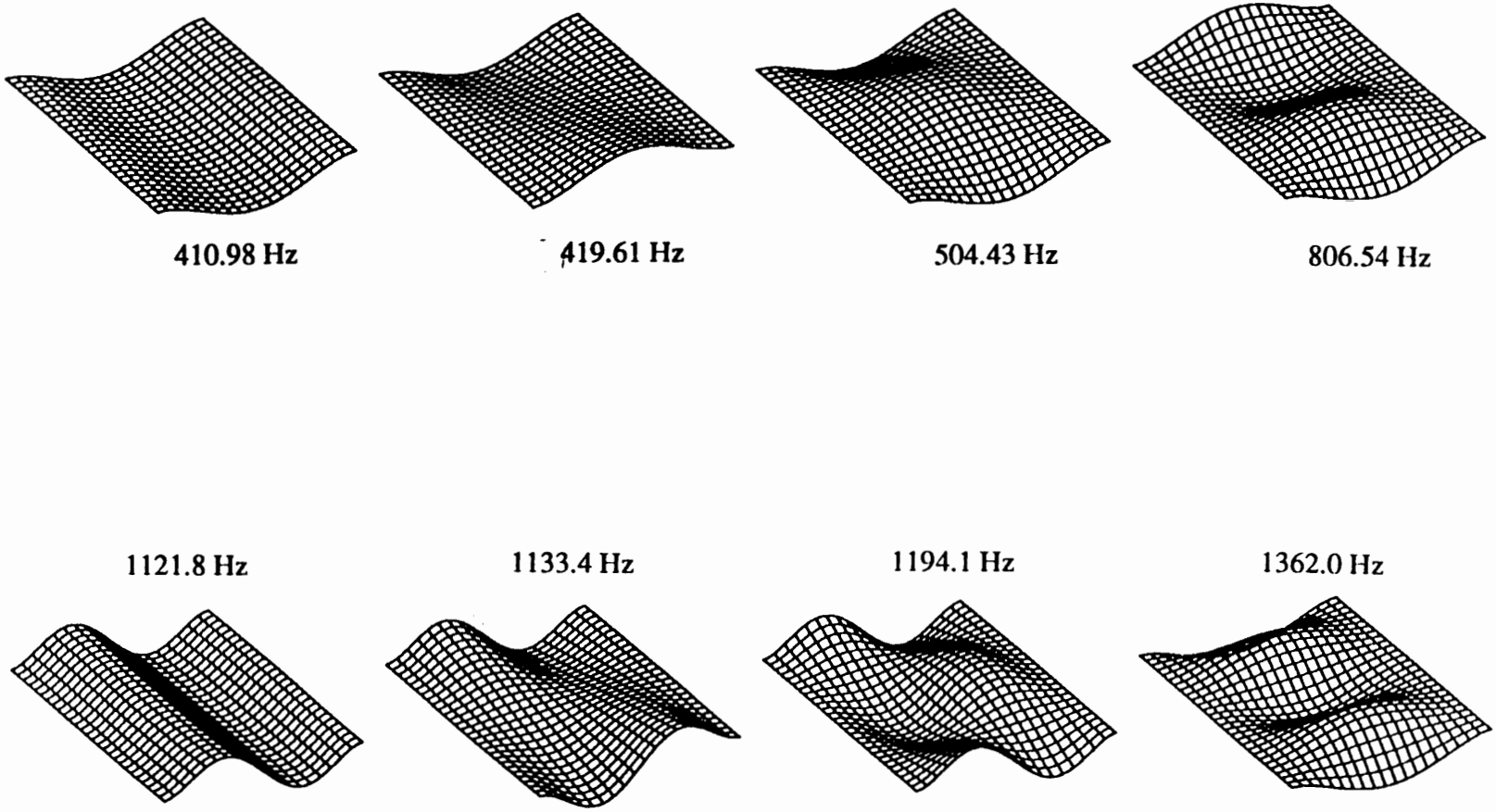

Fig. 6.28 Displacement plots of theoretically obtained mode shapes for the fixed-fixed cross-ply plate configuration.

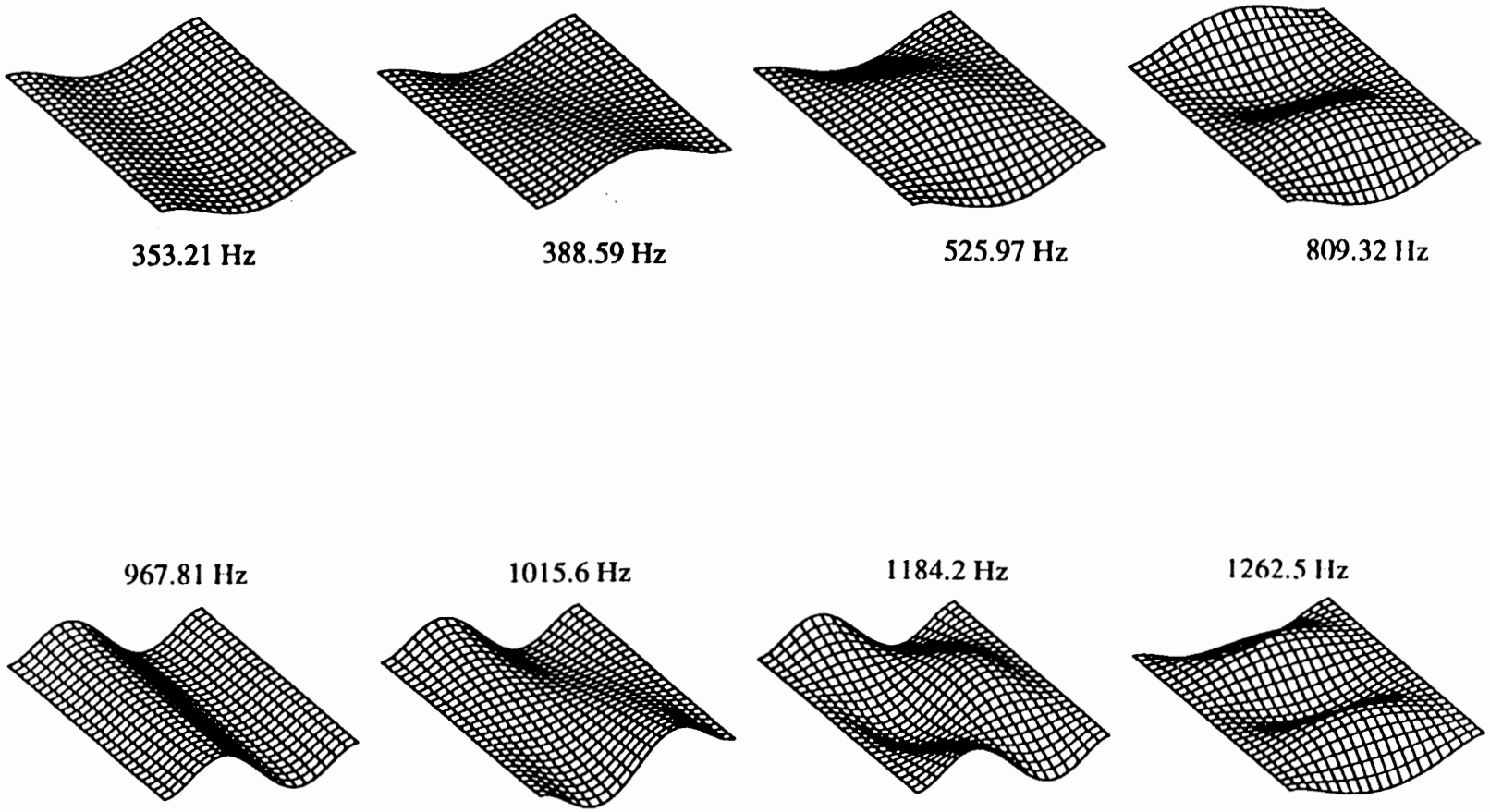

Fig. 6.29 Displacement plots of theoretically obtained mode shapes for the fixed-fixed quasi-isotropic plate configuration.

7. Summary and Recommendations

7.1 Summary

Four separate studies were conducted and the results presented. In all of the studies, we have emphasized the value of combining experimental and theoretical work. With this combined approach, we verified the importance of the nonlinear curvature in modeling of cantilever beams. Also, we found that the addition of quadratic damping to the the model improves the agreement between the experimental and theoretical results for both frequency-response and force-response curves. Without the quadratic damping the experimental and theoretical results did not agree even qualitatively for the first mode.

In the two studies involving the multi-mode responses of the slender cantilever beam, we experimentally discovered a new type of model interaction where the complete response of a low-frequency mode interacts with the modulations of a high-frequency mode. Both static and periodic responses of the low-frequency mode were found. We then developed a model that captures the essential characteristics of this type of motion. A significant characteristic of this type of modal interaction is that a specific frequency relationship is not required between the modes involved as is typical of other modal interactions. The only requirements for this type of modal interaction to occur are that the frequency of one mode is much higher than the other and there is nonlinear coupling between the modes. This result may have implications for flexible structures such as the space station, which have many modes of interest with widely separated frequencies.

We also investigated the natural frequencies and mode shapes of several laminated composite plates in various configurations. Results from experimental modal analysis and FEA are presented and compared. Comparisons between experimental and

FEA are much better than what has been previously reported for the free-hanging configuration where the boundary conditions are well known. Comparisons between the experimental and FEA are poor for the fixed-fixed configuration indicating that the fixed boundary conditions significantly deviate from ideal. In this study, we tried to avoid some of the problems encountered by similar previous studies, such as mass loading the structure, using the maximum amplitude as a measure of the natural frequency, choice of the material properties, and unknown boundary conditions. Moreover, experimentally obtained properties for the material are included. The results of the free-hanging configuration provide accurate experimental natural frequencies for several composite plates, these results can be used to validate future theoretical developments. The results of the fixed-fixed configuration can be used to provide possible explanations for the discrepancies between the measured and calculated natural frequencies previously reported in the literature.

7.2 Recommendations

The following topics concerning the nonlinear vibrations of structures are recommended for future study:

1) Additional experimental investigations need to be conducted to determine if the transfer of energy from a high-frequency excitation to a low-frequency component in the response, similar to that reported in Chapters 4 and 5, occurs in other systems.

2) An analysis should be done that includes the out-of-plane motion coupled with the analysis from Chapter 5 that treats the first mode as a slowly-varying term. This analysis could be used to explain the experimental results reported in Section 4.3.

3) Additional work in identifying appropriate models for damping is needed. The identification of damping models must be done experimentally and on a case by case basis.

4) Investigate if modal interactions can occur through coupling that comes only from nonlinear damping.

5) Experimental investigations of the forced response of laminated composite plates should be conducted. The results of Chapter 6 can be used to chose forcing frequencies such that various resonant conditions would be expected to occur.

References

ABAQUS User's Manual Version 4.8, 1989, Hibbit, Karlsson & Ssorensen, Inc.

Adams, R. D., and Bacon, D. G. C., 1973, "Measurement of the Flexural Damping Capacity and Dynamic Young's Modulus of Metals and Reinforced Plastics," *Journal of Physics D: Applied Physics*, Vol. 6, pp. 27-41.

Ashton, J. E., and Anderson, J. D., 1969, "The Natural Modes of Vibration of Boron-Epoxy Plates," *Shock and Vibration Bulletin*, No. 39, Part 4, pp. 81-91.

Anand, G. V., 1966, "Nonlinear Resonance in Stretched Strings with Viscous Damping," *Journal of Acoustical Society of America*, Vol. 40, pp. 1517-1528.

Baker, W. E., Woolam, W. E., and Yound, D., 1967, "Air and Internal Damping of Thin Cantilever Beams," *International Journal Mechanical Sciences,* Vol. 9, pp. 743-766.

Banks, H. T., and Inman, D. J., 1991, "On Damping Mechanisms in Beams," *Journal of Applied Mechanics*, Vol. 58, pp. 716-723.

Bernasconi, O., and Ewins, D. J., 1989, "Application of Strain Modal Testing to Real Structures," *Proceedings of the 7th International Modal Analysis Conference*, Las Vegas, NV, Jan. 30-Feb. 2.

Bert, C. W., 1973, "Material Damping: An Introductory Review of Mathematical Models, Measures and Experimental Techniques," *Journal of Sound and Vibration*, Vol. 29, pp. 129-153.

Bert, C. W., and Mayberry, B. L., 1969, "Free Vibrations on Unsymmetrically Laminated Anisotropic Plates," *Journal of Composite Materials*, Vol. 3. pp. 282-293.

Bert, C. W., 1985, "Research on Dynamic Behavior of Composite and Sandwitch Plates," *Shock and Vibration Digest*, Vol. 17, pp. 3-15.

Bhimaraddi, A., and Stephens, L. K., 1984, "A Higher-Order Theory for Free Vibrations of Orthotropic, Homogeneous, and Laminated Rectangular Plates," *Journal of Applied Mehcanics*, Vol. 51, pp. 195-198.

Bhimaraddi, A., 1987, "Nonlinear Flexural Vibrations of Rectangular Plates Subjected to In-Plane Forces Uning a New Shear Deformation Theory," *Thin-Walled Structures*, Vol. 5, pp. 309-327.

Brigham, E. O., 1974, *The Fast Fourier Transform*, Prentice Hall Inc., New Jersey.

Burton, T. D., and Kolowith, M., 1988, "Nonlinear Resonances and Chaotic Motion in a Flexible Parametrically Excited Beam," *Proceedings of the Second Conference on Non-linear Vibrations, Stability, and Dynamics of Structures and Mechanisms,* Blacksburg, VA, June 1-3.

Chia, C. Y., 1980, *Nonlinear Analysis of Plates*, McGraw-Hill, New York.

Clary, R. R., 1972, "Vibration Characteristics of Unidirectional Filamentary Composite Material Panels," *Composite Materials: Testing, Design (Second Conference)* , ASTM STP 497, pp. 415-438.

Corelli, D., and Brown, D. L., 1984, "Impact Testing Considerations," *Proceedings of the 2nd International Modal Analysis Conference*, Orlando, FL, Feb. 6-7.

Crandall, S. H., 1970, "The Role of Damping in Vibration Theory," *Journal of Sound and Vibration*, Vol. 11, pp. 3-18.

Crawley, E. F., 1979, "The Natural Modes of Graphite/Epoxy Cantilever Plates and Shells," *Journal of Composite Materials*, Vol. 13, pp. 195-205.

Crespo da Silva, M. R. M., and Glynn, C. C., 1978a, "Nonlinear Flexural-Flexural-Torsional Dyanamics of Inextensional Beams -- I. Equations of Motion," *Journal of Structural Mechanics*, Vol. 6, pp. 437-448.

Crespo da Silva, M. R. M., and Glynn, C. C., 1978b, "Nonlinear Flexural-Flexural-Torsional Dyanamics of Inextensional Beams -- II. Forced Motions," *Journal of Structural Mechanics*, Vol. 6, pp. 449-461.

Cusumano, J. P., and Moon, F.C., 1989, "Low Dimensional Behavior in Chaotic Nonplanar Motions of a Forced Elastic Rod: Experiment and Theory," *Nonlinear Dynamics in Engineering Systems, IUTAM Symposium*, Germany.

Cusumano, J. P., 1990, "Low-Dimensional, Chaotic, Nonplanar Motions of the Elastica: Experiment and Theory," Ph.D. Dissertation, Cornell University, New York.

Dowell, E. H., Traybar, J., and Hodges, D. H., 1977, "An Experimental-Theoretical Correlation Study of Nonlinear Bending and Torsion Deformations of a Cantilever Beam," *Journal of Sound and Vibration*, Vol. 50, pp. 533-544.

Dugundji, J., and Mukhopadhyay, V., 1973, "Lateral Bending-Torsional Vibrations of a Thin Beam Under Parametric Excitation," *Journal of Applied Mechanics,* Vol. 40, pp. 693-698.

Eringen, A. C., 1952, "On the Nonlinear Vibration of Elastic Bars," *Quarterly of Applied Mathematics*, Vol. 9, pp. 361-369.

Evensen, D. A., and Evan-Iwanowski, R. M., 1966, "Effects fo Longitudinal Inertia Upon the Parametric Response of Elastic Column," *Journal of Applied Mechanics*, Vol. 33, pp. 141-148.

Ewins, D. J., 1984, *Modal Testing: Theory and Practice*, Wiley, New York.

Froude, W., 1863, "Remarks on Mr. Scott Russell's Paper on Rolling," *Transactions of Institute of Naval Architects*, Vol. 4, pp. 232-275.

Gade, S., and Herlufsen, H., 1988, "Windows to FFT Analysis," *Sound and Vibration*, Vol. 22, No. 3 , pp. 14-22.

Haddow, A. G., Barr, A. D. S., and Mook, D. T., 1984, "Theoretical and Experimental Study of Modal Interaction in a Two-Degree-of-Freedon Structure," *Journal of Sound and Vibration*, Vol. 97, pp. 451-473.

Haddow, A. G., and Hasan, S. M., 1988, "Nonlinear Oscillation of a Flexible Cantilever: Experimental Results," *Proceedings of the Second Conference on Non-linear Vibrations, Stability, and Dynamics of Structures and Mechanisms*, Blacksburg, VA, June 1-3.

Haight, E. C., and King, W. W., 1971, "Stability of Parametrically Excited Vibrations of and Elastic Rod," *Developments in Theoretical and Applied Mechanics*, Vol. 5, pp. 677-714.

Harris, F. J., 1978, "On the Use of Windows for Harmonic Analysis with the Discrete Fourier Transform," *Proceeding of the IEEE*, Vol. 66, No. 1, pp. 51-83.

Heyliger, P. R., and Reddy, J. N., 1988, "A Higher Order Beam Finite Element for Bending and Vibration Problems," *Journal of Sound and Vibration*, Vol. 126, pp. 309-326.

Hodges, D. H., and Dowell, E. H., 1974, " Nonlinear Equations of Motion for the Elastic Bending and Torsion of Twisted Nonuniform Rotor Blades," NASA TN D-7818.

Hodges, D. H., Crespo da Silva, M. R. M., and Peters, D. A., 1988, "Nonlinear Effects in the Static and Dynamic Behavior of Beams and Rotor Blades," *Vertica*, Vol. 12, pp. 243-256.

Hyer, M. W., 1989, "Introduction to the Mechanics of Fiber-Reinforced Materials and Structures," Virginia Polytechnic Institute and State University, College of Engineering Report VPI-E89-9.

Jeffries, C., and Wiesenfeld, K., 1985, "Observation of Noisy Precursors of Dynamical Instabilities," *Physical Review A*, Vol. 31, No. 2, pp. 1077-1084.

Johnson, J. M., and Bajaj, A. K., 1989, "Amplitued Modulated and Chaotic Dynamics in Resonant Motion of Strings," *Journal of Sound and Vibration*, Vol. 128, pp. 87-107.

Kapania, R. K., and Raciti, S., 1989a, "Recent Advances in Analysis of Laminated Beams and Plates, Part I: Shear Effects and Buckling," *AIAA Journal*, Vol. 27, pp. 923-934.

Kapania, R. K., and Raciti, S., 1989b, "Recent Advances in Analysis of Laminated Beams and Plates, Part II: Vibration and Wave Propagation," *AIAA Journal*, Vol. 27, pp. 934-946.

Leissa, A. W., 1981, "Advances in Vibrations, Buckling, and Postbuckling Studies on Composite Plates," *Composite Structures*, edited by T. H. Marshall, Applied Science Publisters, London, pp. 312-334.

Librescu, L., and Reddy, J. N., 1989, "A Few Remarks Concerning Several Refined Theories of Anisotropic Composite Laminated Plates," *International Journal of Engineering Science*, Vol. 27, pp. 515-527.

Mayberry, B. L., and Bert, C. W., 1968 , "Experimental Investigation of Nonlinear Vibrations of Laminated Anisotropic Panels," *The Shock and Vibration Bulletin*, No. 39, Part 3, pp. 191-199.

Miles, J. W., 1962, "Stability of Forces Oscillations of a Spherical Pendulum," *Quarterly of Applied Mathematics*, Vol. 20, pp. 21-32.

Miles, J. W., 1965, "Stability of Forced Oscillations of a Vibrating String, *Journal of Acoustical Society of America*, Vol. 38, pp. 855-861.

Moon, F. C., and Holmes, P. J., 1979, "A Magneto-Elastic Strange Attractor," *Journal of Sound and Vibration*, Vol. 65, pp. 275-296.

Moon, F. C., 1980, "Experiments on Chaotic Motions of a Forced Nonlinear Oscillator: Strange Attractors," *Journal of Applied Mechanics*, Vol. 47, pp. 638-644.

Moon, F. C., and Holmes, W. T., 1985, "Double Poincaré Sections of a Quasi-Periodically Forced Chaotic Attractor," *Physics Letters A*, Vol. 111, No. 4, pp. 157-160.

Moon, F. C., and Shaw, S. W., 1983, "Chaotic Vibrations of a Beam with Nonlinear Boundary Conditions," *International Journal of Non-Linear Mechanics*, Vol. 18, pp. 465-477.

Narasimha, R., 1968, "Nonlinear Vibration of an Elastic String," *Journal of Sound and Vibration*, Vol. 8, pp. 134-136.

Nayfeh, A. H., Mook, D. T., and Marshall, L. R., 1973, "Nonlinear Coupling of Pitch and Roll Modes in Ship Motions," *Journal of Hydronautics*, Vol. 7, pp. 145-152.

Nayfeh, A. H., and Mook, D. T., 1979, *Nonlinear Oscillations*, Wiley, New York.

Nayfeh, A. H., 1981, *Introduction to Perturbation Techniques*, Wiley, New York.

Nayfeh, A. H., 1983, "Combination Resonances in the Non-Linear Response of Bowed Structures to a Harmonic Excitation," *Journal of Sound and Vibration*, Vol. 90, pp. 457-470.

Nayfeh, A. H., 1984, "On the Low-Frequency Drumming of Bowed Structures," *Journal of Sound and Vibration*, Vol. 94, pp. 551-562.

Nayfeh, A. H., and Zavodney, L. D., 1988, "Experimental Observations of Amplitude- and Phase-Modulated Responses of Two Internally Coupled Oscillators to a Harmonic Excitation," *Journal of Applied Mechanics*, Vol. 55, pp. 706-711.

Nayfeh, A. H., Balachandran, B., Colbert, M. A., and Nayfeh, M. A., 1989, "An Experimental Investigation of Complicated Responses of a Two-Degree-of Freedom Structure," *Journal of Applied Mechanics*, Vol. 56, pp. 960-967.

Nayfeh, A. H., and Balachandran, B., 1993, *Applied Nonlinear Dynamics*, Wiley, New York.

Nayfeh, S. A., Nayfeh, A. H., and Mook, D. T., 1992, "Modal Interactions in a Parametrically and Externally Excited String," *Proceedings of the Fourth Conference on Nonlinear Vibrations, Stability, and Dynamics of Structures and Mechanisms*, Blacksburg, VA, June 7-11.

Nayfeh, T. A., Nayfeh, A. H., and Mook, D. T., 1990, "A Theoretical-Experimental Investigation of a Three-Degree-of-Freedom Structure," *AIAA Paper No. 90-1081, AIAA 31st Structure, Structural Dyanmics and Materials Conference*, Long Beach, CA.

Nelson, F. C., and Greif, R., 1970, "Damping", *Shock and Vibration Computer Programs: Reviews and Summaries*, Vol. 23, pp. 237-245.

Pai, P. F., and Nayfeh, A. H., 1991, "A Nonlinear Composite Plate Theory," *Nonlinear Dynamics*, Vol. 2, pp. 445-477.

Pai, P. F., and Nayfeh, A. H., 1992, "A Nonlinear Composite Beam Theory," *Nonlinear Dynamics*, Vol. 3, pp. 273-303.

Rades, M., 1983, "Identification of the Dyanmic Characteristics of a Simple System with Qaudratic Damping," *Rev. Roum. Sci. Techn.-Méc. Appl.*, Vol. 28, No. 4, pp. 439-446.

Reddy, J. N., 1983, "A Review of the Literature on Finite-Element Modeling of Laminated Composite Plates and Shells," *Shock and Vibration Digest*, Vol. 15, pp. 3-8.

Reddy, J. N., 1984a, "A Simple Higher-Order Theory for Laminated Composite Plates," *Journal of Applied Mechanics*, Vol. 51, pp. 745-762.

Reddy, J. N., 1984b, "A Refined Nonlinear Theory of Plates with Transverse Shear Deformation," *International Journal of Solids and Structrues*, Vol. 20, pp. 881-896.

Reddy, J. N., 1985, "A Review of the Literature on Finite-Element Modeling of Laminated Composite Plates and Shells," *Shock and Vibration Digest*, Vol. 17, pp. 3-8.

Reference Manual for Modal-Plus, 1985, Structural Dynamics Research Corporation.

Reissner, E., 1948, "Finite Deflections of Sandwitch Plates," *Journal of the Aeronautical Sciences*, Vol. 15, pp. 435-440.

Reissner, E., 1953, "On Variational Theory for Finite Elastic Deformation," *Journal of Mathematical Physics*, Vol. 32, pp. 129-135.

Rice, H. J., and Fitzpatrick, J. A., 1991, "The Measurement of Nonlinear Damping in Single-Degree-of-Freedom Systems," *Journal of Vibration and Acoustics*, Vol. 113, pp. 132-140.

Sato, K., Saito, H., and Otomi, K., 1978, "The Parametric Response of a Horizonatal Beam Carrying a Concentrated Mass Under Gravity," *Journal of Applied Mechanics*, Vol. 45, pp. 643-648.

Schmidt, R., 1977, "A Refined Nonlinear Theory of Plates with Transverse Shear Deformations," *Journal of Industrial Mathematics Society*, Vol. 27, Part 1, pp. 23-28.

Singh, G., Rao, G. V., and Iyengar, N. G. R., 1991, "Some Observations on the Large Deflecton Bending of Rectangular Antisymmetric Cross-Ply Plates," *Composite Structures*, Vol. 18, pp. 77-91.

Thomson, W. T., 1981, *Theory of Vibration with Applications,* Prentice-Hall, Inc., New Jersey.

Timoshenko, S. P., 1921, "On the Correction for Shear of the Differential Equation for Tranverse Vibrations of Prismatic Bars," *Philosophical Magazine*, Vol. 41, pp. 744-746.

Timoshenko, S. P., 1922, "On the Transverse Vibrations of Bars of Uniform Cross Sections," *Philosophical Magazine*, Vol. 43, pp. 125-131.

Whitney, J. M., and Leissa, A. W., 1969, "Analysis of Heterogeneous Anisotropic Plates," *Journal of Applied Mechanics*, Vol. 36, pp. 261-266.

Wiesenfeld, K., 1985, "Noisy Precursors of Nonlinear Instabilities," *Journal of Statistical Physics*, Vol. 38, Nos. 5/6, pp. 1071-1097.

Yamaki, M., and Chiba, M., 1983, "Nonlinear Vibrations of a Clamped Rectagular Plate with Initial Deflection and Initial Edge Displacement--Part I: Theory," *Thin-Walled Structures*, Vol. 1, pp. 3-29.

Yamaki, M., and Chiba, M., 1983, "Nonlinear Vibrations of a Clamped Rectagular Plate with Initial Deflection and Initial Edge Displacement--Part II: Experiment," *Thin-Walled Structures*, Vol. 1, pp. 101-119.

Vita

Tony Joseph Anderson was born on August 26, 1960 in Salt Lake City, Utah to Douglas and Janet Anderson. After graduating from high school in 1978, he attended Utah State University on an athletic scholarship in track and cross-country. He received a B.S. degree in Mechanical Engineering from Utah State University in 1983. Because jobs were scarce, he attended Arizona State University, where he worked towards a M.S. in Mechanical Engineering. In 1984 he married Jonna Olson Anderson who he met while at Utah State.

In the fall of 1984, Tony joined Space Data Corporation in Tempe, Arizona. While at Space Data, he worked as a Mechanical Engineer on a wide assortments of tasks related to building and launching rockets. While working at Space Data he continued to work on a masters degree that he received from Arizona State University in 1987. In 1989, Tony, Jonna and family left Arizona for Virginia so Tony could work towards a Ph.D. in the Department of Engineering Science and Mechanics at Virginia Polytechnic Institute and State University. In April 1993, he received a Ph.D. degree in Engineering Mechanics.

Tony and Jonna have three children, Danielle 8, Tana 6, and Kyle 5.